Modeling and Analysis of Cellular Networks using Stochastic Geometry: A Tutorial

Hesham ElSawy, *Member, IEEE*, Ahmed Sultan-Salem, *Member, IEEE*,
Mohamed-Slim Alouini, *Fellow, IEEE*, and Moe Z. Win, *Fellow, IEEE*

Abstract—This paper presents a tutorial on stochastic geometry (SG) based analysis for cellular networks. This tutorial is distinguished by its depth with respect to wireless communication details and its focus on cellular networks. The paper starts by modeling and analyzing the baseband interference in a baseline single-tier downlink cellular network with single antenna base stations and universal frequency reuse. Then, it characterizes signal-to-interference-plus-noise-ratio (SINR) and its related performance metrics. In particular, a unified approach to conduct error probability, outage probability, and transmission rate analysis is presented. Although the main focus of the paper is on cellular networks, the presented unified approach applies for other types of wireless networks that impose interference protection around receivers. The paper then extends the unified approach to capture cellular network characteristics (e.g., frequency reuse, multiple antenna, power control, etc.). It also presents numerical examples associated with demonstrations and discussions. To this end, the paper highlights the state-of-the-art research and points out future research directions.

I. Introduction

STOCHASTIC GEOMETRY (SG) has succeeded to provide a unified mathematical paradigm to model different types of wireless networks, characterize their operation, and understand their behavior [1]–[5]. The main strength of the analysis based on SG, hereafter denoted as SG analysis, can be attributed to its ability to capture the spatial randomness inherent in wireless networks. Furthermore, SG models can be naturally extended to account for other sources of uncertainties such as fading, shadowing, and power control. In some special cases, SG analysis can lead to closed-form expressions that govern system behavior. These expressions enable the understanding of network operation and provide insightful design guidelines, which are often difficult to get from computationally intensive simulations.

SG analysis for wireless networks can be traced back to the late 70's [6]–[10]. At that point in time, SG was first used to design the transmission ranges and strategies in multi-hop ad hoc networks. Then, SG was used to characterize the aggregate interference coming from a Poisson field of interferers [11]–[13].[1] Despite the existence of a large number of interfering sources, it is shown in [11]–[13] that the central limit theorem (CLT) does not apply, and consequently, the aggregate interference does not follow the Gaussian distribution. This is due to the prominent effect of distance-dependent path-loss attenuation, which makes the aggregate interference dominated by proximate interferers. The research outcome in [3], [11], [14]–[16] has shown that the aggregate interference follows the α-stable distribution [13], [17], [18], which is more impulsive and heavy tailed than the Gaussian distribution [19]. In fact, the aggregate interference has been characterized by generalizing shot-noise theory in higher dimensions [13], [20]–[23]. Such characterization has set the foundations for SG analysis, enriched the literature with valuable results, and helped to understand the behavior of several wireless technologies in large-scale setups [1], [6]–[11], [14]–[16], [23]–[33]. However, these results are confined to ad hoc networks with no spectrum access coordination schemes. In wireless networks with coordinated spectrum access, the aforementioned analysis presents pessimistic results.

Due to the shared nature of the wireless spectrum, along with the reliability requirement for information transmission, spectrum access is usually coordinated to mute interference sources near receivers. This can be achieved by separating nearby transmissions over orthogonal resources (i.e., time, frequency, or codes). However, due to the scarcity of resources and the high demand for wireless communication, the wireless resources are reused over the spatial domain. The receivers are usually protected from interference resulting from spatial frequency reuse by interference exclusion regions. Cellular networks, which are the main focus of this tutorial, impose interference protection for users' terminals via the cellular structure.[2] This intrinsic property of cellular networks should be incorporated into analysis. Furthermore, several medium access control protocols exist in ad hoc networks (e.g., carrier sensing multiple access) that impose interference protection around receivers. Accounting for the interference protection around receivers, the aggregate interference is neither α-stable nor Gaussian distributed [34]. In fact, there is no closed-form expression for the interference distribution if interference protection is incorporated into analysis. This makes

---

[1]The Poisson field of interferers means that the transmitters are randomly, independently, and uniformly scattered in the spatial domain, in which the number of transmitters in any bounded region in the space is a Poisson random variable.

[2]The cellular structure guarantees that each user is served by the base station that provides the highest signal strength.

characterizing and understanding the interference behavior a challenging task. This tutorial shows detailed step-by-step interference characterization using stochastic geometry. It also shows the interference effect on key wireless communication performance indicators such as error probability and transmission rate. Since interference coordination is elementary for several types of wireless networks, the analysis in this paper can be extended to other types of wireless networks that impose interference protection around receivers.

To facilitate navigating through this tutorial, we first illustrate the organization of its contents and the relations between its sections as shown in Fig. 1. Sections I to III are introductory sections that introduce SG, present related literature, and define the baseline system model that will be used for the analysis through the subsequent sections. Sections IV and V present exact characterization for the baseband aggregate interference and error rate in cellular networks modeled via the Poisson point process (PPP). As discussed later in the tutorial, the exact analysis presented in Sections IV and V is involved and different from the widely used outage probability and ergodic capacity analysis. Hence, Section VI presents an approximation that simplifies the error rate analysis and unifies it with the outage probability and ergodic capacity framework presented in Section VII. The unified analysis developed in Sections VI and VII are then applied to advanced cellular network system models in Section VIII. Future research directions are then highlighted in Section IX before the paper is concluded in Section X.

A. Using SG for Cellular Networks

SG was mostly confined to ad hoc and sensor networks to account for their intrinsic spatial randomness. In contrast, cellular networks were mostly assumed to be spatially deployed according to an idealized hexagonal grid. Motivated by its tractability, attempts to promote SG to model cellular networks can be traced back to the late 90's [35], [36]. However, success was not achieved until a decade later [37]–[39]. The theoretical and statistical studies presented in [37]–[39] revealed that cellular networks deviate from the idealized hexagonal grid structure and follows an irregular topology that randomly changes from one geographical location to another. The authors in [37] show that the signal-to-interference-plus-noise-ratio (SINR) experienced by users in a simulation with actual base station (BS) locations is upper bounded by the SINR of users in idealistic grid network, and lower bounded by the SINR of users in random network. Interestingly, the random network provides a lower bound that is as tight as the upper bound provided by the idealized grid network. However, the lower bound is preferred due to the tractability provided by SG. The authors in [38] show that the spatial patterns exhibited by actual BS locations in different geographical places can be accurately fitted to random spatial patterns modeled via SG. Furthermore, the results in [38] confirm the tight lower bound provided by the random network to the users' SINR in simulations with actual BS locations. Finally, the authors in [39] show that the SINR in grid network converges to the SINR of random network in a strong

shadowing environment.

Exploiting the tractability of SG, several notable results are obtained for cellular networks. For instance, the downlink baseline operation of cellular networks is characterized in [37]–[48]. Extensions to multi-tier case are provided in [49]–[64]. The uplink case is characterized in [41], [65]–[76]. Range expansion and load balancing are studied in [77]–[81]. Relay-aided cellular networks are characterized in [82]–[86]. Cognitive and self-organizing cellular networks are studied in [87]–[95]. Cellular networks with multiple-input multiple-output (MIMO) antenna system are investigated in [96]–[114]. Cooperation, coordination, and interference cancellation in cellular networks are characterized in [115]–[125]. Energy efficiency, energy harvesting, and BS sleeping for green cellular operation are studied in [126]–[136]. Millimeter (mmW) based communication in cellular network is characterized in [137]–[140]. In-band full-duplex communication for cellular networks is studied in [141]–[145]. Interference correlation across time and space in cellular networks is studied in [146], [147]. The additional interference imposed via underlay device-to-device (D2D) communication in cellular networks is characterized in [148]–[154]. Mobility and cell boundary cross rate are studied in [155]–[160]. Cloud radio access network and backhuling in cellular networks are studied in [161]–[163]. Last but not least, the physical layer security and secrecy in the context of cellular networks are characterized in [164], [165]. A detailed taxonomy for the state-of-the-art stochastic geometry models for cellular networks is given in Table I. By virtue of the results in [35]–[165], SG based modeling for cellular networks is widely accepted by both academia and industry.

B. Motivation & Contribution

Due to the expanding interest in SG analysis, it is required to have a unified and deep, yet elementary, tutorial that introduces SG analysis for beginners in this field. Although there are excellent resources that present SG analysis for wireless networks [3]–[5], [20], [166]–[171], this tutorial is distinguished by characterizing the baseband aggregate interference, introducing error rate analysis, and focusing on cellular networks. The monographs [166]–[168] present an advanced level treatment for SG and delve into details related to SG theory. In [4], [20], [166]–[171] many transceiver characteristics (e.g., modulation scheme, constellation size, matched filtering, signal recovery technique, etc.) are abstracted and the aggregate interference is treated as the sum of the powers of the interfering signals, and hence, the analysis is limited to outage probability, defined as the probability that the SINR goes below a certain threshold, and ergodic rate, defined by the seminal Shannon's formula. The tutorial in [3] delves into fine wireless communication details and presents error probability analysis. However, it is focused on ad hoc networks. The authors in [5] survey the SG related cellular networks literature without delving into the analysis details.

In contrast to [4], [5], [20], [166]–[171], this tutorial delves into baseband interference characterization and symbol/bit error probability analysis while exposing the necessary ma-
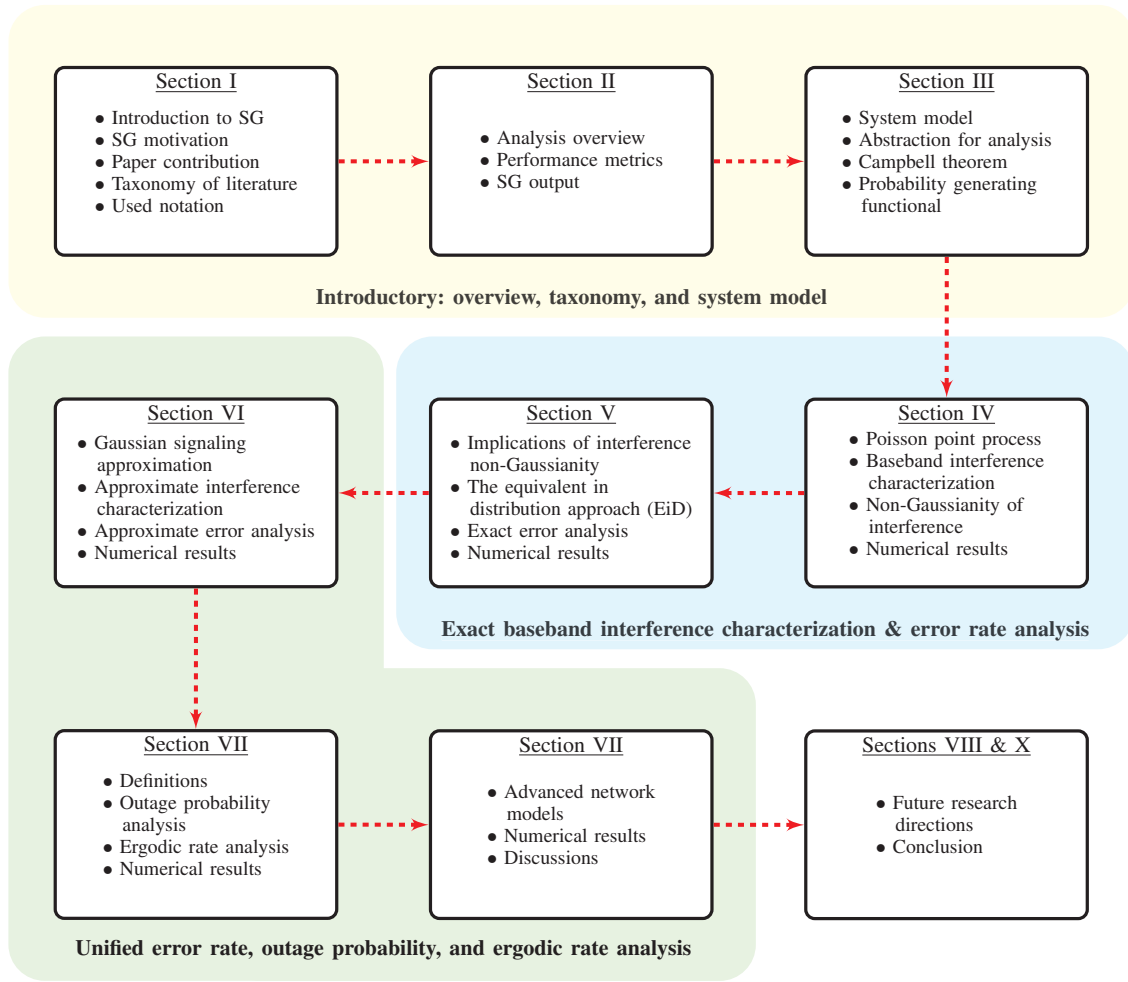
Fig. 1. Organization of the tutorial.

terial from SG theory. Hence, it is more suited for those with wireless communication background. Furthermore, it is focused on the cellular network which is not the case in [3], [4], [20], [166]–[169]. This tutorial also discusses the Gaussian signaling approximation that is taken for granted in the literature. To the best of the authors' knowledge, this is the first time that the accuracy of the Gaussian signaling approximation in large-scale networks is discussed and analytically quantified. Finally, the tutorial elaborates the reasons for the pessimistic performance evaluation obtained via SG analysis and points out potential solutions.

Notation: throughout the paper, $\mathbb{P}\{\cdot\}$ denotes probability, $\mathbb{E}_X\{\cdot\}$ denotes the expectation over the random variable X, $\mathbb{E}\{\cdot\}$ denotes the expectation over all random variables in $\{\cdot\}$, $\kappa_n(X)$ denotes the nth cumulant of the random variable X, $\triangleq$ denotes the definition, $\overset{d}{=}$ denotes the equivalence in distribution, $\sim$ denotes the distribution, and $\mathcal{CN}(a,b)$ denotes the circularly symmetric complex Gaussian distribution with mean a and variance b. The notations $f_X(\cdot)$, $F_X(\cdot)$, $\varphi_X(\cdot)$, and $\mathcal{L}_X(\cdot)$ are used to denote the probability density function (PDF), the cumulative distribution function (CDF),

the characteristic function (CF), and the Laplace transform[3] (LT), respectively, for the random variable X. The indicator function is denoted as $\mathbb{1}_{\{\cdot\}}$, which takes the value 1 when the statement $\{\cdot\}$ is true and 0 otherwise. The set of real numbers is denoted as $\mathbb{R}$, the set of positive integers is denoted as $\mathbb{Z}^+$, the set $\mathbb{Z}^+ \cup \{0\}$ is denoted as $\mathbb{N}$, the set of complex numbers is denoted as $\mathbb{C}$, in which the imaginary unit is denoted as $\jmath = \sqrt{-1}$, real part, imaginary part, and magnitude of a complex number are denoted as $\mathrm{Re}\{\cdot\}$, $\mathrm{Im}\{\cdot\}$, and $|\cdot|$, respectively, the complex conjugate is denoted as $(\cdot)^*$, and the Hermitian conjugate $(\cdot)^H$. The Euclidean norm is denoted as $\|\cdot\|$. $\gamma(a,b) = \int_0^b x^{a-1}e^{-x}dx$ is the lower incomplete gamma function, $Q(x) = \frac{1}{\sqrt{2\pi}}\int_x^\infty e^{-\frac{t^2}{2}}\mathrm{d}t$ is the Q-function, $(a)_n = \frac{\Gamma(a+n)}{\Gamma(a)}$ is the Pochhammer symbol, $_1F_1(a;b;x) = \sum_{n=0}^\infty \frac{(a)_n}{(b)_n}\frac{x^n}{n!}$ is the Kummer confluent hypergeometric function, and $_2F_1(a,b;c;x) = \sum_{n=0}^\infty \frac{(a)_n(b)_n}{(c)_n}\frac{x^n}{n!}$ is the Gauss hypergeometric function [172], [173]. With a slight abuse of notation, $\overset{x=a}{=}$ is used to denote that the current

---

[3]With a slight abuse of notation, we denote the LT of the PDF of a random variable X by the LT of X. The LT of X is defined as $\mathcal{L}_X(s) = \mathbb{E}\{e^{-sX}\}$.

TABLE I
TAXONOMY OF THE LITERATURE FOR CELLULAR NETWORK SG MODELS

Point Process	Metric	System	Technology	References
Poisson	Coverage Probability & Ergodic Rate	Downlink	Single-tier	[37], [39], [42]
			Multi-tier	[49]–[59], [77]–[79], [81]
			MIMO	[96]–[100], [105]–[112], [122], [123], [125], [131], [164]
			Cognitive Cellular	[87]–[95]
			Interference Management & BS Cooperation	[115]–[120], [122]–[125]
			Relaying	[82]–[85]
			Millimeter Wave Communication	[137]–[139]
			Energy Harvesting & Energy Efficiency	[111], [122], [126]–[136]
			Mobility	[155]–[158], [160]
			Cloud Radio Access & Backhauling	[112], [138], [161]–[163]
			Physical-Layer Security	[164], [165]
		Uplink	Single-tier	[65], [69], [71], [73]
			Multi-tier	[65], [68], [70], [74], [75]
			MIMO	[67], [113], [114], [121]
			Energy Efficiency	[130]
			Relaying	[86]
			Internet of Things	[72]
		Full-Duplex	Single-tier	[142], [143], [145]
			Multi-tier	[141], [144]
		Device-to-Device	Half-Duplex	[128], [148]–[152]
			Full-Duplex	[153]
	Error Rate & Throughput	Downlink	Single-tier	[40], [41]
			MIMO	[101]–[103], [110]
			Millimeter Wave Communication	[140]
		Uplink	Single-tier	[41]
			Multi-tier	[66]
		Full-Duplex	Single-tier	[143]
Binomial	Outage Probability & Ergodic Rate	Downlink	Single-tier	[48]
			MIMO	[105]
Hard-core	Outage Probability & Ergodic Rate	Downlink	Single-tier	[62], [63]
			Multi-tier	[64]
			Multi-tier Cognitive	[87]–[90]
		Uplink	MIMO	[104]
Ginibre	Outage Probability & Ergodic Rate	Downlink	Single-tier	[43], [44]
		Uplink	Single-tier	[76]
Poisson Cluster	Outage Probability & Ergodic Rate	Downlink	Multi-tier	[60]
Poisson Hole	Outage Probability & Ergodic Rate	Device-to-Device	Proactive Caching	[154]
General	Outage Probability & Ergodic Rate	Device-to-Device	Single-tier	[45]–[47]
			Multi-tier	[61], [80]

expression is obtained from a substitution for x with a in the directly preceding expression.

II. OVERVIEW OF SG ANALYSIS

Before delving into the modeling details, we first give a broad overview of the SG analysis as well as its outcome. In practice, cellular networks are already deployed and, for a given city, the locations of BSs are already known. However, SG does not model the performance of a specific realization of the cellular network at a specific geographical location. Instead, it gives general analytical model that applies on average for all cellular networks' realizations. For instance,

if we want to analyze the effect of in-band full-duplex communication in cellular networks, instead of repeating the analysis for each and every geographical setup of the cellular networks, we can obtain general performance analysis, guidelines, and design insights that apply when averaging over all distinct realizations. Following the studies in [37], [38], the locations of BSs at different geographical locations form random patterns. Hence, general analysis for cellular networks should be based on the probabilistic spatial distribution of BSs rather than on a specific network realization. Abstracting each BS location to a point in the Euclidean space, SG models the probabilistic BS locations by a stochastic point process

(PP) [174]–[177], which describes the random spatial patterns formed by points in space.

We are interested in the performance of a randomly selected user and/or the average performance of all users, i.e., the average performance of users in all locations. As discussed above, from the network perspective, we are interested in the average performance over all cellular network realizations. Such an average performance metric is denoted as *spatially averaged* (SA) performance, which is the main outcome from SG analysis.[4] Examples of the SA performance metrics of interest in cellular networks are:

- **Outage probability:** the probability that the SINR goes below a certain threshold (T), $\mathbb{P}\{\text{SINR} < T\}$.
- **Ergodic capacity:** the expectation $\mathbb{E}\{\log(1 + \text{SINR})\}$ is denoted as the ergodic capacity, which measures the long-term achievable rate averaged over all channel and interference (i.e., network realization) states [178].
- **Symbol error probability (SEP):** the probability that the decoded symbol is not identical to the transmitted symbol.
- **Bit error probability (BEP):** the probability that the decoded bit is not identical to the transmitted bit.
- **Pairwise error probability (PEP):** the probability that the decoded symbol is s_i given that s_j is transmitted ignoring other possible symbols.
- **Handover rate** the number of cell boundaries crossed over per unit time.[5]

SG gives expressions that relate the aforementioned performance metrics to the cellular network parameters and design variables. Such expressions are then used to understand the network behavior in response to the network parameters and/or design variables. This helps to obtain insights into the network operation and extract design guidelines. Note that, by SG analysis, the obtained design insights hold on average for all realizations of cellular networks. Hence, in light of the obtained expressions, communication system engineers can perform tradeoff studies and take informed design decisions before facing practical implementation issues. It is worth noting that the spatially averaged performance metrics obtained by SG analysis can be interpreted in different ways. For instance, the average SEP can be interpreted as: i) the SEP averaged over all symbols for a randomly selected user, or ii) the SEP averaged over all symbols transmitted within the network. Similar interpretation applies for other performance metrics.

---

[4]Formally, the spatial averaging technique and its interpretation depend on the type of the PP. If the PP is stationary (i.e., translation invariant) and spatially ergodic, then the averaging is w.r.t. the PP distribution and the result is location independent. On the other hand, if the PP is stationary but spatial ergodicity does not hold, then the expectation is done w.r.t. the Palm distribution of the PP [168] and the result is location independent. Finally, if the PP is neither stationary nor spatially ergodic, then the expectation is done w.r.t. the Palm distribution of the PP and the result is location-dependent. Further discussion about this subject can be found in [168, Chapter 8].

[5]Handover rate is not discussed in this tutorial. Interested readers are referred to [155], [156].

III. Baseline System Model & Aggregate Interference Characterization

A. System Model

As a starting point, a baseline two-dimensional single-tier downlink cellular network is considered to introduce the basic SG analysis. It is assumed that all BSs are equipped with single antenna and transmit with the same power P. Other scenarios such as MIMO, uplink, and more advanced downlink models are presented in Section VIII. It is also assumed that each user equipment (UE) is equipped with a single antenna and is associated to its nearest BS. Nearest BS association captures the traditional average received signal strength (RSS) based association for single-tier cellular networks when shadowing is ignored. In this case, the service area of each BS can be geometrically represented by a Voronoi-tessellation [175], [179] as shown in Fig. 2. We assume that BSs have saturated buffers and that every BS has a user to serve (saturation condition). Each BS maps its user data using a general two-dimensional zero-mean unit-power constellation $\mathbf{S} = \{d_1, d_2, \ldots, d_M\}$, where $d_m = a_m \exp\{\jmath\theta_m\}$ and $m = 1, 2, 3, \ldots. M$. If s is a randomly and uniformly selected symbol from $\mathbf{S}$, then $\mathbb{E}\{s\} = 0$ and $\mathbb{E}\{|s|^2\} = 1$. All symbols from all BSs are modulated on the same carrier frequency and are transmitted to the corresponding users. The transmitted signal amplitude attenuates with the distance r according to the power-law $r^{-\frac{\eta}{2}}$, where η is an environmental dependent path-loss exponent.[6] We consider narrowband fading channels where multi-path fading is modeled via independent and identically distributed (i.i.d.) zero-mean unit-variance circularly symmetric complex Gaussian random variables, denoted by h. We are interested in modeling the baseband signal received at an arbitrary user which is located r meters away from his serving BS. The baseband signal (after proper down-conversion and low-pass filtering) can be represented as

$$y = \sqrt{P}\, s\, h\, r^{-\frac{\eta}{2}} + i_{\text{agg}} + n, \tag{1}$$

where s is the intended symbol, $h \sim \mathcal{CN}(0, 1)$, i_{agg} is the baseband aggregate interference experienced from all interfering BSs, and $n \sim \mathcal{CN}(0, N_o)$ is the noise.

B. Network Abstraction

The first step in the analysis is to choose a *"convenient PP"* to abstract network elements (i.e., BSs and users). Then, the performance metrics of interest are expressed as functions of the selected PP. These functions can be evaluated using results from SG. Note that the term *"convenient PP"* is used to denote a PP that balances a tradeoff between tractability and practicality. As will be discussed later, a PP that is perfectly practical may obstruct the model tractability, and hence, approximations are usually sought. For the sake of complete presentation, the paper first sheds light on the tractability

---

[6]The path loss exponent strongly depends on the local terrain characteristics as well as the cell size. Typical values for path-loss exponent are $3 \leq \eta \leq 4$ for urban macro-cells and $2 < \eta \leq 8$ for micro-cells [180].
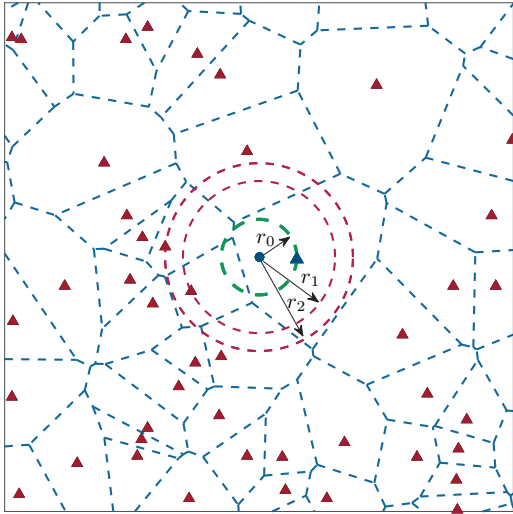
Fig. 2. A realization from a cellular network in which the triangles represent the BSs, the blue triangle/circle represents the test BS/user, red triangles represent interfering BSs, the bold-dashed lines visualize BSs footprints for nearest BS association, and the green dashed circle shows the interference protection imposed by nearest BS association. The locations of other users are omitted for clarity.

issue of general PPs. Then the Poisson point process (PPP) approximation is introduced, which is usually used in the literature due to its tractability.

Consider that each realization for BS locations is abstracted by a general infinite two-dimensional PP, denoted by the set $\Psi = \{x_i; i \in \mathbb{N}\}$,[7] such that $x_i \in \mathbb{R}^2$ represents the coordinates of the ith BS.[8] At the moment, assume that the selected PP Ψ perfectly reflects the correlation between the BSs belonging to the same service provider. Repulsion (i.e., a minimum distance between BSs) is an important form of correlation that exists in cellular networks due to the network planning process.

Without loss of generality, the analysis is conducted, and the performance is evaluated, for a test user which is located at the origin.[9] For notational convenience, it is assumed that the points in the set Ψ are ordered with respect to (w.r.t.) their distances from the origin, see Fig. 2. In this case, the distance from the nth BS to the test user is given by $r_n = \|x_n\|$, and the inequalities ($r_{n-1} < r_n < r_{n+1}$) are satisfied with probability one. For the sake of simple presentation, the set $\tilde{\Psi} = \{\|x_i\|; i \in \mathbb{N}\} = \{r_i; i \in \mathbb{N}\}$ is defined, which consists of the ordered BSs distances to the test user. Due to the RSS-based association rule, the test user is associated with the BS located at x_0 and the baseband received signal by the test user

[7]While a PP can be defined as a random set or a random measure [168, Chapter 2], we restrict the focus of this tutorial on the random set definition.

[8]Each BS is denoted by its location and the terms "point" and "BS" are used interchangeably. Infinite networks are considered for simplicity and due to the negligible contribution from far-away BSs to the aggregate interference. Also, the analysis can be easily modified to finite networks.

[9]The origin is an arbitrary reference point in $\mathbb{R}^2$ which is selected for the analysis. Usually the origin is selected to be the test user's location at which the performance is evaluated. The obtained results do not depend on the choice of the origin for stationary PPs. Otherwise, the analysis is location-dependent.

can be expressed as

$$y_0 = \sqrt{P}s_0 h_0 r_0^{-\frac{\eta}{2}} + \underbrace{\sum_{r_k \in \tilde{\Psi} \setminus r_0} \sqrt{P}s_k h_k r_k^{-\frac{\eta}{2}}}_{i_{\text{agg}}} + n, \qquad (2)$$

where s_0 is the intended symbol, s_k is the interfering symbol from the kth BS, $h_0 \sim \mathcal{CN}(0,1)$ is the intended channel fading parameter, $h_k \sim \mathcal{CN}(0,1)$ is the interfering channel fading parameter. The random variables s_k are i.i.d. $\forall k$. The random variables h_k are also i.i.d. $\forall k$. The symbols and fading parameters are independent of one another. Note that r_0 is excluded from $\tilde{\Psi}$ as the serving BS does not contribute to the interference. It is worth noting that the received signal in the form of (2) also applies to other types of wireless networks that impose an interference protection of r_0 around receivers.

In cellular networks, the serving distance r_0 is a random variable that is parametrized by the BS intensity. As cellular networks become denser, users are more likely to be closer to their serving BSs, and vice versa. For the sake of simple and general analysis, the paper introduces the analysis for a fixed r_0 (i.e., assuming constant r_0) that is decoupled from the intensity λ in Sections IV to VII. Fixing r_0 and letting λ to be varied independently reveals the explicit effect of the interference boundary and interferers intensity on the aggregate interference properties. Furthermore, the scenario of decoupled interference protection region and intensity of interferers has potential applications in wireless networks such as cognitive networks. In cognitive networks, the performance of primary receivers can be protected by either enlarging the spatial interference protection around the primary receiver or lowering the intensity of simultaneously active secondary users [24]. Section VIII relaxes the fixed r_0 assumption and focus on the case where the PDF of r_0 is characterized by the BS intensity λ.

By visual inspection of (2), it is clear that i_{agg} involves numerous sources of uncertainties. Neither the number nor locations of the interfering BSs $\{x_k\}_{k \in \mathbb{Z}^+}$ are known. The set of interfering BSs $\Psi \setminus x_0$ is a random set with infinite cardinality (or random cardinality for finite networks). The following subsections show how to handle this randomness and statistically characterize the aggregate interference in (2). Before getting into the details, it should be emphasized that we do not aim to calculate an instantaneous value for i_{agg}. Instead, we aim to characterize i_{agg} via its PDF, CF, and/or moments. As will be shown later, and also discussed in [3], [5], the distribution of i_{agg} is not Gaussian. This is because the CLT does not hold for i_{agg} as the sum in (2) is dominated by the interference from nearby BSs.

C. SG Analysis for i_{agg} for General Point Process

Due to many sources involving uncertainties, it is not feasible to characterize i_{agg} in an elementary manner (i.e., by evaluating the distribution for sum and product of random variables). Instead, the characterization parameter of interest (e.g., the moments of i_{agg}) is expressed as a function of the PP ($\tilde{\Psi}$), then apply SG results to seek a solution. As shown
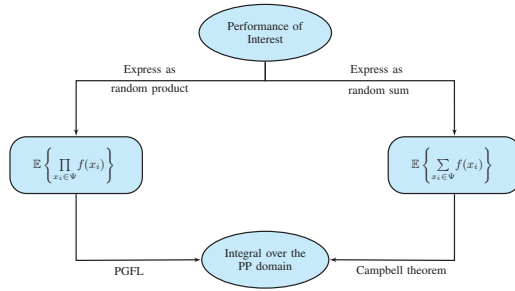
Fig. 3. The two main techniques to handle the PP randomness. The PGFL denotes the probability generating functional, which is defined in the text. The figure illustrates that if the performance of interest is expressed in terms of an expectation over a sum (or a product) of functions in the point process, this expectation can be computed via a tractable integral over the point process (i.e., spatial region in which the point process exists).

in Fig. 3, SG provides two main techniques that transform a function that involves all points in a PP to an integral over the PP domain, namely, Campbell's theorem and the probability generating functional (PGFL).[10] However, as shown in the figure, a certain representation for the parameter of interest is mandatory to exploit these techniques. Since Campbell's theorem requires an expectation over a random sum, it can be directly used to calculate moments. On the other hand, the PGFL requires an expectation over a random product, which makes it suitable to calculate the CF of i_{agg}. Campbell's theorem states that:

Theorem 1 (Campbell Theorem): Let Φ be a PP in $\mathbb{R}^n$ and $f : \mathbb{R}^n \to \mathbb{R}$ be a measurable function, then

$$\mathbb{E}\left\{ \sum_{x_i \in \Phi} f(x_i) \right\} = \int_{\mathbb{R}^n} f(x) \Lambda(\mathrm{d}x) \tag{3}$$

where $\Lambda(\mathrm{d}x)$ is the intensity measure of the PP Φ and $x \in \mathbb{R}^n$ [175, Chapter 1.9]. In case of PPs in $\mathbb{R}^2$ with intensity function $\lambda(x)$, (3) reduces to

$$\mathbb{E}\left\{ \sum_{x_i \in \Phi} f(x_i) \right\} = \int_{\mathbb{R}^2} f(x) \lambda(x) \mathrm{d}x \tag{4}$$

As shown in (3), Campbell's theorem transforms an expectation of a random sum over the PP to an integral involving the PP intensity function. Note that the integration boundaries represent the boundaries of the region where the PP exists. For example, in the case of the depicted system model, the RSS association implies that no interfering BS can exist within the distance r_0. Applying Campbell's theorem, the mean value of the aggregate interference in (2) can be expressed as

$$\mathbb{E}\left\{ i_{\mathrm{agg}} \right\} = \mathbb{E}\left\{ \sum_{r_k \in \tilde{\Psi} \setminus r_0} \sqrt{P} s_k h_k r_k^{-\frac{\eta}{2}} \right\}$$

$$\overset{(a)}{=} \mathbb{E}_{\tilde{\Psi} \setminus r_0}\left\{ \sum_{r_k \in \tilde{\Psi} \setminus r_0} \mathbb{E}_{s_k, h_k}\left\{ \sqrt{P} s_k h_k r_k^{-\frac{\eta}{2}} \right\} \right\}$$

$$\overset{(b)}{=} \int_0^{2\pi} \lambda \int_{r_0}^{\infty} \mathbb{E}_{s,h}\left\{ \sqrt{P} s h r^{-\frac{\eta}{2}} \right\} r \mathrm{d}r \mathrm{d}\theta$$

$$= 2\pi \lambda \sqrt{P} \mathbb{E}\left\{ s \right\} \mathbb{E}\left\{ h \right\} \int_{r_0}^{\infty} r^{-\frac{\eta}{2}+1} \mathrm{d}r$$

$$\overset{(c)}{=} 0 \tag{5}$$

where (a) follows from the linearity of the expectation operator and the independence among the BS locations, the transmitted symbols, and the fading gains; (b) follows from Campbell's theorem and using the two random variables $h \overset{d}{=} h_k$ and $s \overset{d}{=} s_k$, in which the integration is computed in the polar coordinates $(\mathrm{d}x = r \mathrm{d}r \mathrm{d}\theta)$ with a constant intensity function $\lambda(x) = \lambda$; (c) follows from $\mathbb{E}\left\{ s \right\} = 0$, due to the symmetry of the symbols' constellation and the equal probability of the interfering symbols; (c) can also follow from $\mathbb{E}\left\{ h \right\} = 0$.

Campbell's theorem can also be used to find the second moment of interference:

$$\mathbb{E}\left\{ \left(\sum_{r_i \in \Phi} f(x_i) \right)^2 \right\} = \mathbb{E}\left\{ \sum_{x_i \in \Phi} f^2(x_i) + \sum_{x_i, y_i \in \Phi}^{x_i \neq y_i} f(x_i) f(y_i) \right\}$$

$$= \mathbb{E}\left\{ \sum_{x_i \in \Phi} f^2(x_i) \right\} + \mathbb{E}\left\{ \sum_{x_i, y_i \in \Phi}^{x_i \neq y_i} f(x_i) f(y_i) \right\}$$

$$= \int_{\mathbb{R}^n} f^2(x) \Lambda(\mathrm{d}x) + \int_{\mathbb{R}^n} \int_{\mathbb{R}^n} f(x) f(y) \mu^{(2)}(\mathrm{d}x, \mathrm{d}y) \tag{6}$$

where $\mu^{(2)}(\mathrm{d}x, \mathrm{d}y)$ is the second factorial moment [168, Chapter 6] of the PP $\tilde{\Psi}$, which is not always straightforward to compute.[11] From the above discussion, it seems that Campbell's theorem is restricted to compute the first moment of the interference and can be extended to derive the second moment when $\mu^{(2)}$ can be obtained. Therefore, Campbell's theorem is not sufficient to fully characterize i_{agg}.

The second technique to characterize i_{agg} is through the PGFL [168, Definition 4.3]. The PGFL converts random multiplication of functions over PP, in the form of $\mathbb{E}\left\{ \Pi_{x_i \in \Phi} f(x_i) \right\}$, to an integral over the PP domain. As shown in (7), random multiplication is useful to obtain the CF of the aggregate interference i_{agg}, where the first equality in (7) shows the definition of the CF for complex random variables [181, Definition 10.1], and $\boldsymbol{\omega} = \omega_1 + \jmath \omega_2$.

Equation (7) represents the CF of i_{agg} as an expectation over a random product of a function of the process Ψ. Hence, the PGFL of Ψ can be used to compute $\varphi_{i_{\mathrm{agg}}}(\cdot)$. Unfortunately, expressions for the PGFL only exist for a limited number

---

[10]The PP domain is the smallest region in the Euclidean space that contains the PP.

[11]For a homogeneous PPP with intensity λ, the second factorial moment is given by $\mu^{(2)}(\mathrm{d}x, \mathrm{d}y) = \lambda^2 \mathrm{d}x \mathrm{d}y$ [168, Example 6.5].

$$
\begin{aligned}
\varphi_{i_{\text{agg}}}(\boldsymbol{\omega}) &\triangleq \mathbb{E}\left\{\exp\left\{\jmath\text{Re}\left\{\boldsymbol{\omega}^H i_{\text{agg}}\right\}\right\}\right\} \\
&= \mathbb{E}\left\{\exp\left\{\jmath\omega_1\text{Re}(i_{\text{agg}}) + \jmath\omega_2\text{Im}(i_{\text{agg}})\right\}\right\} \\
&= \mathbb{E}\left\{\exp\left\{\jmath\omega_1\sum_{r_k\in\tilde{\Psi}\setminus r_0}\text{Re}(s_k h_k)\sqrt{P}r_k^{-\frac{\eta}{2}} + \jmath\omega_2\sum_{r_k\in\tilde{\Psi}\setminus r_0}\text{Im}(s_k h_k)\sqrt{P}r_k^{-\frac{\eta}{2}}\right\}\right\} \\
&= \mathbb{E}\left\{\exp\left\{\sum_{r_k\in\tilde{\Psi}\setminus r_0}\jmath\sqrt{\frac{P}{r_k^\eta}}(\omega_1\text{Re}(s_k h_k) + \omega_2\text{Im}(s_k h_k))\right\}\right\} \\
&= \mathbb{E}_{\tilde{\Psi}\setminus r_0}\left\{\prod_{r_k\in\tilde{\Psi}\setminus r_0}\mathbb{E}_{s_k,h_k}\left\{\exp\left\{\jmath\sqrt{\frac{P}{r_k^\eta}}\left[\omega_1\text{Re}(s_k h_k) + \omega_2\text{Im}(s_k h_k)\right]\right\}\right\}\right\}
\end{aligned}
\tag{7}
$$

of PPs. Hence, in order to use the PGFL and characterize the aggregate interference via its CF, the PP Ψ should be approximated via one of the PPs with known PGFL.

In conclusion, characterizing the aggregate interference from a general PP $\{\tilde{\Psi}\setminus r_0\}$ is not trivial and may not be analytically tractable. While the PP intensity is sufficient to obtain the mean of i_{agg} associated with a general PP $\{\tilde{\Psi}\setminus r_0\}$ via Campbell's theorem, tractable expressions for higher order moments cannot be generally obtained. Furthermore. the PGFL does not exist for all PPs to characterize the aggregate interference via its CF. Therefore, we have to resort to some approximation to maintain tractability. The most common and widely accepted approximation for the interference associated with $\{\tilde{\Psi}\setminus r_0\}$ is the interference generated from a PPP, which is discussed in the next section.

IV. POISSON POINT PROCESS APPROXIMATION

The PPP is an appealing point process due to its simple PGFL expression (see (90)), which leads to simple evaluation of (7). Furthermore, the homogenous PPP is stationary and spatially ergodic, which further simplifies the analysis. By Slivnyak-Mecke theorem [175], the statistical characteristics seen from a homogenous PPP is independent from the observation location.[12] In other words, the interference characterized at the test arbitrary origin is equivalent (i.e., has equivalent distribution) to the interference characterized at any other location in $\mathbb{R}^2$ including the points in Ψ. The PPP is formally defined as

Definition 1 (Poisson point process (PPP)): A PP $\Phi = \{x_i; i = 1, 2, 3, \ldots\} \subset \mathbb{R}^d$ is a PPP if and only if the number of points inside any compact set $\mathcal{B} \subset \mathbb{R}^d$ is a Poisson random variable, and the numbers of points in disjoint sets are independent.

Useful expressions characterizing the PPP are listed in **Appendix I**.

From the PPP definition, one can see that the PPP does not impose any correlation between its points. The uncorrelated spatial locations of the PPP points may raise concerns about its accuracy to model BSs that are unlikely to be deployed arbitrarily close to each other. Intuitively, BSs locations are better captured via repulsive point processes to reflect the network planning procedure.[13] Fortunately, we are more focused on modeling the aggregate interference generated in a cellular network than on studying the mutual spatial interactions between BSs. The aggregate interference is mainly affected by the number of interfering sources and their relative locations to the test receiver rather than the exact locations of the interfering sources. For instance, Fig. 4(a) shows a PP that exhibits minimum repulsion distance of δ among its points as well as repulsion w.r.t. the test receiver, and Fig. 4(b) shows an approximation of the PPs in Fig. 4(a) by relaxing the mutual repulsion between the interfering points. The PP in Fig. 4(b) mimics the interference in Fig. 4(a) on the test receiver because both have similar interference exclusion regions and same number of interferers. Similarly, the aggregate interference generated from a PPP can provide accurate approximation of the interference generated from a repulsive point process if the parameters of the approximating PPP are carefully chosen.

Although validations for the PPP approximation of the interference generated from different repulsive point processes as well as interference generated using empirical BSs locations (which intrinsically exhibit repulsion) are available in the literature [37]–[39], [62]–[64], [87], [89], [182]–[190]. A closer look into the reasons of such accuracy is given in the sequel.

A. Using PPP for Approximating Interference in Repulsive Point Processes.

This section discusses some examples where the PPP is used to approximate the aggregate interference generated from repulsive point processes. The Matérn Hard Core Point Processes (MHCPP) represents an important class of repulsive point processes that has been extensively used in the literature to model wireless networks [62]–[64], [87], [89], [182]–[188].[14] The MHCPP models random spatial patterns of points that are prohibited to coexist with inter-separation distances less than a predefined repulsive distance δ. The

---

[12]Slivnyak-Mecke theorem for the homogenous PPP states that the reduced Palm distribution is equal to the original distribution [175].
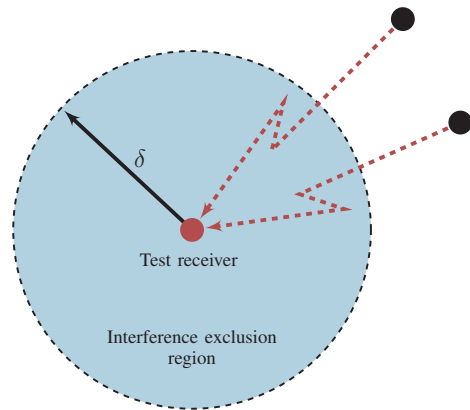
[13]A stochastic PP can be repulsive, attractive, or neutral [168].

[14]The MHCPP comes in three different forms denoted as type-I, type-II, and type-III [191]. The discussion is focused on type-II due to its tractability and applicability to wireless communications [185].
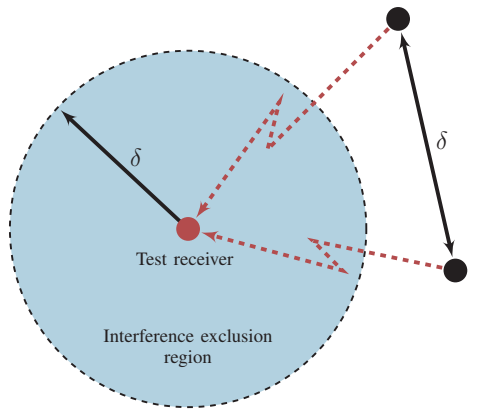
(a) The interference from spatially correlated interferers

(b) the interference from an equi-dense spatially non-correlated interferers

Fig. 4. Simple example for two networks that would generate the same interference at the test receiver. Relaxing the repulsion between the interfering sources will not affect the interference.

Fig. 5. Illustration for the distance dependent mutual interactions between points in MHCPP type-II.

MHCPP is constructed from a PPP, with constant intensity λ, via dependent thinning such that all points retained in the MHCPP satisfy the mutual repulsion of at least δ. The repulsive nature of the MHCPP makes it a suitable candidate to model CSMA ad hoc networks [182]–[188] as well as macro BSs in cellular networks [62]–[64], [87], [89]. However, the PGFL for MHCPP does not exist, which motivates the PPP approximation for the generated aggregate interference. The studies in [62]–[64], [87], [89], [182]–[188] shows that the PPP approximation gives fairly accurate estimate for the interference associated with the MHCPP if the intensity of the approximating PPP and the interference exclusion region around the test receiver are carefully chosen.

To understand the reason for the accurate PPP approximation, we need to look into the mutual spatial correlations between the MHCPP p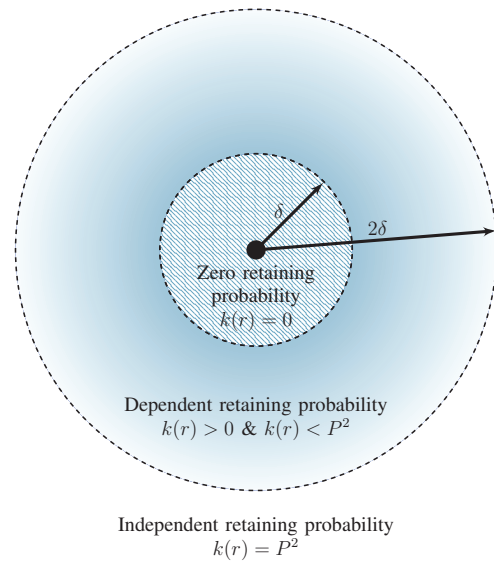oints as a function of their separation distances. Let P be the probability that a point in the parent PPP is retained in the MHCPP and $k(r)$ be the joint probability that two points in the parent PPP separated by distance r are retained together in the MHCPP. Expressions for P and $k(r)$ are given in [192], [175, Section 5.4] and a visual illustration for $k(r)$ as a function of distance is shown in Fig 5. As shown in the figure, mutual spatial correlation between the test receiver, which is assumed to be a point of the MHCPP, and the interfering sources, which are the rest of points in the MHCPP, is confined to the radial distance ranging from δ to 2δ. While the correlation within the distance ranging from 0 to δ can be exactly captured via the interference exclusion region by setting $r_0 = \delta$, the points outside 2δ are seen by the test receiver as a PPP with intensity $P\lambda$ due to the independent retaining probability (cf. Fig.5 and [192]). Consequently, the PPP approximation is accurate because the approximation is mainly confined to the region δ to 2δ, in which the points are assumed to be independently retained with the test receiver (i.e., $k(r)$ is approximated by P^2 for $\delta < r < 2\delta$).

Another elegant technique that relies on the PPP to estimate interference-dependent performance metrics (e.g., outage probability) within repulsive point processes is the interference-to-signal-ratio ($\bar{\mathrm{ISR}}$) technique, where the bar over the S is to indicate that the intended signal is averaged over the fading [193]. The work in [193] shows that the repulsion between interfering sources leads to an approximately constant horizontal shift, denoted as deployment gain [38], for the signal-to-interference-ratio SIR CDF at the test receiver when compared to the PPP interference. Approximate analytical estimates for the deployment gain can be expressed in terms of the ratio between the average $\bar{\mathrm{ISR}}$ for the PPP and the average $\bar{\mathrm{ISR}}$ for the target point process. The results in [193] are quite useful to characterize the performance of a wide range of wireless networks that may inhibit different spatial

interactions amongst their nodes [46], [47], [61], [193].

We conclude the above discussion by emphasizing that the baseline PPP used for approximating the interference in repulsive PPs should be parameterized with two parameters, namely, the intensity $\lambda(x)$ and the interference boundaries, as shown in Fig. 6.[15] Usually, the interference outer boundary is considered infinite due to the large-scale nature of cellular networks and the negligible contribution from faraway BSs to the aggregate interference. Hence, as long as the PPP approximation is considered, the intensity $\lambda(x)$ and inner interference boundary should be carefully estimated. In each of the presented cases in Section VIII, we will highlight how to estimate the intensity and the interference exclusion region.

B. Interference Characterization

As discussed in the previous section, the PPP provides tractable and accurate approximate analysis for several types of intractable repulsive PPs. This section is focused on exact interference characterization in a Poisson field of interferers with interference exclusion of r_0 at the test location.

Let $z_k = h_k s_k$. Then, using the PGFL of a homogeneous PPP (see (90) in **Appendix I**) the CF of the aggregate interference in (7) can be written as in (8) shown on the top of the next page, where (a) follows from the PGFL of the PPP (cf. (90) in **Appendix A**) and that $z \stackrel{d}{=} z_k$; (b) follows from the RSS association (i.e., inner interference boundary is r_0) and substituting z with hs where $h \stackrel{d}{=} h_k$ and $s \stackrel{d}{=} s_k$; (c) follows from the circularly symmetric Gaussian distribution of h; and (d) is obtained by change of variables

$$y = \frac{|\boldsymbol{\omega}|^2 P |d_m|^2}{4 r_0^{\eta}},$$

integration by parts, and uniform symbol distribution. The steps from (a) to (d) in (8) are the SG common steps to derive the CF of the aggregate interference. Note that the CF in (8) is only valid for $\eta > 2$. Otherwise (i.e., $\eta \leq 2$), the instantaneous interference power ($|i_{\text{agg}}|^2$) is infinite almost surely [20]. Putting $r_0 = 0$ in (8), then

$$\varphi_{i_{\text{agg}}}(\boldsymbol{\omega})\big|_{r_0=0} = \exp\left\{ -\frac{\pi \lambda |\boldsymbol{\omega}|^{\frac{4}{\eta}} P^{\frac{2}{\eta}} \mathbb{E}\{|s|^{\frac{4}{\eta}}\} \Gamma\left(1 - \frac{2}{\eta}\right)}{2^{\frac{4}{\eta}}} \right\} \quad (9)$$

which is equivalent to [3, equation (9)] given for ad hoc network. From [3], it can be noted that with no exclusion region around the test receiver the aggregate interference (i_{agg}) has an α-stable distribution with infinite moments. The interference protection of r_0, provided by the basic cellular association, diminishes the interference distribution's heavy tail and results in finite interference moments. To study the moments of the interference, (8) is manipulated to express the CF of the aggregate interference in the following forms[16]

[15] Note that the intensity function $\lambda(x)$ is parameterized by the location x as the PPP is not necessarily homogeneous over the spatial domain.

[16] The expression in (10) is obtained from (8) using the power series expansion of the incomplete Gamma function $\gamma(s, x) = x^s \Gamma(s) e^{-x} \sum_{k=0}^{\infty} \frac{x^k}{\Gamma(s+k+1)}$ and some mathematical manipulations.
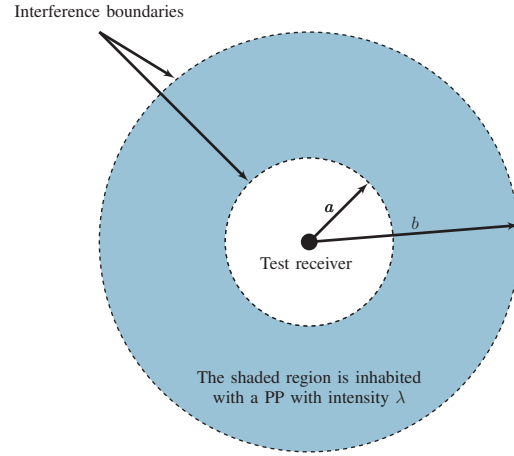

Interference boundaries

a

b

Test receiver

The shaded region is inhabited with a PP with intensity λ

Fig. 6. Intensity and boundaries are the main two parameters for the interference associated with PPP.

$$\varphi_{i_{\text{agg}}}(\boldsymbol{\omega})$$
$$= \exp\left\{ \frac{\pi \lambda}{M} \sum_m r_0^2 \left[1 - {}_1F_1\left(-\frac{2}{\eta}, 1 - \frac{2}{\eta}, -\frac{|\boldsymbol{\omega}|^2 P |d_m|^2}{4 r_0^{\eta}} \right) \right] \right\}$$
$$= \exp\left\{ 2\pi \lambda r_0^2 \sum_{k=1}^{\infty} \frac{(-1)^k |\boldsymbol{\omega}|^{2k} \mathbb{E}\{|s|^{2k}\}}{(\eta k - 2) k!} \left(\frac{P}{4 r_0^{\eta}} \right)^k \right\} \quad (10)$$

While the first form for $\varphi_{i_{\text{agg}}}(\boldsymbol{\omega})$ in (10) is compact and can be used to obtain the PDF of i_{agg} via numerical inversion (e.g., Gil-Pelaez inversion theorem), the second form for $\varphi_{i_{\text{agg}}}(\boldsymbol{\omega})$ in (10) is easy to differentiate and obtain the moments of the i_{agg}. For the sake of simple presentation, moments are obtained from cumulants using the Faà di Bruno's formula [194]. Following [195], the nth cumulant per dimension for the complex interference signal is defined as

$$\kappa_n = \kappa_n \left(\text{Re}\{i_{\text{agg}}\} \right)$$
$$= \kappa_n \left(\text{Im}\{i_{\text{agg}}\} \right)$$
$$= \left. \frac{\partial^n \ln\left(\varphi_{i_{\text{agg}}}(|\boldsymbol{\omega}|) \right)}{j^n \partial \omega_1^n} \right|_{|\boldsymbol{\omega}|=0}$$
$$= \left. \frac{\partial^n \ln\left(\varphi_{i_{\text{agg}}}(|\boldsymbol{\omega}|) \right)}{j^n \partial \omega_2^n} \right|_{|\boldsymbol{\omega}|=0} \quad (11)$$

Note that $\kappa_n \left(\text{Re}\{i_{\text{agg}}\} \right) = \kappa_n \left(\text{Im}\{i_{\text{agg}}\} \right)$. This is because the interference signal is circularly symmetric as the CF in (10) is a function of $|\boldsymbol{\omega}|$ only. For notational convenience, the real and imaginary parts are dropped and the per dimension n^{th} cumulant is denoted as $\kappa_n(i_{\text{agg}}) = \kappa_n(\text{Re}\{i_{\text{agg}}\}) = \kappa_n(\text{Im}\{i_{\text{agg}}\})$. Using this notation, the per dimension cumulants are

$$\kappa_n(i_{\text{agg}}) = \begin{cases} 0, & n \text{ is odd} \\ \frac{\pi \lambda P^{\frac{n}{2}} (n)_{n/2}}{2^{n-1}(\frac{\eta n}{2}-2)} r_0^{2-\frac{\eta n}{2}} \mathbb{E}\{|s|^n\}, & n \text{ is even} \end{cases} \quad (12)$$

From the cumulants, the per-dimension moments can be obtained using the Faà di Bruno's formula [194] as

$$\varphi_{i_{\mathrm{agg}}}(\boldsymbol{\omega}) = \mathbb{E}_{\tilde{\Psi}\backslash r_0}\left\{\prod_{r_k\in\tilde{\Psi}}\mathbb{E}_{z_k}\left\{\exp\left\{\jmath\sqrt{\frac{P}{r_k^{\eta}}}(\omega_1\mathrm{Re}\{z_k\}+\omega_2\mathrm{Im}\{z_k\})\right\}\right\}\right\}$$

$$\overset{(a)}{=}\exp\left\{-\int_{\mathbb{R}^2}\left(1-\mathbb{E}_z\left\{\exp\left\{\jmath\sqrt{\frac{P}{r^{\eta}}}(\omega_1\mathrm{Re}\{z\}+\omega_2\mathrm{Im}\{z\})\right\}\right\}\right)\Lambda(dr)\right\}$$

$$\overset{(b)}{=}\exp\left\{-2\pi\lambda\int_{r_0}^{\infty}\left(1-\mathbb{E}_s\mathbb{E}_h\left\{\exp\left\{\jmath\sqrt{\frac{P}{r^{\eta}}}(\omega_1\mathrm{Re}\{hs\}+\omega_2\mathrm{Im}\{hs\})\right\}\right\}\right)rdr\right\}$$

$$\overset{(c)}{=}\exp\left\{-2\pi\lambda\int_{r_0}^{\infty}\left(1-\mathbb{E}_s\left\{\exp\left\{-\frac{|\boldsymbol{\omega}|^2P|s|^2}{4r^{\eta}}\right\}\right\}\right)rdr\right\}$$

$$\overset{(d)}{=}\exp\left\{\frac{\pi\lambda}{M}\sum_m\left[r_0^2\left(1-e^{-\frac{|\boldsymbol{\omega}|^2P|d_m|^2}{4r_0^{\eta}}}\right)-\left(\frac{|\boldsymbol{\omega}|^2P|d_m|^2}{4}\right)^{\frac{2}{\eta}}\gamma\left(1-\frac{2}{\eta},\frac{|\boldsymbol{\omega}|^2P|d_m|^2}{4r_0^{\eta}}\right)\right]\right\} \tag{8}$$

$$\mathbb{E}\left\{\mathrm{Re}\left\{i_{\mathrm{agg}}\right\}^n\right\} = \begin{cases} 0, & n\text{ is odd} \\ \kappa_2, & n=2 \\ \kappa_4+3(\kappa_2)^2, & n=4 \\ \kappa_6+15\kappa_2(\kappa_4+(\kappa_2)^2), & n=6 \\ \vdots & \vdots \end{cases} \tag{13}$$

The expected aggregate interference power can be expressed as

$$\mathbb{E}\left\{|i_{\mathrm{agg}}|^2\right\} = \frac{2\pi\lambda Pr_0^{2-\eta}}{\eta-2}. \tag{14}$$

The per dimension kurtosis is

$$\mathrm{kur} \triangleq \frac{\kappa_4}{\kappa_2} = \frac{3(\eta-2)^2\mathbb{E}\left\{|s|^4\right\}}{4\pi\lambda(\eta-1)r_0^2}. \tag{15}$$

The CF in (10), the cumulants in (12), the expected interference power in (14), and the kurtosis in (15) show several interesting facts about the aggregate interference in the depicted system model:

- The interference is circularly symmetric complex random variable as shown in (8) and (10).
- Since the CFs in (8) and (10) does not match the CF of the Gaussian distribution, the interference is not Gaussian and the CLT does not apply.[17]
- The interference power is infinite at $\eta=2$ or $r_0=0$ as shown in (14).
- All interference cumulants, and hence moments, are finite for $\eta>2$ and $r_0>0$ as shown in (12) and (13).
- The interference distribution has a positive and finite kurtosis for $\eta>2$ and $r_0>0$ as shown in (15), which indicates that it has a heavier tail than the Gaussian distribution.

- The interference power decays with the interference exclusion radius at the rate of $r_0^{2-\eta}$ for $\eta>2$ as shown in (14).
- The interference power increases linearly with the intensity λ and power P as shown in (14).

C. Numerical Results for i_{agg}

This section provides numerical results to visualize some properties of the aggregate interference in PPP networks with interference exclusion region. Also, the numerical results show how the aggregate interference in PPP networks is related to the Gaussian and α-stable distributions. Fig. 7 shows the PDF of $\mathrm{Re}\{i_{\mathrm{agg}}\}$ against the α-stable and Gaussian PDFs with the same parameters.[18] The figure confirms the heavy (fast-decaying) tail of the i_{agg} when compared to the Gaussian (α-stable) PDF. With a smaller exclusion distance r_0, the interference i_{agg} approaches the α-stable distribution. As r_0 increases, i_{agg} approaches the Gaussian distribution.

To see the relation between i_{agg}, Gaussian, and α-stable distributions more clearly, the relative Kolmogorov–Smirnov (KS) distance is shown in Fig. 8.[19] Note that the KS statistic compares the entire CDFs and does not capture deviations in the tail probabilities. The figure shows that i_{agg} can neither be classified as Gaussian nor as α-stable distributed. However, as r_0 increases, i_{agg} deviates from the α-stable distribution and approaches the Gaussian distribution. Furthermore, as the intensity increases, the rate at which i_{agg} deviates from the α-stable distribution and approaches the Gaussian distribution increases. This is because increasing the intensity of interferers populates the interference boundary with more interferers, and hence, the aggregate interference summation in (2) has more terms with comparable variances. On the contrary, at low intensity the interference summation in (2) is dominated by a small number of interferers, which renders the limit theorem inapplicable.

---

[17]The CLT does not apply to the interference term in (2) due to the drastic effect of path-loss on the variance of each term, which leads to a summation of a large number of non i.i.d. random variables.

[18]Due to the circular symmetry of i_{agg} the PDF of $\mathrm{Im}\{i_{\mathrm{agg}}\}$ is similar to that of $\mathrm{Re}\{i_{\mathrm{agg}}\}$ given in Fig. 7.

[19]The KS distance measures the maximum distance between two CDFs $F_1(\cdot)$ and $F_2(\cdot)$, and is defined as $\mathrm{KS}=\sup_x|F_1(x)-F_2(x)|$.
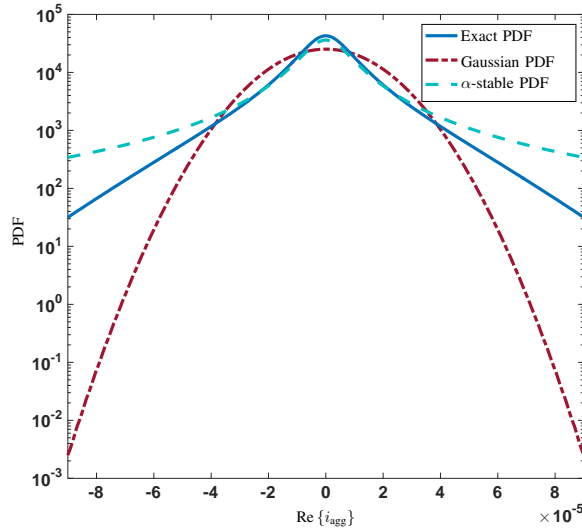
(a)
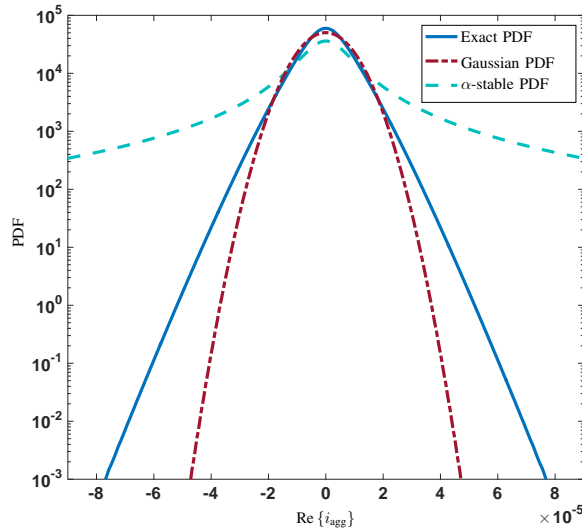
(b)

Fig. 7. The PDF of Re$\{i_{\text{agg}}\}$ obtained by numerically inverting (10) at $\lambda = 1$ BS/km^2, $P = 10$ W and $\eta = 4$ for a) $r_0 = 250$ m and b) $r_0 = 500$ m .

It is important to note that convergence of the aggregate interference PDF to the Gaussian PDF at large r_0 may be useful in simplifying interference-dependent performance analysis. However, such convergence mainly holds in a scenario with decoupled (i.e., independent) r_0 and λ, which is not typical in cellular networks.

D. Section Summary

This section motivates the use of PPP for network abstraction in order to obtain tractable results. The CF of the aggregate baseband interference is derived and its moments are obtained. It is shown that the aggregate interference in PPP networks with exclusion region around the receiver is neither Gaussian nor α-stable distributed. Then, some characteristics
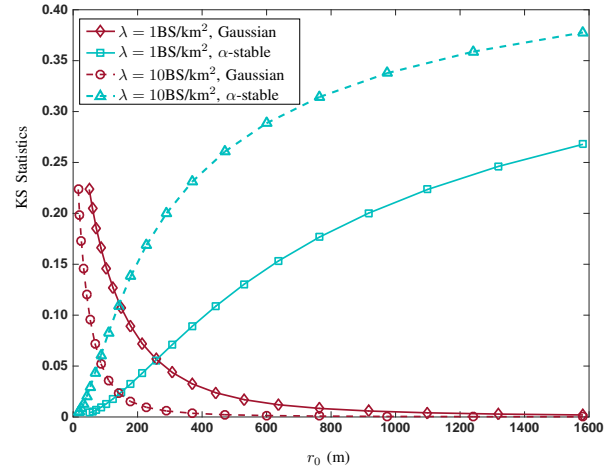

Fig. 8. The KS statistic for i_{agg} when compared to a Gaussian and α-stable distributions.

of the baseband aggregate interference are highlighted and discussed. The next section turns the focus to error probability performance.

V. EXACT ERROR PROBABILITY ANALYSIS

Error probability is a tangible measure used to fairly judge the performance of communication systems. Error probability captures fine system details (e.g., modulation scheme, receiver type, symbol constellation, etc.) and is considered the most revealing metric about the system behavior [196]–[198]. It includes bit error probability (BEP), symbol error probability (SEP), and pairwise error probability (PEP). In the context of wireless networks, error probability has mainly been studied and conducted for additive white Gaussian noise (AWGN) or Gaussian interference channels [198]. This section illustrates how to generalize the error probability analysis to the cellular networks domain. Without loss of generality, we focus on the SEP, denoted by $\mathcal{S}$, for coherent maximum likelihood detector with M-QAM modulation scheme given by [198, chapter 8],

$$\mathcal{S} = w_1 Q\left(\sqrt{\beta_1 \Upsilon}\right) + w_2 Q^2\left(\sqrt{\beta_2 \Upsilon}\right), \quad (16)$$

where , $w_1 = 4\frac{\sqrt{M}-1}{\sqrt{M}}$, $w_2 = -4\left(\frac{\sqrt{M}-1}{\sqrt{M}}\right)^2$, $\beta_1 = \beta_2 = \frac{3}{(M-1)}$ are modulation-dependent weighting factors, and Υ is the the signal-to-noise-ratio (SNR). It is worth noting that by changing the factors w_1, w_2, β_1, and β_2, the SEP and BEP can be calculated for different modulation schemes and constellation sizes as shown in Appendix II.

All parameters in the SEP expression in (16) are deterministic and the expression is derived based on the Gaussian distribution of the noise, in which the SNR Υ is the signal power divided by the variance of the Gaussian noise. As shown in the previous section, the aggregate interference in the depicted system model is not Gaussian, and hence, the cellular network does not maintain the same assumptions that

are used to derive (16). Therefore, (16) cannot be directly applied to calculate the SEP in cellular networks.

One elegant solution to apply (16) to study the error performance in the depicted large-scale cellular network is to represent the interference as a conditional Gaussian random variable [14], [40], [66]. Hence, treating interference as noise, (16) is legitimate to calculate the conditional error probability. Then, an averaging step is required to obtain the unconditional error probability. This is known in the literature by the *Equivalent-in-Distribution* (EiD) approach, as it relies on the equivalence in distribution between the interference and the sum of randomly scaled Gaussian random variables. The rest of this section is devoted to the exact error performance characterization via the EiD approach. We first show how to represent the interference as a conditional Gaussian random variable, then we exploit this representation to calculate the spatial average SEP (ASEP), denoted as $\overline{S}$, in cellular networks.

A. Conditional Gaussian Representation for Interference

The conditional Gaussian representation of the interference is obtained by exploiting the fact that matching CFs implies equivalent distributions. This idea originates in [14], where the authors use the decomposition property of stable random variables to represent the α-stable interference in ad hoc networks in terms of a randomly scaled Gaussian random variable. The idea of the Gaussian representation for the aggregate interference to conduct error probability analysis was then extended to cellular network in [40], where it was first denoted as the *EiD* approach. However, since the aggregate interference in cellular networks is not α-stable, the conditional Gaussian representation in [40] was obtained in terms of an infinite series of randomly scaled Gaussian random variables. This paper follows a slightly different approach than [40] and obtains the Gaussian representation of the aggregate interference in cellular networks via a single randomly scaled standardized complex Gaussian random variable. While the conditional Gaussian representation used in this paper leads to the same final result as in [40], it simplifies the notation and analysis.[20] The proposed conditional Gaussian representation of the aggregate interference in cellular networks is presented in the following lemma.

Lemma 1: Consider the baseband aggregate interference i_{eq} shown in (2) with the CF shown in (10), then

$$i_{eq} \overset{d}{=} \sqrt{\mathcal{B}}G, \qquad (17)$$

where $G \sim \mathcal{CN}(0, 1)$ is a standard complex Gaussian random variable and $\mathcal{B}$ is a positive real random scale independent of G and has the following LT

$$\mathcal{L}_{\mathcal{B}}(z) = \exp\left\{\sum_{k=1}^{\infty} a_k z^k\right\}, \qquad (18)$$

where

$$a_k = (-1)^k 2\pi\lambda r_0^2 \left(\frac{P}{r_o^\eta}\right)^k \frac{\mathbb{E}\left\{|s|^{2k}\right\}}{(\eta k - 2)k!}.$$

Proof: The EiD approach is obtained by matching the characteristic functions of i_{eq} and $\sqrt{\mathcal{B}}G$ with an equality sign. The CF of i_{eq} is given in (10). The CF of $\sqrt{\mathcal{B}}G$ is obtained as

$$\varphi_{\sqrt{\mathcal{B}}G}(\boldsymbol{\omega}) \triangleq \mathbb{E}_{\mathcal{B},G}\left\{\exp\left\{\jmath\omega_1\text{Re}\left\{\sqrt{\mathcal{B}}G\right\} + \jmath\omega_2\text{Im}\left\{\sqrt{\mathcal{B}}G\right\}\right\}\right\}$$
$$= \mathbb{E}_{\mathcal{B}}\left\{\exp\left\{-\frac{\mathcal{B}|\boldsymbol{\omega}|^2}{4}\right\}\right\}$$
$$= \mathcal{L}_{\mathcal{B}}\left(\frac{\mathcal{B}|\boldsymbol{\omega}|^2}{4}\right), \qquad (19)$$

where the second equality follows from the standard complex Gaussian distribution of G and the independence between $\mathcal{B}$ and G. The equality $\varphi_{i_{eq}}(\boldsymbol{\omega}) = \varphi_{\sqrt{\mathcal{B}}G}(\boldsymbol{\omega})$ is satisfied if and only if the LT of $\mathcal{B}$ is selected as in (18), which leads to the desired EiD between i_{eq} and $\sqrt{\mathcal{B}}G$. $\qquad\square$

Exploiting the Gaussian representation for i_{agg}, the baseband received signal at the test UE can be rewritten as

$$y_0 \overset{d}{=} \sqrt{P}s_0h_0r_0^{-\frac{\eta}{2}} + \underbrace{\sqrt{\mathcal{B}}G}_{i_{eq}} + n,$$
$$= \sqrt{P}s_0h_0r_0^{-\frac{\eta}{2}} + \tilde{n}, \qquad (20)$$

where $\tilde{n} = i_{eq} + n$. Since G is a standard circularly symmetric Gaussian random variable, conditioning on $\mathcal{B}$, the lumped interference plus noise term $\tilde{n}$ is a circularly symmetric complex Gaussian random variable with variance $(\mathcal{B} + N_0)$. This representation is the key that merges SG analysis and the rich literature available on AWGN based performance analysis. Since $\tilde{n}$ in (20) is conditionally Gaussian, the SEP expression in (16) as well as other SNR based expressions for AWGN channels can be applied to conduct error performance in cellular networks, as shown in the next subsection.

B. ASEP with Non-Gaussian Cellular Network Interference

Let $\Xi = h_0 \cup \mathcal{B}$. Then following [198], the conditional average SINR, when treating interference as noise, is given by

$$\bar{\Upsilon}(r_0|\Xi) = \frac{\mathbb{E}_{s_0}\{\mathbb{E}\{y_0\}\mathbb{E}\{y_0^*\}\}}{\mathbb{E}\{y_0y_0^*\} - \mathbb{E}\{y_0\}\mathbb{E}\{y_0^*\}}$$
$$= \frac{P|h_0|^2\mathbb{E}\{|s_0|^2\}r_0^{-\eta}}{\mathcal{B} + N_0}$$
$$= \frac{P|h_0|^2r_0^{-\eta}}{\mathcal{B} + N_0}. \qquad (21)$$

Conditioning on Ξ, the SINR in (21) is similar to the legacy SNR in (16) but with increased noise variance of $\mathcal{B} + N_0$. Hence, rewriting (16), the ASEP with interference can be expressed as

---

[20]The proposed Gaussian representation also alleviates a minor deficiency of negative variances that appears in the intermediate steps (see [40, Eq. (5)]) of the EiD approach presented in [40]. Nevertheless, we confirm the validity of the results presented in [40], in which the negative variances cancels out in final error probability expression.

$$\bar{\mathcal{S}}(r_0|\Xi) = w_1 Q\left(\sqrt{\beta_1 \bar{\Upsilon}(r_0|\Xi)}\right) + w_2 Q^2\left(\sqrt{\beta_2 \bar{\Upsilon}(r_0|\Xi)}\right). \quad (22)$$

Let $\zeta = \frac{\mathcal{B}}{P r_0^{-\eta}}$. Then, the unconditional ASEP can be obtained by an additional averaging step as in (24) shown on the top of next page. Note that (24) is unconditional with respect to the elements of Ξ, but it is still conditional on r_0. The equality (a) in (24) follows from the lemma proposed in [199], which is also given in **Appendix III**.[21] The LT of ζ can be directly obtained from (18) as

$$
\begin{aligned}
&\mathcal{L}_\zeta(z) \\
&= \exp\left\{ 2\pi\lambda r_0^2 \sum_{k=1}^{\infty} \frac{(-1)^k z^k \mathbb{E}\left\{|s|^{2k}\right\}}{(\eta k - 2)k!} \right\}, \\
&= \exp\left\{ \pi\lambda r_0^2 \left(1 - \frac{1}{M} \sum_{m=1}^{M} {}_1F_1\left(-\frac{2}{\eta}; 1 - \frac{2}{\eta}; -z|d_m|^2\right)\right) \right\}.
\end{aligned}
$$
(23)

Substituting the LT of ζ into (24), the ASEP is characterized via Theorem 2 given at the top of the next page.

C. Section Summary

This section explains the steps for exact ASEP calculation via the EiD approach. The EiD approach is used to express the aggregate interference as a conditional Gaussian random variable, which makes the available AWGN based ASEP expressions legitimate to conduct error probability analysis for cellular networks. The EiD approach proceeds as follows:

1) **Interference Characterization:** Use SG to obtain the characteristic function of the aggregate complex interference signal i_{agg} in the form of (10).
2) **Gaussian Representation:** Express the interference via a randomly scaled standardized complex Gaussian random variable $i_{eq} = \sqrt{\mathcal{B}}G$ and calculate the coefficients $a_k, \forall k$ of the LT of $\mathcal{B}$ in (18) to match the CF in (10), which ensures equivalence in distribution.
3) **Conditional Analysis:** Condition on $\mathcal{B}$ and obtain the conditional ASEP via AWGN based expression with the conditional SINR as in (22).
4) **Averaging:** Decondition over the non-Gaussian random variables to obtain ASEP as in (24).

Although exact, the ASEP expression given in (25) is quite complex and computationally intensive due to the integral over an exponential function with a sum of hypergeometric functions in the exponent. Furthermore, the complexity of the EiD approach increases for advanced system models with Nakagami-m fading and/or multiple antennas [101]. Therefore, approximations and more abstract analysis are conducted in the literature to seek simpler and more insightful performance expressions, as will be shown in the next sections.

---

[21]Let Y be a Gamma random variable, [199] shows that the expectation in the form of $\mathbb{E}\left\{Q\left(\sqrt{Y/X}\right)\right\}$ and $\mathbb{E}\left\{Q^2\left(\sqrt{Y/X}\right)\right\}$ can be computed in terms of the LT of X. In our case, $Y = |h_0|^2$ is an exponential distribution which is a special case of gamma distribution.

VI. Gaussian Signaling Approximation

The complexity of the EiD approach is due to the fact that it statistically accounts for the transmitted symbol by each interfering source. Abstracting such information highly facilitates the analysis. The idea of Gaussian signaling approximation can be found in [200], [201] for BPSK and QPSK symbols for a single interfering link. The Gaussian signaling approximation idea was extended to M-QAM symbols in downlink and uplink cellular networks in [41]. Instead of assuming that each interfering transmitter maps its data using a distinct constellation, it can be assumed that each transmitter randomly selects its transmitted symbol from a Gaussian constellation with unit variance.[22] As shown in this section, the Gaussian signaling approximation directly achieves the conditional Gaussian representation for aggregate interference. Hence, the ASEP expressions for AWGN channels are legitimate to be used. Furthermore, the Gaussian signaling approximation circumvents the complexity of the EiD approach without compromising the modeling accuracy.

This section first validates the Gaussian signaling approximation and shows that it does not change the distribution of the aggregate interference. The section also shows the effect of the Gaussian signaling approximation on the interference moments as well as on the approximate error probability performance.

A. Validation

The Gaussian signaling approximation does not approximate the aggregate interference by a Gaussian random variable. Instead, it assumes that each interferer chooses a symbol s from complex Gaussian distribution such that $\mathbb{E}\{|s|^2\} = 1$. Then, the transmitted symbol by each interfering BS x_i experiences the location-dependent path-loss $r_i^{-\eta/2}$ and encounters independent random fading h_i before reaching the test receiver. The main idea in the Gaussian signaling approximation is to abstract the information carried in the aggregate interference to facilitate error probability analysis. The baseband signal representation in the Gaussian signaling approximation is similar to (2), except that s_k has a complex Gaussian distribution with a unit variance. Following the same steps as in (8) and (10), the CF of the approximate aggregate interference $\hat{i}_{\text{agg}}$ is obtained as

$$
\begin{aligned}
&\varphi_{\hat{i}_{\text{agg}}}(\boldsymbol{\omega}) \\
&= \exp\left\{ -\frac{\pi\lambda P|\boldsymbol{\omega}|^2}{2(\eta-2)r_0^{\eta-2}} {}_2F_1\left(1, 1 - \frac{2}{\eta}; 2 - \frac{2}{\eta}; -\frac{P|\boldsymbol{\omega}|^2}{4r_0^\eta}\right) \right\} \\
&= \exp\left\{ 2\pi\lambda r_0^2 \sum_{k=1}^{\infty} \frac{(-1)^k |\boldsymbol{\omega}|^{2k}}{\eta k - 2} \left(\frac{P}{4r_0^\eta}\right)^k \right\}
\end{aligned}
$$
(26)

Equation (26) shows that the aggregate interference signal is circularly symmetric, which implies that the distribution and moments of the real and imaginary parts of $\hat{i}_{\text{agg}}$ are identical.

---

[22]Note that if the interfering BSs are coded and operating close to capacity, then the signal transmitted by each is Gaussian [15]. However, we are interested in the Gaussian signaling as an approximation for the interfering symbols which are drawn from the distinct constellation **S**.

$$\bar{\mathcal{S}}(r_0) = w_1 \mathbb{E}\left\{ Q\left(\sqrt{\beta_1 \bar{\Upsilon}(r_0|\Xi)}\right)\right\} + w_2 \mathbb{E}\left\{ Q^2\left(\sqrt{\beta_2 \bar{\Upsilon}(r_0|\Xi)}\right)\right\}$$

$$= w_1 \mathbb{E}\left\{ Q\left(\sqrt{\frac{|h_0|^2}{\frac{N_0 r_0^\eta}{P\beta_1} + \frac{\zeta}{\beta_1}}}\right)\right\} + w_2 \mathbb{E}\left\{ Q^2\left(\sqrt{\frac{|h_0|^2}{\frac{N_0 r_0^\eta}{P\beta_2} + \frac{\zeta}{\beta_2}}}\right)\right\}$$

$$\overset{(a)}{=} \sum_{c=1}^2 w_c \left(\frac{1}{2c} - \frac{c}{\sqrt{\pi}} \int_0^\infty \frac{Q(\sqrt{2z}\mathbb{1}_{\{c=2\}})}{\sqrt{z}} \exp\left\{-z\left(1 + \frac{2N_0 r_0^\eta}{P\beta_c}\right)\right\} \mathcal{L}_\zeta\left(\frac{2z}{\beta_c}\right) dz\right). \tag{24}$$

Theorem 2: Consider cellular network modeled via a PPP with intensity λ in Rayleigh fading environment with universal frequency reuse and no intra-cell interference. Then, the downlink ASEP with M-QAM modulated signals for a user located at the distance r_0 away from his serving BS, is expressed as

$$\bar{\mathcal{S}}(r_0) = \sum_{c=1}^2 w_c \left(\frac{1}{2c} - \frac{c}{\sqrt{\pi}} \int_0^\infty \frac{Q(\sqrt{2z}\mathbb{1}_{c=2})}{\sqrt{z}} \exp\left\{-z\left(1 + \frac{2N_0 r_0^\eta}{P\beta_c}\right) - \pi\lambda r_0^2 \left(\frac{1}{M}\sum_{m=1}^M {}_1F_1\left(-\frac{2}{\eta}; 1 - \frac{2}{\eta}; -\frac{2z|d_m|^2}{\beta_c}\right) - 1\right)\right\} dz\right). \tag{25}$$

Following the same notation in (12), the real and imaginary parts are dropped, and the per dimension n^{th} cumulant is denoted as $\kappa_n\left(\hat{i}_{\text{agg}}\right) = \kappa_n\left(\text{Re}\{\hat{i}_{\text{agg}}\}\right) = \kappa_n\left(\text{Im}\{\hat{i}_{\text{agg}}\}\right)$. Using this notation, the cumulants of $\hat{i}_{\text{agg}}$ are given by

$$\kappa_n(\hat{i}_{\text{agg}}) = \begin{cases} 0, & n \text{ is odd} \\ \frac{\pi\lambda P^{\frac{n}{2}} n!}{2^{n-1}(\frac{\eta n}{2} - 2)} r_0^{2 - \frac{n\eta}{2}}, & n \text{ is even.} \end{cases} \tag{27}$$

Further, the moments can be obtained as in (13) and the aggregate interference power can be expressed as

$$\mathbb{E}\left\{\left|\hat{i}_{\text{agg}}\right|^2\right\} = \frac{2\pi\lambda P r_0^{2-\eta}}{\eta - 2}. \tag{28}$$

Comparing (26) with (10), it can be observed that both CFs have equivalent forms but with slightly different coefficients.[23] Also, comparing (28) with (14), it can be observed that both $\hat{i}_{\text{agg}}$ and i_{agg} have equivalent powers. Hence, all the characteristics described for i_{agg} in Section IV hold for $\hat{i}_{\text{agg}}$. Fig. 9 compares the PDF of $\hat{i}_{\text{agg}}$ with the PDF of i_{agg}. The figure shows that the PDF $\hat{i}_{\text{agg}}$ matches that of i_{agg} with high accuracy. Comparing (12) with (27), it can be observed that the difference between i_{agg} and $\hat{i}_{\text{agg}}$ exists only in even cumulants with orders higher than two, as highlighted in Table II. Our numerical results in Section VI-B (e.g., see Fig. 10) show that such differences have minor effect on the SINR-dependent performance metrics such as the ASEP.

B. Approximate Error Probability Analysis

The Gaussian signaling assumption highly simplifies the analysis steps and reduces the computational complexity for the error probability expression. To visualize the conditional Gaussian representation of the aggregate interference, the

TABLE II
PER-DIMENSION CUMULANT COMPARISON FOR $\eta = 4$.

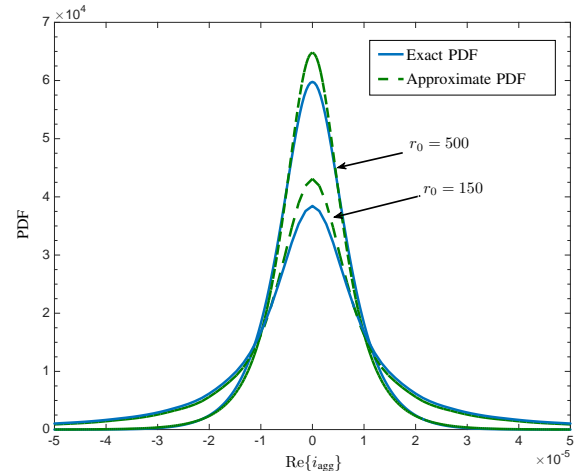| Cumulants	4-QAM	16-QAM	Gaussian
κ_2	$\frac{\pi\lambda P}{2r_0^2}$	$\frac{\pi\lambda P}{2r_0^2}$	$\frac{\pi\lambda P}{2r_0^2}$
κ_4	$\frac{0.25\pi\lambda P^2}{r_0^6}$	$\frac{0.33\pi\lambda P^2}{r_0^6}$	$\frac{0.5\pi\lambda P^2}{r_0^6}$
κ_6	$\frac{0.375\pi\lambda P^3}{r_0^{10}}$	$\frac{0.735\pi\lambda P^3}{r_0^{10}}$	$\frac{2.25\pi\lambda P^3}{r_0^{10}}$
kur $\triangleq \frac{\kappa_4}{\kappa_2^2}$	$\frac{1}{\pi\lambda r_0^2}$	$\frac{1.32}{\pi\lambda r_0^2}$	$\frac{2}{\pi\lambda r_0^2}$

Fig. 9. The PDF of i_{agg} obtained by numerically inverting (10) and (26) at $\lambda = 1$ BS/km^2, $P = 10$ W and $\eta = 4$ for $r_0 = 150$ m and $r_0 = 500$ m .

---

[23]Note that (26) is related to (10) by substituting for $\mathbb{E}\{|s|^{2n}\} = n!$, which is the case when $s \sim \mathcal{C}(0, 1)$.

baseband signal at the test receiver given in (2) is rewritten with the Gaussian signaling approximation as

$$y_0 \approx \sqrt{P}s_0 h_0 r_0^{-\frac{\eta}{2}} + \underbrace{\sum_{r_k \in \tilde{\Psi} \setminus r_0} \sqrt{P}\tilde{s}_k h_k r_k^{-\frac{\eta}{2}}}_{\hat{i}_{\mathrm{agg}}} + n, \qquad (29)$$

where s_0 is the useful symbol that is randomly drawn form the constellation $\mathbf{S}$, and $\tilde{s}_k$ is an interfering symbol randomly drawn from a Gaussian constellation. Due to the Gaussian signaling assumption, conditioning on the network geometry (i.e., $r_k \in \tilde{\Psi}$, $\forall k$) and channel gains (i.e., h_0 and h_k, $\forall k$), the received signal y_0 is conditional Gaussian. Particularly, the conditional aggregate interference $\hat{i}_{\mathrm{agg}} \sim \mathcal{CN}(0, \mathcal{I}_{\mathrm{agg}})$ with $\mathcal{I}_{\mathrm{agg}} = \sum_{r_k \in \tilde{\Psi} \setminus r_0} P|h_k|^2 r_k^{-\eta}$. Hence, approximating the interfering symbols with Gaussian signals directly achieves the conditional Gaussian representation of the aggregate interference and renders the AWGN based ASEP expressions legitimate to be used. The SINR in (21), with the Gaussian signaling approximation, can be expressed as

$$\begin{aligned}\bar{\Upsilon}(r_0|h_0, \mathcal{I}_{\mathrm{agg}}) &= \frac{\mathbb{E}_{s_0}\{\mathbb{E}\{y_0\}\mathbb{E}\{y_0^*\}\}}{\mathbb{E}\{y_0 y_0^*\} - \mathbb{E}\{y_0\}\mathbb{E}\{y_0^*\}} \\ &= \frac{P|h_0|^2 \mathbb{E}\{|s_0|^2\}r_0^{-\eta}}{\sum_{r_k \in \tilde{\Psi} \setminus r_0} P|h_k|^2 r_k^{-\eta} + N_0} \\ &= \frac{P|h_0|^2 r_0^{-\eta}}{\mathcal{I}_{\mathrm{agg}} + N_0}.\end{aligned} \qquad (30)$$

Similar to the EiD case in (24), the unconditional ASEP in the Gaussian signaling approximation is expressed as in (31).[24] Similar to (24), equality (a) in (31) follows from the lemma proposed in [199], which is given in **Appendix III**. The ASEP in (31) requires the LT of $\mathcal{I}_{\mathrm{agg}}$, which is characterized in the following lemma.

Lemma 2: The LT of the aggregate inter-cell interference in one-tier cellular network modeled via a PPP with constant transmit power P, intensity λ, Rayleigh fading, and nearest BS association is given by

$$\mathcal{L}_{\mathcal{I}_{\mathrm{agg}}}(z) = \exp\left\{-\frac{2\pi\lambda z P r_0^{2-\eta}}{\eta - 2}\,_2F_1\left(1, 1 - \frac{2}{\eta}; 2 - \frac{2}{\eta}; -\frac{zP}{r_0^\eta}\right)\right\}. \qquad (32)$$

Proof: See **Appendix IV**. □

Remark 1: A special case of Lemma 2 is for $\eta = 4$, which is a common practical value for path-loss exponent in outdoor urban environments. In this case, unlike the EiD approach ASEP in (25), the LT of $\mathcal{I}_{\mathrm{agg}}$ expression reduces from the Gauss hypergeometric function $_2F_1(.,.;.;.)$ to the elementary inverse tangent function as

$$\mathcal{L}_{\mathcal{I}_{\mathrm{agg}}}(z) \stackrel{(\eta=4)}{=} \exp\left\{-\pi\lambda\sqrt{zP}\arctan\left(\frac{\sqrt{zP}}{r_0^2}\right)\right\}. \qquad (33)$$

Accordingly, the ASEP for the downlink communication links is provided by Theorem 3, given at the top of the next page, which is obtained by plugging (32) and (33) into (31). The ASEP expression in (34) contains a single integration over

[24] The ASEP is unconditional because the expectation in (31) w.r.t. $\mathcal{I}_{\mathrm{agg}}$ and h_0, however, the expressions is still for a given r_0.
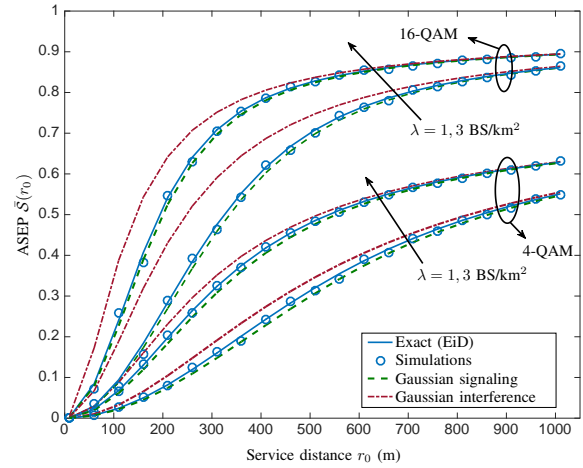

Fig. 10. ASEP vs the service distance r_0 for 4-QAM and 16-QAM constellations and $\eta = 4$.

an exponential function with a single Gauss hypergeometric function in the exponent for any constellation size M. This considerably reduces the computational complexity required to evaluate the ASEP when compared to (25), which contains a constellation size dependent summation of confluent hypergeometric functions in the exponent. Furthermore, the Gauss hypergeometric function in (34) reduces to the elementary $\arctan(\cdot)$ in (35) for $\eta = 4$, which further reduces the computational complexity required to evaluate the ASEP.

Fig. 10 compares the ASEP obtained via the EiD approach (25), the Gaussian signaling approximation (34), the Gaussian aggregate interference with variance in (14), and Monte Carlo simulation for different BS intensities. The figure shows that the Gaussian interference approximation provides an upper bound for the ASEP, in which the bound accuracy depends on the constellation size, interference exclusion radius r_0, and BS intensity λ. Hence, assuming Gaussian aggregate interference may result in a loose estimate for the ASEP. On the other hand, the close match between the Gaussian signaling approximation and the exact analysis validates the Gaussian signaling approximation and shows that it accurately captures the ASEP. The figure also shows that the gap between the Gaussian signaling approximation and the exact analysis diminishes for higher constellations as discussed in Section VI-A (cf. Table II). Last but not least, the figure manifests the prominent effect of the interferers' intensity and interference boundary on the network performance, which are the two main parameters that characterize the interfering PPP as discussed in Section IV.

Fig. 10 also shows that the Gaussian interference approximation becomes tighter at higher intensity and larger interference exclusion distance, which occurs only in a decoupled r_0 and λ scenario. As discussed in Section III-B, r_0 and λ are coupled through (88) in cellular systems. Consequently, the Gaussian interference approximation will result in a loose ASEP estimate in the context of cellular networks.

$$\bar{\mathcal{S}}(r_0) = w_1 \mathbb{E}\left\{ Q\left(\sqrt{\beta_1 \bar{\Upsilon}(r_0|h_0, \mathcal{I}_{\text{agg}})} \right) \right\} + w_2 \mathbb{E}\left\{ Q^2\left(\sqrt{\beta_2 \bar{\Upsilon}(r_0|h_0, \mathcal{I}_{\text{agg}})} \right) \right\}$$

$$\overset{(a)}{=} \sum_{c=1}^{2} w_c \left(\frac{1}{2c} - \frac{c}{\sqrt{\pi}} \int_0^\infty \frac{Q(\sqrt{2z}\mathbb{1}_{\{c=2\}})}{\sqrt{z}} \exp\left\{ -z\left(1 + \frac{2N_0 r_0^\eta}{P\beta_c} \right) \right\} \mathcal{L}_{\mathcal{I}_{\text{agg}}}\left(\frac{2z r_0^\eta}{P\beta_c} \right) \mathrm{d}z \right) \tag{31}$$

Theorem 3: Consider cellular network modeled via a PPP with intensity λ in a Rayleigh fading environment with universal frequency reuse and no intra-cell interference. Then, the downlink ASEP, with M-QAM modulated useful signal and Gaussian interfering signals, for a user located at the distance r_0 away from his serving BS, is expressed as

$$\bar{\mathcal{S}}(r_0) = \sum_{c=1}^{2} w_c \left(\frac{1}{2c} - \frac{c}{\sqrt{\pi}} \int_0^\infty \frac{Q(\sqrt{2z}\mathbb{1}_{c=2})}{\sqrt{z}} \exp\left\{ -z\left(1 + \frac{2N_0 r_0^\eta}{P\beta_c} \right) - \frac{4\pi\lambda z r_0^2}{\beta_c(\eta-2)} {}_2F_1\left(1, 1 - \frac{2}{\eta}; 2 - \frac{2}{\eta}; -\frac{2z}{\beta_c} \right) \right\} \mathrm{d}z \right) \tag{34}$$

$$\overset{\eta=4}{=} \sum_{c=1}^{2} w_c \left(\frac{1}{2c} - \frac{c}{\sqrt{\pi}} \int_0^\infty \frac{Q(\sqrt{2z}\mathbb{1}_{c=2})}{\sqrt{z}} \exp\left\{ -z\left(1 + \frac{2N_0 r_0^4}{P\beta_c} \right) - \pi\lambda r_0^2 \sqrt{\frac{2z}{\beta_c}} \arctan\left(\sqrt{\frac{2z}{\beta_c}} \right) \right\} \mathrm{d}z \right). \tag{35}$$

C. Section Summary

This section motivates the Gaussian signaling approximation for interfering symbols to facilitate the ASEP analysis in cellular networks. We first validate the Gaussian signaling approximation by showing that it preserves the distribution of the aggregate interference signal and provides matching odd and second cumulants, as well as matching interference power for any constellation size. Difference between the exact interference and the interference based on Gaussian signaling only exists for even cumulants with orders higher than two.

The effect of the Gaussian signaling approximation on the ASEP expression can be observed by comparing (25) with (34). One can see that the Gaussian signaling approximation reduces the sum of M hypergeometric functions in the exponent for the constellation size M, to a single hypergeometric function exponent. This highly reduces the computational complexity to evaluate the ASEP without sacrificing the ASEP accuracy. Furthermore, for the special case of $\eta = 4$ the expression for the ASEP reduces to a computationaly simple inverse tangent function, which is not the case for the exact EiD.

The Gaussian signaling approximation also facilitates the derivation steps to obtain the ASEP. Particularly, the analysis requires the LT of the aggregate interference power ($\mathcal{I}_{\text{agg}}$), which is easier to derive and simpler to evaluate than the CF of the baseband aggregate interference required by the EiD approach. Furthermore, the LT of $\mathcal{I}_{\text{agg}}$ can be used to compute several other performance metrics. As will be shown in the next section, the Gaussian signaling unifies the computation of the ASEP, outage probability, and ergodic capacity.

VII. Outage Probability and Ergodic Rate

Error probability expressions provide a tangible characterization of network performance and capture the effect of several system factors. However, as shown in the Section V and Section VI, the ASEP expressions are involved, even with the Gaussian signaling approximation. Consequently, several researchers resort to more conceptual analysis relying on quantities such as outage probability and ergodic rate. Such

abstracted analysis sacrifices the model depth for simplicity leading to simple expressions that characterize high-level network behavior, highlight general tradeoffs, and facilitate network design.

A. Definition of Outage Probability and Ergodic Rate

For AWGN channels, the maximum rate per unit bandwidth (BW) that can be reliably transmitted, also known as the spectral efficiency, is defined by Shannon's capacity expression given by [178]:

$$C = \log(1 + \text{SNR}) \tag{36}$$

where the SNR in (36) is the instantaneous signal-to-noise ratio. Shannon's capacity formula assumes that the additive noise is Gaussian and that coded trasmission is employed with codewords drawn from a Gaussian codebook. If this expression is extended to include interference, then the interference signal should also be Gaussian. This is the case when the interfering BSs also employ Gaussian codebooks, which is equivalent to the use of Gaussian signaling in Section VI. Similar to (29), the baseband aggregate interference signal is Gaussian conditioned on the PPP, which validates lumping the aggregate interference with the noise term. That is, treating interference as noise, the instantaneous SINR (Υ) in (30) is analogous to the SNR in (36) for Gaussian interfering symbols $\tilde{s}_k$ when conditioning on the interfering BSs locations $r_k \in \tilde{\Psi} \setminus r_0$. Therefore, (36) is legitimate to compute the link capacity in the depicted large-scale cellular network. However, an additional averaging step over Υ is required, which leads to the following ergodic rate per unit BW definition

$$\mathcal{C} = \mathbb{E}\{\ln(1 + \Upsilon)\}$$
$$\overset{(a)}{=} \int_0^\infty \mathbb{P}\{\ln(1 + \Upsilon) > t\}\,\mathrm{d}t$$
$$= \int_0^\infty \mathbb{P}\{\Upsilon > e^t - 1\}\,\mathrm{d}t$$
$$\overset{(b)}{=} \int_0^\infty \frac{(1 - F_\Upsilon(y))}{y + 1}\,\mathrm{d}y \tag{37}$$

where (a) follows because $\log(1 + \Upsilon)$ is a positive random variable, (b) is obtained by change of variables, and $F_\Upsilon(\cdot)$ is the CDF of the SINR (Υ). Shannon's capacity expression in (36) can also be used to define the outage probability. Let R be the transmission rate. Then, the outage probability is defined as the probability that the transmission rate is greater than the channel capacity, given by

$$
\begin{aligned}
\mathcal{O}(R) &= \mathbb{P}\left\{\log\left(1 + \Upsilon\right) < R\right\} \\
&= \mathbb{P}\left\{\Upsilon < e^R - 1\right\}
\end{aligned}
\tag{38}
$$

where Υ denotes the instantaneous SINR (i.e., as in (30) without conditioning on either h_0 or $\mathcal{I}_{\text{agg}}$). Hence, the rate outage probability depends on interference and/or fading.

Outage probability can also be defined based on the bit error probability (BEP) [202]. In this case, the outage probability is defined as the probability that the BER exceeds a certain threshold ϵ. Exploiting the Gaussian signaling approximation, the BER based outage probability is given by

$$
\begin{aligned}
\mathcal{O}(\epsilon) &= \mathbb{P}\left\{\text{BER} > \epsilon\right\} \\
&\approx \mathbb{P}\left\{w_1 Q(\beta_1 \Upsilon) > \epsilon\right\} \\
&= \mathbb{P}\left\{\Upsilon < \frac{1}{\beta_1} Q^{-1}\left(\frac{\epsilon}{w_1}\right)\right\}
\end{aligned}
\tag{39}
$$

where (39) ignores the $Q^2(\cdot)$ term of (16).

Most of the SG literature does not discriminate between the two forms of outage probabilities in (38) and (39). Instead, the outage probability is treated in an abstract manner with a unified abstracted threshold value (T), as follows:

$$
\begin{aligned}
\mathcal{O}(T) &= \mathbb{P}\left\{\Upsilon < T\right\} \\
&= F_\Upsilon(T)
\end{aligned}
\tag{40}
$$

Equations (37) and (40) show that the SINR CDF is sufficient to characterize both the outage probability and ergodic rate. The SINR CDF is obtained in the next section.

B. SINR CDF

The SINR CDF is given by

$$
\begin{aligned}
F_\Upsilon(T) &= \mathbb{P}\left\{\Upsilon < T\right\} \\
&= \mathbb{P}\left\{\frac{P|h_0|^2 r_0^{-\eta}}{\mathcal{I}_{\text{agg}} + N_0} < T\right\} \\
&\overset{(a)}{=} \mathbb{E}_{\mathcal{I}_{\text{agg}}}\left\{F_{|h_0|^2}\left(\frac{T(\mathcal{I}_{\text{agg}} + N_0)}{P r_0^{-\eta}}\right)\right\} \\
&\overset{(b)}{=} 1 - e^{\frac{-T N_0 r_0^\eta}{P}} \mathcal{L}_{\mathcal{I}_{\text{agg}}}\left(\frac{T r_0^\eta}{P}\right)
\end{aligned}
\tag{41}
$$

where (b) follows from the exponential distribution of $|h_0|^2$ and the definition of the LT. It is worth highlighting that (a) in (41) cannot be always computed. This is because the PDF of the interference power $\mathcal{I}_{\text{agg}}$ is not available in closed-form, except for very special cases which are not of practical

interest for cellular networks [20], [166]–[169].[25] However, the exponential distribution of $|h_0|^2$ enables expressing the CDF of the SINR in terms of the LT of $\mathcal{I}_{\text{agg}}$. The LT of $\mathcal{I}_{\text{agg}}$ is given in Lemma 2, which is used to characterize the ergodic rate and outage probability in the following theorem.

Theorem 4: Consider a cellular network modeled via a PPP with intensity λ in a Rayleigh fading environment with universal frequency reuse and no intra-cell interference. The downlink ergodic rate for a user located at the distance r_0 away from his serving BS can expressed as

$$
\begin{aligned}
&\mathcal{C}(r_0) \\
&= \int_0^\infty \frac{\exp\left\{-\frac{t N_0 r_0^\eta}{P} - \frac{2\pi\lambda t r_0^2}{\eta-2}{}_2F_1\left(1, 1-\frac{2}{\eta}; 2-\frac{2}{\eta}; -t\right)\right\}}{t+1} \mathrm{d}t \\
&\overset{\eta=4}{=} \int_0^\infty \frac{\exp\left\{-\frac{t N_0 r_0^4}{P} - \pi\lambda\sqrt{t} r_0^2 \arctan\left(\sqrt{t}\right)\right\}}{t+1} \mathrm{d}t,
\end{aligned}
\tag{42}
$$

and outage probability for a user located at the distance r_0 away from his serving BS can expressed as

$$
\begin{aligned}
&\mathcal{O}(r_0, T) \\
&= 1 - \exp\left\{-\frac{T N_0 r_0^\eta}{P} - \frac{2\pi\lambda T r_0^2}{\eta-2}{}_2F_1\left(1, 1-\frac{2}{\eta}; 2-\frac{2}{\eta}; -T\right)\right\} \\
&\overset{\eta=4}{=} 1 - \exp\left\{-\frac{T N_0 r_0^4}{P} - \pi\lambda\sqrt{T} r_0^2 \arctan\left(\sqrt{T}\right)\right\}.
\end{aligned}
\tag{43}
$$

Proof: The theorem is obtained by plugging the LT expressions (32) and (33) into (41) to get the SINR CDF, which is then used to compute the ergodic rate and the outage probability as in (37) and (40), respectively. $\square$

Fig. 11 validates (42) and (43) against Monte Carlo simulation. Similar to Fig. 10, the results in Fig. 11 show the effect of interferers' intensity and interference boundary on the network performance. Hence, the outage probability and ergodic rate can be used as an alternative and simpler way to characterize the network behavior.[26] However, such simplicity comes at the expense of abstractions that may hide the true network behavior. As shown in Fig. 11(b) the network performance is a function of the abstracted SINR threshold value, which gives a constellation oblivious performance measure. On the other hand, Fig. 10 clearly shows the true ASEP for each modulation scheme.

C. Section Summary

The outage probability and ergodic rate can be defined in terms of the SINR CDF. This may lead to closed-form simple expressions which help to characterize the network performance. It is worth mentioning that the Gaussian signaling approximation provides a unified approach to characterize SINR related performance metrics. Thas is, the outage probability,

---

[25]The interference distribution can be only found for special cases of PPP networks in which the interference boundaries (cf. Fig. 6) go from 0 to ∞ [11], which is not suitable to model cellular networks that enforce an inner interference boundary of r_0.
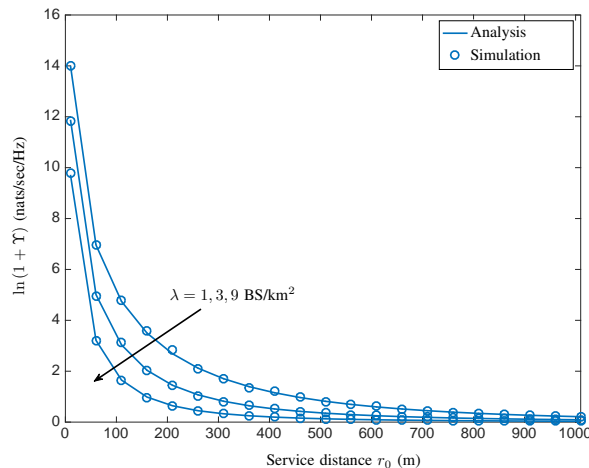
[26]The outage and ergodic rate expressions (43) and (42) are simpler than the ASEP expressions (25) and (34)
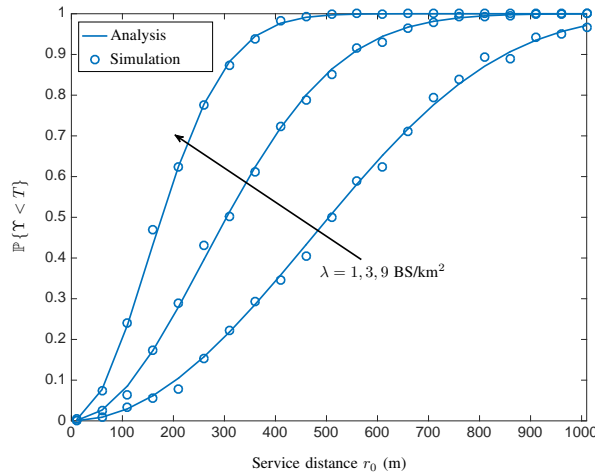
(a) Outage probability for different BS intensities at $T = 1$ and $\eta = 4$.
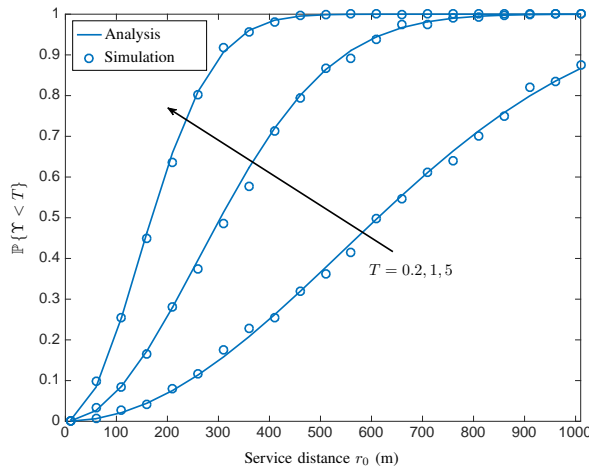
(b) Outage probability for different SINR thresholds at $\lambda = 3$ BS/km^2 and $\eta = 4$.

(c) Ergodic rate per unit BW for different BS intensities at $\eta = 4$.

Fig. 11. Outage probability and ergodic rate vs the service distance r_0.

ergodic capacity, and also ASEP under Gaussian signaling approximation require obtaining the LT of the aggregate interference power as in (32). Then, these quantities are computed by plugging the LT of $\mathcal{I}_{\text{agg}}$ into (43), (42), and (34), respectively.

VIII. ADVANCED NETWORK MODELS

This section is focused on the analysis based on Gaussian signaling approximation. Hence, we only show $\mathcal{L}_{\mathcal{I}_{\text{agg}}}(\cdot)$ and we neither calculate $\{\sigma_q^2\}_{q=1}^{\infty}$ nor $\mathcal{L}_\zeta(\cdot)$. As shown in the previous sections, the ASEP, outage probability, and ergodic rate expressions are all functions of the LT of the aggregate interference. Therefore, throughout this section, we show how the LT of the aggregate interference changes for each network model. For the sake of concise presentation, the LT of the aggregate interference plus noise is defined as

$$
\begin{aligned}
\mathcal{L}_{\mathcal{I}+N}(z) &= \mathbb{E}\left\{\exp\{-z(\mathcal{I}_{\text{agg}} + N_0)\}\right\} \\
&= \exp\{-zN_0\}\mathbb{E}\left\{\exp\{-z\mathcal{I}_{\text{agg}}\}\right\} \\
&= \exp\{-zN_0\}\mathcal{L}_{\mathcal{I}_{\text{agg}}}(z)
\end{aligned}
\tag{44}
$$

where the second equality in (44) follows because the noise variance N_0 is a constant. Using the LT of the aggregate interference plus noise, the ASEP in (31) and the outage probability in (41) can be rewritten as

$$
\bar{S}(r_0) = \sum_{c=1}^{2} w_c \left(\frac{1}{c} - \frac{c}{\sqrt{\pi}} \int_0^\infty \frac{e^{-z} Q(\sqrt{2z}\mathbb{1}_{\{c=2\}})}{\sqrt{z}} \mathcal{L}_{\mathcal{I}+N}\left(\frac{2zr_0^\eta}{P\beta_c} \right) dz \right)
\tag{45}
$$

and

$$
F_\Upsilon(T) = 1 - \mathcal{L}_{\mathcal{I}+N}\left(\frac{Tr_0^\eta}{P} \right).
\tag{46}
$$

Hence, we focus on the LT of the aggregate interference plus noise evaluated at $\frac{ar_0^\eta}{P}$, where $a = \beta_c^{-1}$ for ASEP evaluation, and $a = T$ for outage probability and ergodic rate evaluation.

As discussed in Section III-B, as far as the PPP is considered, the interference exclusion region (denoted hereafter as $r_{\mathcal{I}}$) and the intensity λ are the two main parameters that discriminate the LT of the interference in different network models [203]. Note that the baseline network model used in the previous sections assumed a single-tier cellular network with no interference coordination. Hence, the interference exclusion distance is equivalent to the service distance (i.e., $r_{\mathcal{I}} = r_0$) and the interferers' transmit powers are equivalent. However, this might not always be the case. In the next sections, we discriminate between the interference exclusion distance $r_{\mathcal{I}}$ and the service distance r_0. We will also discriminate between the interferers' transmit power $P_{\mathcal{I}}$ and the serving BS transmit power P_0. Then, using (33) and (44), the LT of the interference plus noise can be generalized to (47) shown on the top of the next page. Then, substituting $z = \frac{ar_0^4}{P_0}$ into (47), the expressions (48), (49), and (50) are obtained. While (47) represents the general case, (49) and (50) give simplified versions of the LT of interference in the special

$$\mathcal{L}_{\mathcal{I}+N}(a, \lambda, r_0, r_{\mathcal{I}}) = \exp\left\{-zN_0 - \frac{2\pi\lambda z P_{\mathcal{I}} r_{\mathcal{I}}^{2-\eta}}{\eta-2} \,_2F_1\left(1, 1-\frac{2}{\eta}; 2-\frac{2}{\eta}; -\frac{zP_{\mathcal{I}}}{r_{\mathcal{I}}^{\eta}}\right)\right\}. \tag{47}$$

$$\mathcal{L}_{\mathcal{I}+N}(a, \lambda, r_0, r_{\mathcal{I}}) = \exp\left\{-\frac{aN_0 r_0^{\eta}}{P_0} - \frac{2\pi\lambda a r_0^{\eta} P_{\mathcal{I}} r_{\mathcal{I}}^{2-\eta}}{P_0(\eta-2)} \,_2F_1\left(1, 1-\frac{2}{\eta}; 2-\frac{2}{\eta}; -\frac{ar_0^{\eta}P_{\mathcal{I}}}{P_0 r_{\mathcal{I}}^{\eta}}\right)\right\} \tag{48}$$

$$\stackrel{N_0=0}{=} \exp\left\{-\frac{2\pi\lambda a r_0^{\eta} P_{\mathcal{I}} r_{\mathcal{I}}^{2-\eta}}{P_0(\eta-2)} \,_2F_1\left(1, 1-\frac{2}{\eta}; 2-\frac{2}{\eta}; -\frac{ar_0^{\eta}P_{\mathcal{I}}}{P_0 r_{\mathcal{I}}^{\eta}}\right)\right\} \tag{49}$$

$$\stackrel{\eta=4}{=} \exp\left\{-\pi\lambda\sqrt{\frac{aP_{\mathcal{I}}}{P_0}}r_0^2 \arctan\left(\left(\frac{r_0}{r_{\mathcal{I}}}\right)^2 \sqrt{\frac{aP_{\mathcal{I}}}{P_0}}\right)\right\}. \tag{50}$$

cases of interference-limited scenario (i.e., $N_o \to 0$) with general path-loss exponent and interference limited scenario with $\eta = 4$ respectively. The simplifying scenarios given by (49) and (50) are important as they lead to simple and insightful expressions for the ASEP, outage probability, and ergodic rate. Equations (48), (49), and (50) give the LT of interference plus noise that serves as a basis for the analysis in the sequel.

A. Random Link Distance r_0

As discussed in Section III-B, random link distance is an intrinsic property of the baseline cellular network model. Due to the employed association rule, the link distance distribution is characterized by the BS intensity as shown in (88). Hence, averaging over the link distance distribution is required to obtain the spatially average performance. Note that the random service distance r_0 does not change any of the previous analysis and only adds an additional averaging step over r_0. This is because both the aggregate interference and the useful signal power in (30) depend on the service distance r_0. Hence, we first obtain the conditional (i.e., on r_0) LT of the aggregate interference as in (32) and then conduct the averaging step over r_0. Note that the service distance r_0 in (45) and (46) appears within the LT of $\mathcal{I}+N$ only, and hence, the averaging step over r_0 only affects the LT expression. That is, the ASEP and the SINR CDF are given in terms of the spatially averaged LT (i.e., after averaging over r_0). It is worth mentioning that in the subsequent case studies, random service distance is always considered and the spatially averaged LT is calculated.

By averaging over r_0, the LT is given by (51), (52), and (53), for the general case, interference limited scenario, and interference limited scenario with $\eta = 4$, respectively. The ASEP and the SINR CDF are obtained by substituting (51) (or equivalently (52) or (53) depending on the noise variance and η) into (45) with $a = \beta^{-1}$ and into (46) with $a = T$, respectively. It can be observed from (51) that the LT of the interference plus noise cannot be obtained in closed-from for general system parameters. Four approaches to approximate (51) in closed-form are presented in [204]. Alternatively, the simplifying cases shown in (52) and (53), obtained by ignoring noise and setting $\eta = 4$ can also be used to find closed-from expressions for the LT. Such simplicity reveals several insights into the performance of the cellular network. For instance, under a interference-limited operation, (52) and (53)

along with (45) show that the ASEP depends only on the modulation scheme parameters w_c and β_c. Consequently, the outage probability is only a function of the threshold value T and the ergodic rate is constant as shown from (52) and (53) along with (46).

Figs. 12 and 13 validate (51) via Monte Carlo simulation for outage probability (i.e., $a = T$) and ASEP (i.e., $a = \beta^{-1}$), respectively. At interference limited regime, Fig. 12 shows that the ASEP is independent of both the noise variance and BS intensity and only depends on the constellation size. However, the BS intensity controls the turning point at which the performance becomes sensitive to the noise variance. This is because the intended signal power and interference power scales together at the same rate with the BS intensity as shown in [37]. Fig. 12 also shows that the Gaussian interference upper bound is always loose at the interference limited regime and the bound gap is independent from the BS intensity. This is due to the coupling between r_0 and λ imposed by the association rule in cellular networks, which is conceptually different form the results shown in Fig. 10 for the decoupled r_0 and λ scenario. Increasing the noise variance, the Gaussian noise dominates the SINR, which diminishes the effect of the Gaussian interference approximation on the ASEP accuracy. Last but not least, Fig. 12 confirms the accuracy of the Gaussian signaling approximation for estimating the ASEP in all cases.

Fig. 13 plots (46) using the LTs in (51) and (53) to emphasize the negligible effect of noise on outage probability for full-loaded network scenario (i.e., all BSs are interfering with the test user). On the other hand, noise may have prominent effect on the outage probability at low network load as discussed in the next section.

B. Load-Aware Modeling

The previous sections assume universal frequency reuse for a single channel and $\lambda_u \gg \lambda$, such that each BS always has a user to serve. However, in practice, multiple channels are available per BS and some channels may be left idle (i.e., some BSs might not be fully loaded). The results in [79], [87], [89], [90], [128] show that assuming fully-loaded network leads to a pessimistic performance evaluation. Hence, load-awareness is essential for practical performance assessment. In a load-aware model, the SINR-dependent performance analysis is conducted for each channel and the per-channel

$$\mathcal{L}_{\mathcal{I}+N}(a, \lambda) = \int_0^\infty 2\pi\lambda r e^{-\pi\lambda r^2} \mathcal{L}_{\mathcal{I}+N}(a, \lambda, r, r)\, dr$$

$$= \int_0^\infty 2\pi\lambda r \exp\left\{ -\frac{aN_0 r^\eta}{P_0} - \frac{2\pi\lambda a r^2}{(\eta-2)} {}_2F_1\left(1, 1 - \frac{2}{\eta}; 2 - \frac{2}{\eta}; -a\right) - \pi\lambda r^2 \right\} dr \qquad (51)$$

$$\overset{N_0=0}{=} \int_0^\infty 2\pi\lambda r \exp\left\{ -\frac{2\pi\lambda a r^2}{(\eta-2)} {}_2F_1\left(1, 1 - \frac{2}{\eta}; 2 - \frac{2}{\eta}; -a\right) - \pi\lambda r^2 \right\} dr$$

$$= \frac{1}{\frac{2a}{(\eta-2)} {}_2F_1\left(1, 1 - \frac{2}{\eta}; 2 - \frac{2}{\eta}; -a\right) + 1} \qquad (52)$$

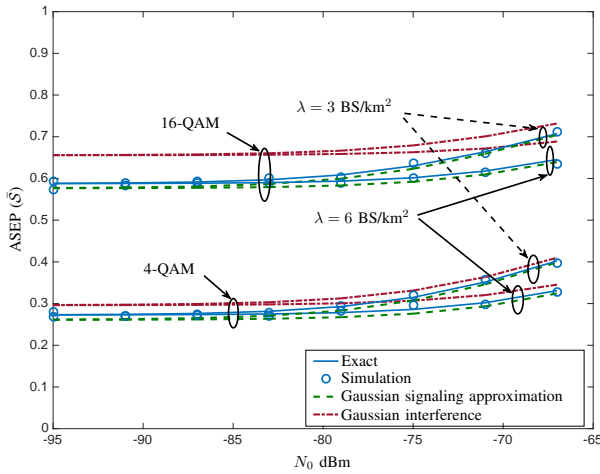$$\overset{\eta=4}{=} \frac{1}{\sqrt{a}\arctan(\sqrt{a}) + 1} \qquad (53)$$

Fig. 12. ASEP vs the noise variance N_0 for $\eta = 4$ and different BSs activity factor (p). As p decreases less interferers are active in the network, and hence, the aggregate interference decreases and the noise becomes more prominent.

access probability in each BS is taken into account. Let $\mathbf{N}$ be the set of available channels, and without loss of generality, it is assumed that each BS randomly and uniformly selects a channel to assign for each user request.[27] Following [128], the probability that a generic channel is used by a randomly selected BS is given by

$$p = \mathbb{P}\{n_j \in \mathbf{N} \text{ is used}\}$$
$$= \sum_{k=1}^{N} \mathbb{P}\{\mathcal{U} = k\} \frac{\binom{N-1}{k-1}}{\binom{N}{k}} + \mathbb{P}\{\mathcal{U} > N\}$$
$$= 1 - \sum_{k=1}^{N} \mathbb{P}\{\mathcal{U} = k\} \frac{N-k}{N} \qquad (54)$$

where N is the number of channels in $\mathbf{N}$, $\mathbb{P}\{\mathcal{U} = k\}$ is the probability mass function (PMF) of the number of users served

[27]If each BS assigns the channels based on the channel quality index (CQI), to exploit multi-user diversity, and all the channel gains are identically distributed, then, for a generic user at a generic time instant, each of the channels has the same probability to be the channel with the highest CQI.

by each BS, which is given by (92) when the UEs follow a PPP independent from the BS locations.

From the SINR perspective, the analysis in the load-aware case is similar to Section VIII-A. However, the intensity of interfering BSs is thinned by the per channel access probability p. Hence, the intensity λ in the LT expression in Lemma 2 is replaced by the intensity of active BSs per channel $p\lambda$. On the other hand, the distribution of the service distance r_0 remains the same (i.e., with intensity λ) as each user has the opportunity to be associated with the complete set of BSs. However, a user only receives interference from the subset of active BSs (i.e., the BSs using the same channel). Also, the interference exclusion region is equal to the service distance (i.e., $r_{\mathcal{I}} = r_0$). Hence, the LT of the aggregate interference is given by (55), (56), and (57) shown on the top of the next page.

Equations (55), (56), and (57) show that load-awareness can be easily incorporated into the analysis via the activity factor p. The effect of the activity factor p is shown in Fig. 13. The figure also shows the accuracy of (56), and (57) for different values of p.

C. Uplink Transmission

The previous sections focused on the downlink transmissions, where the BSs are the transmitters and the UEs are the receivers. This section studies the uplink case, where the BSs and UEs roles are reversed. In addition to the baseline model, it is assumed that the UEs constitute an independent PPP with intensity $\lambda_u \gg \lambda$ such that each BS always has a user to serve on each channel. The user association per-channel is shown in Fig. 14, in which there is only one active uplink user per cell due to the employed universal frequency reuse with no intra-cell interference. As shown in the figure, user association does not impose spatial interference protection (i.e., r_0) as in the downlink scenario. That is, an interfering uplink user may be much closer to a BS than its indented user. Hence, per-UE power control is a crucial assumption in the uplink case to limit inter-cell interference, as shown in [65], [69]. For simplicity, full channel inversion power control is assumed, in which each user inverts path-loss to maintain a constant average power level of ρ at the serving BS. That is, if the UE

$$\mathcal{L}_{\mathcal{I}+N}(a,\lambda) = \int_0^\infty 2\pi\lambda r e^{-\pi\lambda r^2} \mathcal{L}_{\mathcal{I}+N}(a,p\lambda,r,r)\,\mathrm{d}r$$

$$= \int_0^\infty 2\pi\lambda r \exp\left\{ -\frac{aN_0 r^\eta}{P_0} - \frac{2\pi p\lambda a r^2}{(\eta-2)} {}_2F_1\left(1, 1-\frac{2}{\eta}; 2-\frac{2}{\eta}; -a\right) - \pi\lambda r^2 \right\}\mathrm{d}r \tag{55}$$

$$\overset{N_0=0}{=} \int_0^\infty 2\pi\lambda r \exp\left\{ -\frac{2\pi p\lambda a r^2}{(\eta-2)} {}_2F_1\left(1, 1-\frac{2}{\eta}; 2-\frac{2}{\eta}; -a\right) - \pi\lambda r^2 \right\}\mathrm{d}r$$

$$= \frac{1}{p\left(\frac{2a}{(\eta-2)} {}_2F_1\left(1, 1-\frac{2}{\eta}; 2-\frac{2}{\eta}; -a\right) + \frac{1}{p}\right)} \tag{56}$$

$$\overset{\eta=4}{=} \frac{1}{p\left(\sqrt{a}\arctan(\sqrt{a}) + \frac{1}{p}\right)}. \tag{57}$$
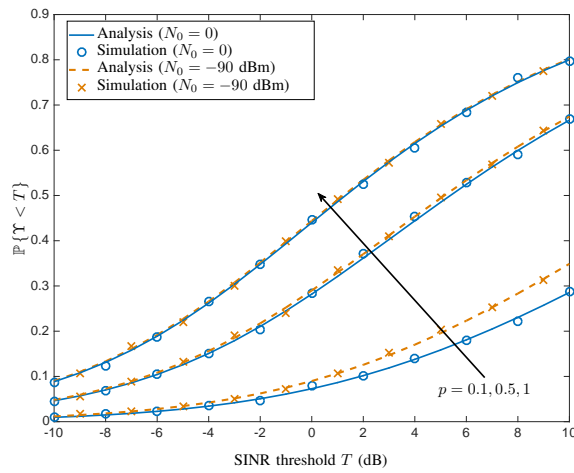

Fig. 13. Outage probability vs the SINR threshold for $\lambda = 3$ BS/km^2, $\eta = 4$, and different BSs activity factor (p). As p decreases less interferers are active in the network, and hence, the aggregate interference decreases and the noise becomes more prominent.

is located r meters away from its serving BS, the transmit power should be ρr^η to have the average signal power level of ρ at the serving BS.

Without loss of generality, the test BS is assumed to be located at the origin. Although the complete set of UEs constitutes a PPP with intensity λ_u, the subset of UEs scheduled on one channel (i.e., interfering UEs) do not constitute a PPP. Due to the unique channel assignment per BS, only one active user per channel is allowed in each Voronoi cell as shown in Fig. 14. This brings correlation, in the form of repulsion, among the set of interfering users. To facilitate the analysis and maintain tractability, the set of interfering UEs is approximated with a PPP. Since there is only one active user in each Voronoi cell, the intensity of the approximate PPP is selected to be equal to the BS intensity λ. In this case, the PGFL of the PPP is legitimate to be used as an approximation to obtain the LT of the aggregate interference in uplink cellular networks. The accuracy of this approximation is verified in Fig. 15 as well as in [65], [66], [69]–[71], [74], [75].

Although the set of interfering UEs is approximated via a PPP, the LT in (47) cannot be directly used. This is because the employed power control imposes a constant received signal power ρ at the test BS. As a result, the SINR expression for the uplink is different from that of the downlink case presented in (30). The SINR at the test BS in the uplink case is given by

$$\Upsilon_u = \frac{\rho h}{N_0 + \mathcal{I}}. \tag{58}$$

Due to the limited power of the UEs, the noise cannot be ignored from (58) as both ρ and $\mathcal{I}$ may be comparable to the noise power.[28] Hence, the noise is prominent to the uplink operation as opposed to the interference-limited downlink scenario. Replacing z by $\frac{a}{\rho}$ in (47), the starting LT for the uplink case is given by (59) and (60), which are no longer functions of r_0. Nevertheless, the distributions of the service distances r_0 affect the interference power $P_{\mathcal{I}_i}$ from each UE due to the employed power control. In other words, the transmission power of each UE is a function of the random distance to his serving BS. The distances between the interfering UEs and their serving BSs can be fairly approximated via i.i.d. random variables with the distribution in (88) [65], [67], [70], which leads to i.i.d. approximation for the transmission powers for all interfering UEs. Consequently, (59) should be averaged over the distribution of $P_{\mathcal{I}}$. Note that the averaging over $P_{\mathcal{I}}$ is done within the PGFL expression (i.e., within the exponential function of (59) and (60)) because $P_{\mathcal{I}}$ takes a different realization for each interfering user.

The interference boundary for the uplink is given by

$$r_{\mathcal{I}} > \left(\frac{P_{\mathcal{I}}}{\rho}\right)^{\frac{1}{\eta}}, \tag{61}$$

which is calculated from the employed power control and the association rule. That is, each user adjusts its power to maintain the power level ρ at his nearest BS. Hence, the interfering power from any other user at the test BS satisfies $P_{\mathcal{I}} r_{\mathcal{I}}^{-\eta} < \rho$, which leads to the boundary in (61). Substituting $r_{\mathcal{I}}$ back into (59) and (60), then

[28]Note that the moments of the aggregate interference $\mathcal{I}$ depend on ρ.

$$\mathcal{L}_{\mathcal{I}+N}(a,\lambda,r_\mathcal{I}) = \exp\left\{-\frac{aN_0}{\rho} - \frac{2\pi\lambda}{\eta-2}\mathbb{E}_{P_\mathcal{I}}\left\{\frac{aP_\mathcal{I}}{\rho r_\mathcal{I}^{\eta-2}}\,{}_2F_1\left(1,1-\frac{2}{\eta};2-\frac{2}{\eta};-\frac{aP_\mathcal{I}}{\rho r_\mathcal{I}^\eta}\right)\right\}\right\} \tag{59}$$

$$\overset{\eta=4}{=} \exp\left\{-\frac{aN_0}{\rho} - \pi\lambda\mathbb{E}_{P_\mathcal{I}}\left\{\sqrt{\frac{aP_\mathcal{I}}{\rho}}\arctan\left(\left(\frac{1}{r_\mathcal{I}}\right)^2\sqrt{\frac{aP_\mathcal{I}}{\rho}}\right)\right\}\right\} \tag{60}$$
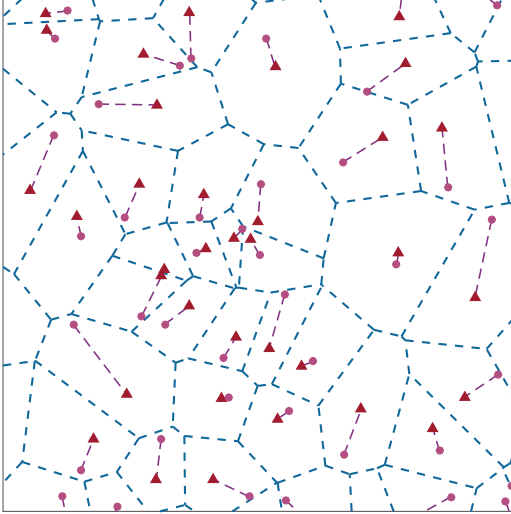

Fig. 14. Single-tier cellular network in which the triangles indicate the MBSs, the circles indicate UEs.

Fig. 15. Outage probability vs SINR threshold for the uplink at $\lambda = 3$ BS/km^2, $\eta = 4$, and different values of ρ for different values of SNR $= \frac{\rho}{N_0}$.

$$\mathcal{L}_{\mathcal{I}_{\text{agg}}}(a,\lambda)$$
$$= \exp\left\{-\frac{aN_0}{\rho} - \frac{2\pi\lambda a}{(\eta-2)\rho^{\frac{2}{\eta}}}\mathbb{E}\left\{P_\mathcal{I}^{\frac{2}{\eta}}\right\}{}_2F_1\left(1,1-\frac{2}{\eta};2-\frac{2}{\eta};-a\right)\right\} \tag{62}$$

$$\overset{\eta=4}{=} \exp\left\{-\frac{aN_0}{\rho} - \pi\lambda\mathbb{E}\left\{\sqrt{P_\mathcal{I}}\right\}\sqrt{\frac{a}{\rho}}\arctan\left(\sqrt{a}\right)\right\}. \tag{63}$$

The power $P_\mathcal{I} = \rho r^\eta$, where r has the PDF in (88). Hence, $\mathbb{E}\left\{P_\mathcal{I}^{\frac{2}{\eta}}\right\} = \frac{\rho^{\frac{2}{\eta}}}{\pi\lambda}$. Substituting $\mathbb{E}\left\{P_\mathcal{I}^{\frac{2}{\eta}}\right\}$ into (62) and (63), then

$$\mathcal{L}_{\mathcal{I}_{\text{agg}}}(a,\lambda)$$
$$= \exp\left\{-\frac{aN_0}{\rho} - \frac{2a}{(\eta-2)}{}_2F_1\left(1,1-\frac{2}{\eta};2-\frac{2}{\eta};-a\right)\right\} \tag{64}$$

$$\overset{\eta=4}{=} \exp\left\{-\frac{aN_0}{\rho} - \sqrt{a}\arctan\left(\sqrt{a}\right)\right\}, \tag{65}$$

which is independent of the BS intensity λ. Furthermore, the interference terms in (64) and (65) are independent from the power control threshold ρ. Hence, the SNR $= \frac{\rho}{N_0}$ may have a prominent effect on the outage probability. More advanced uplink system models with fractional power control and/or maximum transmit power constraint can be found in [65]–[67], [69]–[71].

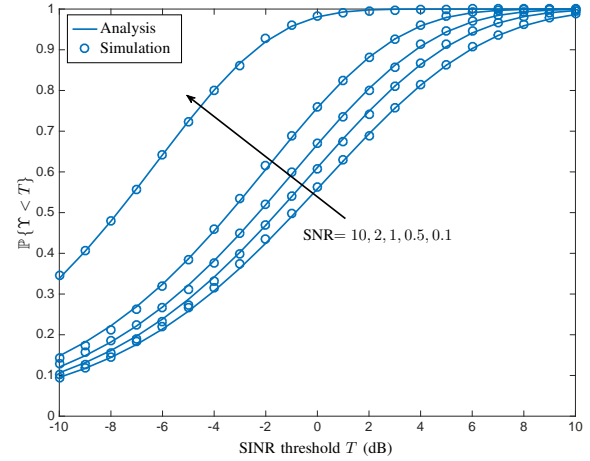Fig. 15 verifies (64) and the PPP approximation for the interfering UEs. Comparing Fig. 15 with Fig. 13, it can

be observed that the uplink transmission has higher outage probability than the downlink counterpart. This is because uplink transmissions have limited transmission power and the association does not impose geographical interference protection for the uplink transmission. Hence, the uplink is more vulnerable to outages than the downlink. Comparison between uplink and downlink performance can be found in [65].

D. Multi-tier Cellular Networks

Cellular networks are no longer single-tiered networks with operator's deployed macro BSs (MBSs) only. Because MBSs are expensive to deploy in terms of time and money, cellular operators tend to expand their networks via small BSs (SBSs) to cope with the increasing capacity demand and device populations. Some of these SBSs can be deployed directly by users in a plug and play fashion such as the LTE femto access points, which are installed by users at their homes and/or workplaces. Therefore, modern cellular networks are multi-tiered networks that are composed of MBSs and several types of SBSs (e.g., micro, pico, femto).

The common assumption in SG analysis is to model multi-tier cellular networks via mutually independent tiers of BSs. On each tier, the BS locations follow an independent PPP which is characterized by its own transmission power P_k, intensity λ_k, and path-loss exponent η_k. It is usually assumed that UEs are associated to BSs according to a biased RSS strategy, which is controlled by a set of bias factors

$\{B_1, B_2, \ldots, B_k, \ldots\}$.[29] The bias factors are manipulated to control the load served by each network tier as shown in Fig. 16. Let $\tilde{\Psi}_k = \{r_{0,k}, r_{1,k}, r_{2,k}, ..\}$ be the set of the ordered distances between a test user at the origin and the BSs in Ψ_k, in which $r_{i-1,k} < r_{i,k} < r_{i+1,k}$, for $\forall i \in \mathbb{Z}^+$. Then, assuming K tiers of BSs, the test UE chooses to associate with tier $k \in \{1, 2, ..., K\}$ if

$$B_k P_k r_{0,k}^{-\eta_k} > B_i P_i r_{0,i}^{-\eta_i}; \quad i \in \{1, 2, ..., K\}, \quad i \neq k. \tag{66}$$

For simplicity, we focus on the case where all tiers have a common path-loss exponent $\eta_k = 4$. The general case analysis can be found in [49], [79]. Hence, the association rule becomes

$$B_k P_k r_{0,k}^{-4} > B_i P_i r_{0,i}^{-4}; \quad i \in \{1, 2, ..., K\}, \quad i \neq k. \tag{67}$$

The performance in each tier may differ according to its parameters. Thus, per-tier performance is usually conducted. Let us focus on a generic tier k. Looking into (45) and (46), one can see that the LT of the aggregate interference power should be evaluated at $\frac{ar_{0,k}^4}{P_k}$ to conduct the performance analysis for tier k. The aggregate interference in this case is the cumulative interference coming from all tiers. Assuming universal frequency reuse across all tiers, the aggregate interference from all tiers can be calculated as

$$\mathcal{L}_{\mathcal{I}_{\text{agg}}}(a, \boldsymbol{\Lambda}, r_{0,k}, \boldsymbol{R}) = \mathbb{E}\left\{e^{-z\sum\limits_{i=1}^{K} \mathcal{I}_i}\right\}$$

$$\overset{(a)}{=} \prod_{i=1}^{K} \mathbb{E}\left\{e^{-z\mathcal{I}_i}\right\}$$

$$= \prod_{i=1}^{K} \mathcal{L}_{\mathcal{I}_i}(z, \lambda_i, r_{\mathcal{I}_i}). \tag{68}$$

where $\boldsymbol{\Lambda} = \{\lambda_i\}_{i=1}^K$, $\boldsymbol{R} = \{r_{\mathcal{I}_i}\}_{i=1}^K$, (a) follows from the independence between the different tiers, and $r_{\mathcal{I}_i}$ and $\mathcal{I}_i$ are, respectively, the interference boundary for the ith tier and the aggregate interference from the ith tier.

The LT of the interference from each tier is similar to (50). The per-tier interference boundary is obtained from the association rule given in (67). For a user who is associated with tier k with the association distance $r_{0,k}$, the ith tier interference should have the intensity λ_i and interference boundary
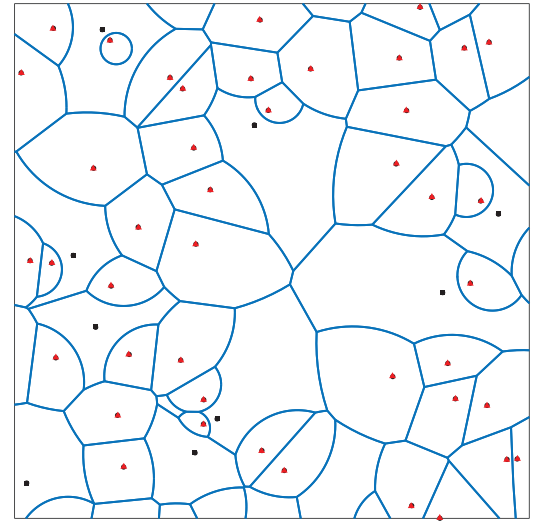
$$r_{\mathcal{I}_i} = r_{0,i} > \left(\frac{B_i P_i}{B_k P_k}\right)^{\frac{1}{4}} r_{0,k}. \tag{69}$$

From (50) with $P_0 = P_k$ and $P_{\mathcal{I}} = P_i$, the LT for the per-tier interference can be expressed as
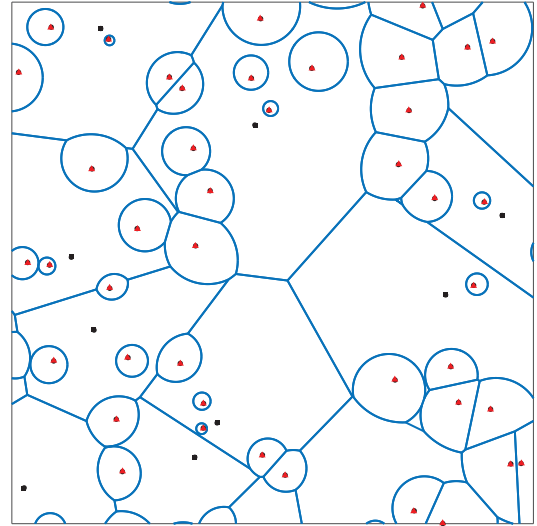
(a) With no biasing ($B_2 = B_1$)

(b) With biasing ($B_2 = 10B_1$)

Fig. 16. Two-tier cellular network with the same BS locations and different bias factors, in which the squares indicate the MBSs, the triangles indicate the SBSs for $P_1 = 50P_2$, $\lambda_1 = 0.2\lambda_2$ and $\eta = 4$. Biasing is used to increase the coverage of SBSs to offload users from the MBSs to the SBSs.

$$\mathcal{L}_{\mathcal{I}_i}^{(k)}(a, \lambda_i, r_{0,k}, r_{\mathcal{I}_i}) =$$
$$\exp\left\{-\pi\lambda_i\sqrt{\frac{aP_i}{P_k}}r_{0,k}^2 \arctan\left(\sqrt{\frac{aB_k}{B_i}}\right)\right\}. \tag{70}$$

Combining (68) and (70), the LT of the aggregate interference experienced by a user in tier k is

$$\mathcal{L}_{\mathcal{I}_{\text{agg}}}^{(k)}(a, \boldsymbol{\Lambda}, r_{0,k}, \boldsymbol{R}) =$$
$$\exp\left\{-\sum_{i=1}^{k}\pi\lambda_i\sqrt{\frac{aP_i}{P_k}}r_{0,k}^2 \arctan\left(\sqrt{\frac{aB_k}{B_i}}\right)\right\}. \tag{71}$$

Similar to Section VIII-A, the service distance $r_{0,k}$ is random with the PDF shown in (94), which is a function of the relative values of the tiers' powers, bias factors, and path-loss exponents. In our case (i.e., $\eta_k = 4, \forall k$), the service distance distribution for a user in the kth tier reduces to

$$f_{r_{0,k}}(x) = 2\pi \left(\sum_{i=1}^{K} \sqrt{\frac{B_i P_i}{B_k P_k}} \lambda_i \right) x \exp \left\{ -\pi \sum_{l=1}^{K} \sqrt{\frac{B_l P_l}{B_k P_k}} \lambda_l x^2 \right\}.$$
(72)

The spatially averaged LT for users in the kth tier is then given by

$$
\begin{aligned}
&\mathcal{L}_{\mathcal{I}_{\text{agg}}}^{(k)}(a, \boldsymbol{\Lambda}) \\
&= \int_0^\infty \mathcal{L}_{\mathcal{I}_{\text{agg}}}^{(k)} \left(a, \boldsymbol{\Lambda}, r, \left\{ \frac{B_i P_i}{B_k P_k} r \right\}_{i=1}^{K} \right) f_{r_{0,k}}(r) \mathrm{d}r \\
&= \frac{\sum_{i=1}^{K} \sqrt{B_i P_i} \lambda_i}{\sum_{l=1}^{K} \sqrt{B_l P_l} \lambda_l \left(1 + \sqrt{\frac{a B_k}{B_l}} \arctan\left(\sqrt{\frac{a B_k}{B_l}} \right) \right)}.
\end{aligned}
$$
(73)

For $\eta = 4$, the tier association probability in (93) reduces to

$$\mathcal{A}_k = \frac{\lambda_k \sqrt{B_k P_k}}{\sum_{i=1}^{K} \lambda_i \sqrt{B_i P_i}}.$$
(74)

Using (74) the averaged LT is given by

$$
\begin{aligned}
&\mathcal{L}_{\mathcal{I}_{\text{agg}}}(a, \boldsymbol{\Lambda}) \\
&= \sum_{k=1}^{K} \mathcal{A}_k \mathcal{L}_{\mathcal{I}_{\text{agg}}}^{(k)}(a, \boldsymbol{\Lambda}) \\
&= \sum_{k=1}^{k} \left(\sum_{i=1}^{k} \frac{\lambda_i}{\lambda_k} \sqrt{\frac{B_i P_i}{B_k P_k}} \left[1 + \sqrt{\frac{a B_k}{B_i}} \arctan\left(\sqrt{\frac{a B_k}{B_i}} \right) \right] \right)^{-1}.
\end{aligned}
$$
(75)

If unbiased RSS association is adopted (i.e., $B_k = 1, \forall k$), then the LT reduces to

$$\mathcal{L}_{\mathcal{I}_{\text{agg}}}(a, \boldsymbol{\Lambda}) = \frac{1}{1 + \sqrt{a} \arctan\left(\sqrt{a} \right)}.$$
(76)

Despite the different transmission powers and intensities of BSs in multi-tier cellular networks, the simple expression in (76) shows that the unbiased RSS association reduces the SINR-dependent performance metrics to the single-tier case, which is independent from network parameters (i.e., numner of tiers, transmission powers, intensities of BSs, etc.).

E. Interference Coordination and Frequency Reuse

For simplicity, we study a user-centric interference coordination with frequency reuse in a single-tier cellular network modeled via a PPP with intensity λ. Due to the randomized network structure modeled by the PPP, the traditional hexagonal grid tailored frequency reuse schemes cannot be employed. Therefore, it is assumed that the available spectrum is divided into Δ sub-bands and that frequency reuse is adopted via coordination among the BSs [115]. As shown in Fig. 17, each BS uses a frequency sub-band which is not used by the $\Delta - 1$ BSs closest to its serving user. The main problem in frequency reuse is that the positions of interfering BSs are
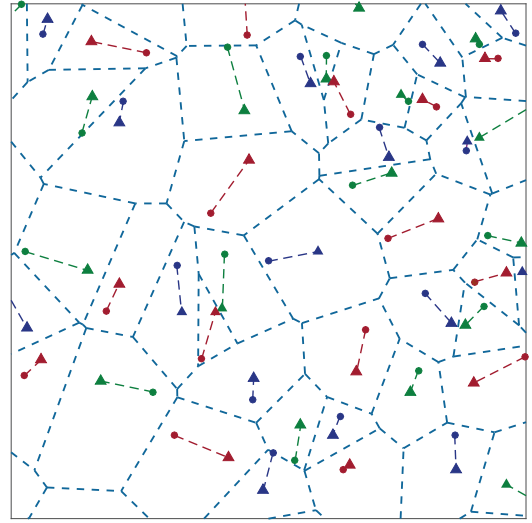

Fig. 17. User-centric coordinated frequency reuse with $\Delta = 3$, in which the BSs are represented by triangles and UEs are represented by circles. BSs using the same frequency are highlighted with similar color.

correlated (i.e., the BSs that are using the same sub-band), which violates the PPP assumption. For analytical tractability, the usual method that is used in such cases is to approximate the set of interfering BSs with a PPP with intensity $\frac{\lambda}{\Delta}$. It is well perceived that approximating a repulsive PP by a PPP that have equivalent intensity gives an accurate estimate for the interference if the exclusion distance $r_{\mathcal{I}}$ around the test receiver is accurately calculated [5], [65], [87], [188], [192]. In our case, since each BS selects one of the Δ sub-bands, the intensity of the interfering BSs on each sub-band is λ/Δ. Exploiting the equi-dense PPP approximation, the LT of the aggregate interference in the form of (50) is legitimate to be used

$$\mathcal{L}_{\mathcal{I}_{\text{agg}}}\left(a, \frac{\lambda}{\Delta}, r_0, r_{\mathcal{I}}\right) = \exp \left\{ -\pi \frac{\lambda}{\Delta} \sqrt{a} r_0^2 \arctan\left(\left(\frac{r_0}{r_{\mathcal{I}}} \right)^2 \sqrt{a} \right) \right\}.$$
(77)

The adopted user-centric coordination imposes an increased geographical interference protection around UEs, and hence, $r_{\mathcal{I}} > r_0$. Particularly, since each BS is using a frequency which is not used by the nearest $\Delta - 1$ neighbors, the geographical interference protection is given by $r_{\mathcal{I}} = r_{\Delta-1}$. Note that $r_{\Delta-1}$ and r_0 are correlated with the joint PDF in (89). Averaging over the joint PDF of $r_{\Delta-1}$ and r_0, the spatially averaged LT of the aggregate interference is given by (78).

It is important to highlight that the conditional PDF in (89) is based on the BS intensity λ not $\frac{\lambda}{\Delta}$. This is because the UEs have the opportunity to associate with the complete set of BSs with intensity λ. However, once associated, it communicates on one of the Δ sub-bands which interferes with a subset of the BSs with intensity $\frac{\lambda}{\Delta}$.

It is obvious that interference coordination and frequency reuse have complicated the analysis, resulting in a double integral expression for the spatially averaged LT of interference

$$\mathcal{L}_{\mathcal{I}_{\text{agg}}}\left(a, \frac{\lambda}{\Delta}\right) = \int_0^\infty \int_x^\infty \frac{4(\pi\lambda)^\Delta y(y^2 - x^2)^{\Delta-2}}{\Gamma(\Delta - 1)} \exp\left\{-\pi\lambda\left(\frac{\sqrt{a}x^2}{\Delta}\arctan\left(\left(\frac{x}{y}\right)^2\sqrt{a}\right) - y^2\right)\right\} \mathrm{d}y\mathrm{d}x \tag{78}$$
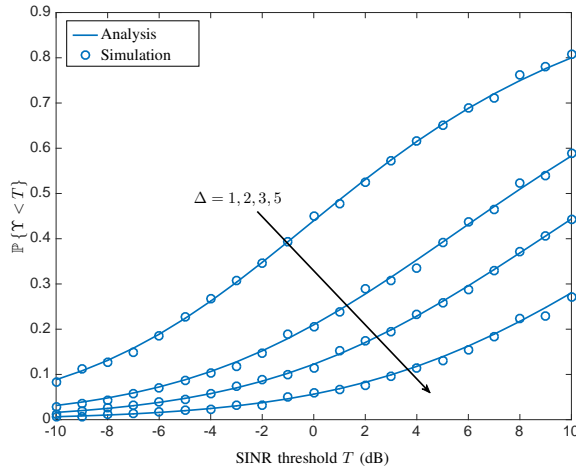

Fig. 18. Outage probability for coordinated frequency reuse with $\lambda = 3$ BS/km^2, $\eta = 4$, and $\Delta = 1$, 2, ,3, and 5.

in (78). However, such expression is still valuable as it can be efficiently evaluated in terms of time and complexity when compared to Monte Carlo simulations.

Fig. 18 validates (78) and shows the effect of the coordinated frequency reuse on the network outage probability. As shown in (77) and (78), coordinated frequency reuse affects both the interference boundary and the interferers intensity. This explains the significant performance improvement shown in Fig. 18 for increasing the reuse factor Δ.

F. General Fading

All of the above analysis is based on the exponential power fading (i.e., Rayleigh environment) assumption, which enables expressing the ASEP, outage probability, and ergodic rate using the LT of the aggregate interference. Assuming general fading on the interfering links, the analytical tractability is not affected as all performance metrics can still be expressed using the LT of the aggregate interference. Nevertheless, the expression of the LT of the aggregate interference may become more involved. Tractability issues occur when the fading of the useful link power gain is not exponentially distributed. In this case, the outage probability and ASEP can no longer be expressed in terms of the LT of the aggregate interference.[30] In [5], the authors discuss four techniques which are used in the literature to extend SG analysis to other fading environments. These techniques are to:

- approximate the interference using a certain PDF via moments fitting, in which the moments are obtained for

[30]Unlike outage probability and ASEP, the ergodic rate can always be expressed in terms of the LT of the aggregate interference (cf. [205, Lemma 1]), and hence, can be evaluated for general fading environment [51].

the interference LT;

- resort to bounds by considering dominant interferers only and/or statistical inequalities;
- use Plancherel-Parseval theorem to obtain the aforementioned performance metrics via complex integrals in the Fourier transform domain;
- inversion (e.g., Gil-Pelaez inversion theorem [42]).

We will not delve into the details of these techniques as they are already discussed in [5]. However, two important cases are highlighted below.

1) Nakagami-m: The first scenario where the above analysis holds is the Nakagami-m fading with integer m. For the ASEP analysis, [199] obtains expressions for $\mathbb{E}\{\text{erfc}(h/x)\}$ and $\mathbb{E}\{\text{erfc}^2(h/x)\}$ using the LT of X, where h is gamma distributed with integer shape parameter as shown in Appendix III. Note that the LT of the aggregate interference in Nakagami-m fading changes from (50) to

$$\mathcal{L}_{\mathcal{I}_{\text{agg}}}(a, \lambda, r_0, r_{\mathcal{I}})$$
$$= \exp\left\{-\pi\lambda r_0^2 {}_2F_1\left(-\frac{2}{\eta}, m, 1 - \frac{2}{\eta}, -\left(\frac{r_0}{r_{\mathcal{I}}}\right)^\eta \frac{aP_{\mathcal{I}}}{P_0}\right)\right\}. \tag{79}$$

The outage probability and ergodic rate can be computed from the CDF of the SINR as shown in Section VII. In the Nakagami-m case, the authors in [206] show that if m is an integer, the CDF of the SINR can be expressed in terms of the LT of the aggregate interference using the following identity

$$t^n f(t) \xrightarrow{LT} (-1)^k \frac{d^k \mathcal{L}_{f(t)}(s)}{ds^k}. \tag{80}$$

Let h be a gamma random variable with shape parameter U and scale parameter 1. From (41), the CDF of the SINR can be expressed

$$F_\Upsilon(T) = \int_x F_h\left(\frac{T\mathcal{I}_{\text{agg}}}{Pr_0^{-\eta}}\right) f_{\mathcal{I}_{\text{agg}}}(x)\mathrm{d}x$$
$$\stackrel{(a)}{=} 1 - \int_x \sum_{u=0}^{U-1} \frac{1}{u!}\left(\frac{T\mathcal{I}_{\text{agg}}r_0^\eta}{P}\right)^u e^{-\frac{T\mathcal{I}_{\text{agg}}r_0^\eta}{P}} f_{\mathcal{I}_{\text{agg}}}(x)\mathrm{d}x$$
$$\stackrel{(b)}{=} 1 - \sum_{u=0}^{U-1} \frac{(-1)^u}{u!}\left(\frac{Tr_0^\eta}{P}\right)^u \frac{\mathrm{d}^u \mathcal{L}_{I_{\text{agg}}}(z)}{\mathrm{d}z^u}\bigg|_{z=\frac{Tr_0^\eta}{P}} \tag{81}$$

where (a) follows from the CDF of the gamma distribution with integer shape parameter, and (b) follows from switching the integral and summation order, the LT definition, and the identity in (80).

2) Additional Slow Fading: When an additional slow fading is incorporated into the analysis on top of the exponential or Nakagami-m fading, the analysis remains tractable if the RSS association adapts to the slow fading. That is, the users are always associated to the BS that provides the highest received signal strength. Applying the displacement theorem

[168], the effect of shadowing is captured by scaling the intensity of the PPP with the shadowing fractional moment $\mathbb{E}\left\{x^{\frac{2}{\eta}}\right\}$, where x is the shadowing random variable [50].

G. Multiple Input Multiple Output (MIMO) Antenna Systems

Due to the vast diversity of available MIMO techniques and the significant differences between their operations, it is difficult to present a unified analytical framework for all MIMO case studies. Further, we do not want to lose the tutorial flavor and delve into MIMO systems details, which already exist elsewhere in the literature. Therefore, this section presents a simple receive diversity MIMO case study just to convey the idea of extending SG analysis to MIMO systems. MIMO with transmit diversity is discussed in the next section in the context of network MIMO.

This section considers a downlink cellular network with receive diversity, where each BS is equipped with a single antenna and each UE is equipped with N_r antennas. The receive diversity scenario is particularly selected for simplicity, but its method of analysis can be applied to more realistic MIMO configurations [110]. Note that in SG analysis, the multiple antennas are usually assumed to be collocated. The channel gain vector between a transmitting antenna and the N_r receiving antennas is denoted by $\boldsymbol{h} \in \mathbb{C}^{N_r \times 1}$, which is assumed to be composed of i.i.d circularly symmetric unit variance complex Gaussian random variables. Also, it is assumed that the UEs have perfect channel information for the intended channel vector $\boldsymbol{h}_0$. Assuming maximum ratio combining (MRC) receivers, the baseband received signal at the input of the decoder can be represented as

$$
\begin{aligned}
y &= \boldsymbol{h}_0^H \left(\sqrt{P} r_0^{-\frac{\eta}{2}} \boldsymbol{h}_0 s_0 + \sum_{r_j \in \tilde{\Psi} \backslash r_0} \sqrt{P} r_j^{-\frac{\eta}{2}} \boldsymbol{h}_j s_j + \boldsymbol{n} \right) \\
&= \sqrt{P} r_0^{-\frac{\eta}{2}} \boldsymbol{h}_0^H \boldsymbol{h}_0 s_0 + \sum_{r_j \in \tilde{\Psi} \backslash r_0} \sqrt{P} r_j^{-\frac{\eta}{2}} \boldsymbol{h}_0^H \boldsymbol{h}_j s_j + \boldsymbol{h}_0^H \boldsymbol{n}
\end{aligned} \quad (82)
$$

where $\boldsymbol{n} \in \mathbb{C}^{N_r \times 1}$ is the noise vector with i.i.d complex Gaussian elements. Conditioning on $\Xi = \left\{ \boldsymbol{h}_0, \boldsymbol{h}_i, \tilde{\Psi} \right\}$ and exploiting the Gaussian signaling assumption, the SINR can be expressed as

$$
\begin{aligned}
\Upsilon(\Xi) &= \frac{P r_0^{-\eta} \boldsymbol{h}_0^H \boldsymbol{h}_0 \boldsymbol{h}_0^H \boldsymbol{h}_0}{\sum\limits_{r_j \in \tilde{\Psi} \backslash r_0} P r_j^{-\eta} \boldsymbol{h}_0^H \boldsymbol{h}_j \boldsymbol{h}_j^H \boldsymbol{h}_0 + N_0 \boldsymbol{h}_0^H \boldsymbol{h}_0} \\
&= \frac{P r_0^{-\eta} \boldsymbol{h}_0^H \boldsymbol{h}_0}{\sum\limits_{r_j \in \tilde{\Psi} \backslash r_0} P r_j^{-\eta} \frac{\boldsymbol{h}_0^H \boldsymbol{h}_j \boldsymbol{h}_j^H \boldsymbol{h}_0}{\boldsymbol{h}_0^H \boldsymbol{h}_0} + N_0} \\
&= \frac{P r_0^{-\eta} g_0}{\sum\limits_{r_j \in \tilde{\Psi} \backslash r_0} P r_j^{-\eta} g_j + N_0}
\end{aligned} \quad (83)
$$

where g_0 and g_j in (83) are the effective channel gains for the employed MIMO scheme. Let $h_{0,k}$ be the kth element of $\boldsymbol{h}_0$, then $g_0 = \sum_{k=1}^{N_r} h_{0,k}^H h_{0,k}$ is a summation of N_r unit-mean exponential random variables. Hence, g_0 is gamma distributed with shape parameter N_r and rate parameter 1.
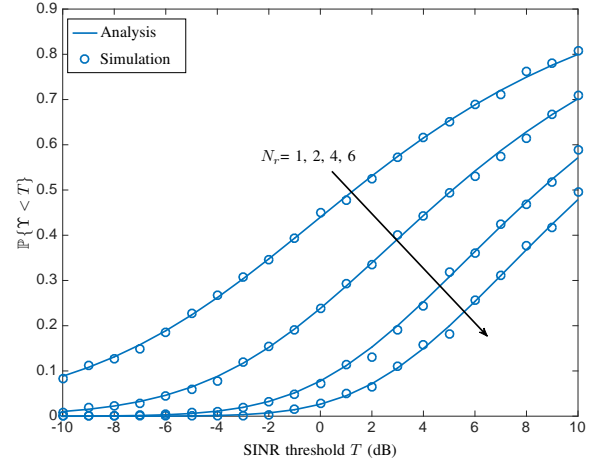

Fig. 19. The effect of receive diversity on the outage probability $\lambda = 3$ BS/km^2 and $\eta = 4$.

On the other hand, due to the independence between $\boldsymbol{h}_0$ and $\boldsymbol{h}_i$, the effective channel gain for the ith interfering link (g_i) is a unit-mean exponential random variable. Note that the exponential distribution of g_i follows from the fact that $\frac{\boldsymbol{h}_0^H \boldsymbol{h}_j \boldsymbol{h}_j^H \boldsymbol{h}_0}{|\boldsymbol{h}_0|^2} \overset{d}{=} h_{j1} h_{j1}^H$, which can be proved by conditioning on h_0 and showing that $h_j \sim \mathcal{CN}(0, 1)$. Since the MRC receiver leads to a gamma distributed intended channel gain, ASEP and SINR CDF can be obtained as in the case of Nakagami-m fading described in Section VIII-F1. For instance, the CDF of the SINR can be found as

$$
F_\Upsilon(T) = 1 - \sum_{u=0}^{N_r-1} \frac{(-1)^u}{u!} \left(\frac{T r_0^\eta}{P} \right)^u \left. \frac{\mathrm{d}^u \mathcal{L}_{I_{\text{agg}}}(z)}{\mathrm{d} z^u} \right|_{z = \frac{T r_0^\eta}{P}} \quad (84)
$$

where $\mathcal{L}_{I_{\text{agg}}}(z)$ is given in (47) with $r_\mathcal{I} = r_0$. Fig. 19 validates (84) and shows the effect of receive diversity on the network outage probability.

From the simple example presented above, one can see that even in Rayligh fading environment, the fading in MIMO networks is no longer exponential, and hence, the analysis is more involved. Also, analyzing the distribution of the interfering signals is challenging as the interfering signal from each BS is multiplied by the precoding matrix tailored for processing the intended signal. Further, correlations within the interference at the antenna branches may impose additional complexity to the MIMO analysis. Nevertheless, the SG analysis has been greatly developed in recent years and modeled the performance of many MIMO setups with and without interference correlation [96]–[102], [104]–[110].

H. Network MIMO

In the previous section, it is implicitly assumed that the multiple antennas are collocated. In contrast, when several BSs cooperate to form a MIMO system, the antenna separations are prominent and should be taken into consideration. This section considers a downlink single-tier cellular network with single antenna BSs. User centric CSI agnostic coordinated

multi-point (CoMP) transmission is enabled [118], [119], in which each user is served by his nearest n BSs. In this case, the test user receives n non-coherent copies of his intended symbol from the n nearest BSs, and the received baseband signal can be expressed as

$$y = \sum_{i=0}^{n-1} \sqrt{P} r_i^{-\frac{\eta}{2}} h_i s_0 + \sum_{r_j \in \tilde{\Psi} \setminus \{r_0, r_1, ..., r_{n-1}\}} \sqrt{P} r_j^{-\frac{\eta}{2}} h_j s_j + n \quad (85)$$

where the set $\{r_0, r_1, ..., r_{n-1}\}$ is excluded from $\tilde{\Psi}$ in (85) as the nearest n BSs do not contribute to the interference. The SINR can be written as

$$\Upsilon = \frac{|\sum_{i=0}^{n-1} \sqrt{P} r_i^{-\frac{\eta}{2}} h_i|^2}{\sum\limits_{r_j \in \tilde{\Psi} \setminus \{r_0, r_1, ..., r_{n-1}\}} P r_j^{-\eta} |h_j|^2 + N_0} \quad (86)$$

where $|\sum_{i=0}^{n-1} \sqrt{P} r_i^{-\frac{\eta}{2}} h_i|^2$ is exponentially distributed with mean $\sum_{i=0}^{n-1} P_i r_i^{-\eta}$. Substituting

$$z = \frac{a}{\sum_{i=0}^{n-1} P r_i^{-\eta}}$$

into (47) and integrating over the joint PDF of the distances $f(r_0, r_1, ... r_n)$, the spatially averaged LT is given (87). Note that cooperation increases the geographical interference protection region to $r_{\mathcal{I}} = r_{n-1}$ because the nearest n BSs cooperate to serve the intended user and do not contribute to the aggregate interference. More advanced models for network MIMO with transmission precoding and location aware cooperation are given in [117]–[120].

I. Discussion

This section discusses some numerical results obtained via SG analysis. Figs. 10-13, 15, 18, and 20 show high outage probability and ASEP values. Hence, it may be argued that the PPP results are pessimistic and do not reflect realistic system performance. However, such results are mainly due to the system model and assumptions rather than from the PPP abstraction. That is, the universal frequency reuse, the saturated network model, and the peak transmit power of the BSs are the main reason for the poor performance shown in Figs. 10-13, 15, 18, and 20. To show that the system model, not the PPP, are the main reasons for such pessimistic performance, we give the following two arguments. First, the results in [38], [193] shows that the PPP captures the same SIR trends as other repulsive point processes using the same system model. That is, the PPP abstraction gives a horizontally shifted version of the SIR CDF curve for repulsive point processes, where such horizontal shift is denoted as *deployment gain*. Second, Fig. 20 shows that the PPP can provide acceptable numerical values for the performance measures when more sophisticated system model is applied. Particularly, Fig. 20 shows the outage probability obtained for a PPP cellular network with receive diversity and frequency reuse, which are basic components of modern networks [207]. Receive diversity and frequency reuse are incorporated into the analysis by using (78) and (81).

Fig. 20(a) shows the explicit and combined effects of receive diversity and frequency reuse on the network outage probability. Fig. 20(b) shows the combined effect of receive diversity and frequency reuse for different reuse factors and different numbers of receive antennas. Figs. 20(a) and 20(b) show that incorporating simple network management techniques into the analysis leads to realistic values for the outage probability. For instance, with only two receive antennas and a reuse factor of 3, the outage probability at $T = 0$ dB drops from almost 50% (cf. Figs. 11, and 13) to below 5%. Incorporating more practical system parameters (e.g., power control and multi-slope path-loss) would further reduce the outage probability.

To recap, with the appropriate system model, SG analysis with the PPP assumption can capture realistic network performance and gives acceptable performance characterization. Sometimes we are interested in trends rather than absolute values. In this case, it is better to keep a simple system model to facilitate the analysis and to obtain insightful performance expressions. These expressions could be used to understand the network behavior in response to different network parameters and desing variables. However, it should be understood that the corresponding results are illustrative to the network behavior and do not give the true numerical values for the performance metrics.

IX. FUTURE RESEARCH DIRECTION

SG analysis can be used to characterize the performance of large-scale setup wireless networks. For instance, it is well known that minimum Euclidean distance receivers are optimal if the intended symbol is disturbed by Gaussian noise. However, in large-scale networks where the intended symbol is disturbed by non-Gaussian interference in addition to the Gaussian noise, the optimal detector is unknown. Furthermore, results obtained for single point-to-point links cannot be directly generalized to large-scale networks. For instance, in a point-to-point link, the BER decreases with the transmit power. This fact does not hold for large-scale networks as the increased power of the useful signal is canceled by the increased interference power. In this regard, SG paves the way to better understanding and more efficient operation of large-scale wireless networks. We highlight below some venues to extend SG for better models of wireless networks.

A. New Point Processes

Exploring new tractable PP for modeling wireless networks is a fundamental research direction for SG analysis. Although we have shown that the PPP provides a good approximation for interference associated with repulsive point processes, the PPP alone is not enough to model all wireless networks. Wireless networks' topologies may include other complex correlations among the network elements rather than the simplified repulsion discussed in this paper. For instance, 5G networks define several types of communication including device-to-device (D2D) communication, vehicle-to-vehicle (V2V) communication, and machine-to-machine communication on top of the legacy device-to-BS communication [208]. These

$$\mathcal{L}_{\mathcal{I}_{agg}}(a, \lambda) = \int\int_{0 < r_0 < r_1 < \ldots < r_{n-1} < \infty} \ldots \int \exp\left\{ -\pi\lambda \sqrt{\frac{a}{\sum_{i=0}^{n-1} r_i^{-4}}} \arctan\left(\frac{1}{r_{n-1}^2} \sqrt{\frac{a}{\sum_{i=0}^{n-1} r_i^{-4}}} \right) \right\} f(r_0, r_1, \ldots, r_n) dr_0 dr_1 \ldots dr_{n-1} \qquad (87)$$
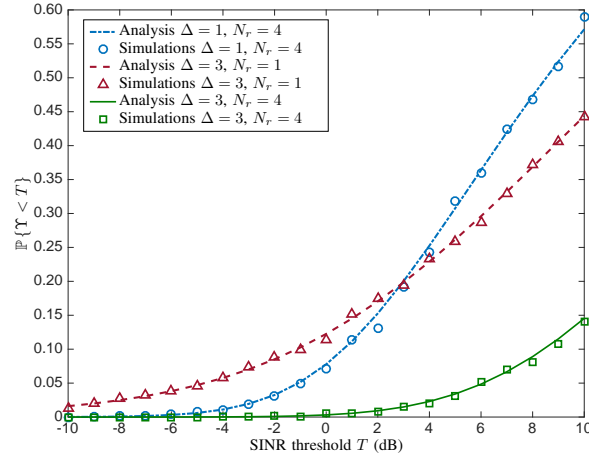
(a)
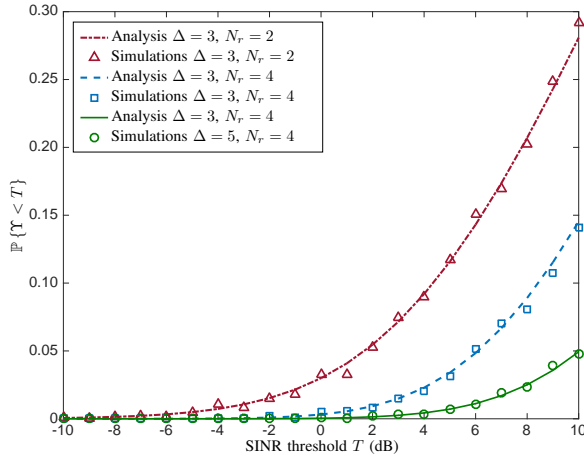
(b)

Fig. 20. The effect of receive diversity and coordinated frequency reuse on the outage probability.

various types of communications create complex topological structures that cannot be captured by PPP. This is because PPP is only characterized by its intensity and interference boundary, which offers limited degrees of freedom to model different topological structures. Hence, it is essential to develop SG models for wireless networks via new PPs. In this regard, there have been efforts invested to study new PPs in the context of cellular networks. For instance, Poisson cluster processes and Gauss-Poisson process for modeling attractive behavior between points are studied in [20], [60], [209], [210]. Repulsive point processes such as the Matérn hard core point process, the Ginibre point process, and the determinantal point process are studied in [43], [44], [76], [87]–[90], [211], [212].

There are even efforts to characterize the asymptotic behavior of networks following general point processes [213], [214]. In some cases when it is difficult to obtain explicit performance metrics in some network models, stochastic ordering can be exploited to compare their performances [98], [215]. Note that the developed models using the aforementioned non-Poisson point processes (e.g., Matérn, Giniber, and determinantal processes) are mostly for the baseline network model due to their involved analytical nature. Hence, besides exploring new point processes, extending existing non-Poisson based models to advanced network setup is also a potential research direction.

B. Characterizing New Technologies

Techniques used for transmissions and network management in wireless networks are continuously evolving to enhance the network performance and cope with the ever-increasing traffic demand. Usually, a proposal for a new technique starts with a theoretical idea followed by prototyping testbeds. However, it is challenging and costly to expose these techniques to realistic tests in large-scale setup. In this case, SG can serve as an initial and fast evaluation step for validating and quantifying the associated performance. For instance, in-band full-duplex (FD) communication, which emerges for recent advances in self-interference cancellation techniques, is optimistically promoted to double the spectral efficiency for wireless networks [216], [217]. While this is true for a point-to-point link, it is not necessarily true in large-scale networks due to the increased interference level. In fact, [143] employed SG analysis to demonstrate the vulnerability of uplink to downlink interference and the negative effect that FD communication can impose on the uplink transmission. Then, in the light of the SG model in [143], the authors proposed a solution to alleviate the negative impact of FD communication on the uplink transmission. Similar examples exist for other new technologies such as D2D communication [148]–[152], coordinated multi-point transmission [118]–[120], offloading and load balancing [77]–[81], uplink/downlink decoupling [70], massive MIMO [109], and so on.

The above discussion shows the important role of SG in evaluating the gains associated with new technologies before the implementation step. Hence, it can be decided beforehand whether the new technology is worth the investment or not. Hence, performance characterization in large-scale networks via SG will always be a future research direction as long as new technologies are being proposed to enhance the performance of cellular networks as well as other types of large-scale networks.

C. More Involved Performance Characterization

In the context of cellular networks, SG is mainly confined to model interference and characterize outage, error probability, and transmission rate. An important direction for research is to extend SG analysis to model more performance metrics. For instance, SG can be used to model other physical layer related parameters in large-scale setups such as secrecy rate [25]–[27], which is the fundamental performance metric in physical layer security. Looking into the literature, there are initiatives to assess physical layer security in cellular networks via the secrecy rate performance metric [164], [165]. However, this field of research is not mature enough to address the security problems imposed on 5G networks. In 5G networks there are massive D2D, M2M, and V2V communications on the top of the legacy user-to-BS communications. These different types of communications may serve applications (e.g., eHealth, smart city automation) which requires some level of privacy and confidentiality. Hence, developing secrecy rate models for modern cellular networks with D2D, M2M, and V2V communications is an interesting future research direction.

Stochastic geometry can also be extended beyond SINR characterization. For instance, cell boundary cross rate and cell dwell time are two fundamental performance metrics in cellular networks to design the handover procedure. The handover models available in the literature are mostly based on the circular approximation for the cell shape, which does not comply with recent measurements in [37], [38], [189], [190]. Hence, more accurate handover models for cellular network are required. In this regards, there are some initiatives to use SG to characterize handover in cellular networks as in [155]–[160]. However, complete handover designs based on SG are yet to be developed.

Developing new techniques for managing cellular networks may also define new performance metrics to be characterized. For instance, it is advised to transport and cache popular files in the cellular network edge during off-peak time to maximize the utilization of the core network and enhance the end user quality of service [218]. In this case, the hitting probability, i.e., the probability that a user finds the requested file in a nearby BS, becomes a meaningful performance metric. Recently, models for hitting probability via stochastic geometry are developed and used to propose solutions to the caching problems based on file popularity [219]. Last but not least, SG analysis can be extended beyond physical and MAC layers to higher layer protocols such as routing and data forwarding [220]. It also can be used to assess signal processing techniques applied to large scale networks [221], [222].

D. Statistical Network Optimization

Cellular operators always seek an optimized operation of their networks. Modern cellular networks are composed of a massive number of network elements (i.e., BSs, users, devices, machines, etc.) which makes a centralized instantaneous optimization for the network infeasible. That is, it is infeasible to select serving BS, assign powers, allocate channels, and choose the mode of operation for each and every network element. In this context, SG analysis can be exploited for statistically optimized operation, which creates a tradeoff among complexity, signaling, and performance. While instantaneous optimization guarantees best performance at any time instant, statistical optimization provides optimal averaged performance on long-term scale to reduce signaling and processing overheads. Note that statistical network parameters (e.g., distribution for channel gains, network elements spatial distribution and intensity, and so on.) change on longer time scales when compared to other instantaneous parameters such as channel realizations and users locations. For statistical network optimization, the performance objective functions and constraints can be formulated via SG analysis, which guarantees an optimal spatially averaged performance. Some efforts are invested in statistical network for cellular networks using SG [223], [224]. However, to the best of the authors' knowledge, merging statistical and instantaneous optimization to balance performance, complexity, and signaling overhead is an open research problem.

X. Conclusion

We present a tutorial on stochastic geometry (SG) analysis for cellular networks. We first characterize interference in cellular networks by deriving its characteristic function and moments. Then, exact error performance analysis and approximate one are conducted. We show that approximating the interfering symbols by Gaussian signals facilitates the analysis and simplifies the symbol error rate expressions without sacrificing accuracy. Then, we present the abstracted outage and ergodic rate analysis, which is used to further simplify the analysis and the performance expressions. To this end, we present a unified technique to compute error probability, outage probability, and ergodic rate for several system models in cellular networks. In particular, we show how the intensity and boundary of the PPP should be determined based on the network characteristics. We also present numerical examples and discussed the pessimistic performance obtained by SG. We show that with the proper network model, SG is capable of capturing realistic network performance. Finally, we point out future research directions for SG in the context of cellular networks.

APPENDIX I
THE POISSON POINT PROCESS

The distance distribution between a generic location in $\mathbb{R}^2$ to the nearest point in a PPP Φ with intensity λ is given by

$$f_{r_0}(r) = 2\pi\lambda r e^{-\pi\lambda r^2}, \qquad r > 0 \tag{88}$$

The joint distance distribution between a generic location in $\mathbb{R}^2$ to the nearest and n^{th} points in a PPP Φ with intensity λ is given by

$$f_{r_0, r_n}(x, y) = \frac{4(\pi\lambda)^{n+1}}{\Gamma(n)} xy(y^2 - x^2)^{n-1} e^{-\pi\lambda y^2}, \tag{89}$$

where $0 \leq x \leq y \leq \infty$.

Let $f : \mathbb{R}^n \to \mathbb{R}$ be a measurable function and $\Phi \in \mathbb{R}^n$ be a PPP, then by the PGFL we have:

$$\mathbb{E}\left\{\prod_{x_i \in \Phi} f(x_i)\right\} = \exp\left\{-\int_{\mathbb{R}^n}(1 - f(x))\Lambda(dx)\right\}. \quad (90)$$

Let V be the area of a generic PPP-Voronoi cell, then

$$f_V(v) \approx \frac{(\lambda c)^c v^{c-1} e^{-c\lambda v}}{\Gamma(c)}, \qquad 0 \le v < \infty \quad (91)$$

where $c = 3.57$ is a constant defined for the Voronoi tessellation in the $\mathbb{R}^2$ [225].

Consider two independent PPPs Φ_b and Φ_u with intensities λ_b and λ_u. Using the approximate PDF in (91) for the Voronoi tessellation constructed w.r.t. Φ_b, the probability mass function of the number of point of Φ_u existing in a generic Voronoi cell of Φ_b is given by

$$\mathbb{P}\{\mathcal{U} = n\} = \frac{\Gamma(n+c)}{\Gamma(n+1)\Gamma(c)}\frac{(\lambda_u)^n(\lambda_b c)^c}{(\lambda_b c + \lambda_u)^{n+c}}, \quad (92)$$

where $n = 0, 1, 2, \cdots$.

In a K-tier cellular network with intensities $\{\lambda_i\}_{k=1}^K$, bias factors $\{B_i\}_{k=1}^K$, and path-loss exponent $\{\eta_k\}_{k=1}^K$, the probability that a user associate with tier k is given by [226, Lemma 1]

$$\mathcal{A}_k = 2\pi\lambda_k \int_0^\infty r \exp\left\{-\pi\sum_{i=1}^K \lambda_i \left(\frac{B_i P_i}{B_k P_k}\right)^{\frac{2}{\eta_i}} r^{\frac{2\eta_k}{\eta_j}}\right\} dr. \quad (93)$$

The service distance $r_{0,k}$ distribution for a user associated to a BS in the kth tier is given by [226, Lemma 3]

$$f_{r_{0,k}}(x) = \frac{2\pi\lambda_k x}{\mathcal{A}_k}\exp\left\{-\pi\sum_{i=1}^K \lambda_i \left(\frac{B_i P_i}{B_k P_k}\right)^{\frac{2}{\eta_i}} x^{\frac{2\eta_k}{\eta_j}}\right\}. \quad (94)$$

APPENDIX II

Let BPSK denote binary phase shift keying , BFSK denote binary frequency shift keying, QPSK denote quadrature phase shift keying, M-QAM denote M-quadrature amplitude modulation, M-PAM denote M-pulse amplitude modulation, DE-BPSK denote differential encoded BPSK, and MSK denote minimum shift keying. Then (16) holds for these schemes with the parameters given in Table III.

APPENDIX III
LEMMA 1 IN [199].

Let $Y \sim Gamma(m, m)$ be a unit mean gamma distributed random variable, X be a real random variable with the LT $\mathcal{L}_x(\cdot)$, and C be a constant. The authors in [199] proposed a technique to calculate averages in the form of $\mathbb{E}\left\{Q\left(\sqrt{\frac{Y}{X+C}}\right)\right\}$ and $\mathbb{E}\left\{Q^2\left(\sqrt{\frac{Y}{X+C}}\right)\right\}$. These averages are

TABLE III
TABLE OF MODULATION-SPECIFIC PARAMETERS

Scheme	c	w_c	β_c
BPSK	1	1	
	2	0	-
BFSK	1	1	1
	2	0	-
QPSK	1	2	1
	2	-1	1
M-QAM	1	$4\frac{\sqrt{M}-1}{\sqrt{M}}$	$\frac{3}{(M-1)}$
	2	$-4\left(\frac{\sqrt{M}-1}{\sqrt{M}}\right)^2$	$\frac{3}{(M-1)}$
M-PAM	1	$\frac{2(M-1)}{M}$	$\frac{6}{(M^2-1)}$
	2	0	-
M-PSK	1	2	$2\sin^2(\frac{\pi}{M})$
Upper-bound	2	0	-
DE-BPSK	1	2	2
	2	-2	2
MSK	2	1	2
	2	0	-

given by

$$\mathbb{E}\left\{Q\left(\sqrt{\frac{Y}{X+C}}\right)\right\} = \frac{1}{2} - \frac{\Gamma(m+\frac{1}{2})}{\Gamma(m)}\frac{1}{\pi}.$$
$$\int_0^\infty \frac{1}{\sqrt{z}}e^{-z(1+2mC)}\,{}_1F_1\left(1 - m; \frac{3}{2}, z\right)\mathcal{L}_X(2mz)\,\mathrm{d}z, \quad (95)$$

$$\overset{m=1}{=} \frac{1}{2}\left(1 - \frac{1}{\sqrt{\pi}}\int_0^\infty \frac{e^{-z(1+2C)}\mathcal{L}_X(2z)}{\sqrt{z}}\mathrm{d}z\right), \quad (96)$$

and

$$\mathbb{E}\left\{Q^2\left(\sqrt{\frac{Y}{X+C}}\right)\right\} = \frac{1}{4} - \frac{m}{\pi}\int_0^\infty e^{-2zmC}$$
$$\mathcal{L}_X(2mz)\int_0^{\frac{\pi}{4}}{}_1F_1\left(m+1; 2, \frac{-z}{\sin^2\vartheta}\right)\frac{\mathrm{d}\vartheta}{\sin^2\vartheta}\mathrm{d}z, \quad (97)$$

$$\overset{m=1}{=} \frac{1}{4} - \frac{1}{\sqrt{\pi}}\int_0^\infty \frac{e^{-z(1+2C)}Q(\sqrt{2z})\mathcal{L}_X(2z)}{\sqrt{z}}\mathrm{d}z. \quad (98)$$

APPENDIX IV
POOF OF LEMMA 2

Following [37], let $\mathcal{I}_{agg} = \sum_{r_k \in \tilde{\Psi}\backslash r_0} sP|h_i|^2 r_i^{-\eta}$, then the LT of $\mathcal{I}_{agg}$ can be derived as

$$\mathcal{L}_{\mathcal{I}_{agg}}(s) = \mathbb{E}_{\tilde{\Psi}} \left\{ \prod_{r_k \in \tilde{\Psi} \setminus r_0} \mathbb{E}_{h_i} \left\{ \exp\left\{ -sP|h_i|^2 r_i^{-\eta} \right\} \right\} \right\}$$

$$= \exp\left\{ -\int_{\mathbb{R}^2} \left(1 - \mathbb{E}_h\{\exp\{-sP|h|^2 r^{-\eta}\}\} \right) \Lambda(dr) \right\}$$

$$= \exp\left\{ -2\pi\lambda \int_{r_0}^{\infty} \left(1 - \mathbb{E}_h\{\exp\{-sP|h|^2 r^{-\eta}\}\} \right) r\,dr \right\}$$

$$= \exp\left\{ -2\pi\lambda \int_{r_0}^{\infty} \left(1 - \frac{1}{1 + sPr^{-\eta}} \right) r\,dr \right\}$$

$$= \exp\left\{ -2\pi\lambda \int_{r_0}^{\infty} \left(\frac{sP}{r^{\eta} + sP} \right) r\,dr \right\}$$

$$= \exp\left\{ -2\pi\lambda(sP)^{\frac{2}{\eta}} \int_{\frac{r_0}{(sP)^{\frac{1}{\eta}}}}^{\infty} \left(\frac{x}{x^{\eta} + 1} \right) dx \right\}$$

$$= \exp\left\{ -\frac{2\pi\lambda sPr_0^{2-\eta}}{\eta - 2} {}_2F_1\left(1, 1 - \frac{2}{\eta}; 2 - \frac{2}{\eta}; -\frac{sP}{r_0^{\eta}} \right) \right\}. \tag{99}$$

ACKNOWLEDGMENT

REFERENCES

[1] M. Z. Win, P. C. Pinto, A. Giorgetti, M. Chiani, and L. Shepp, "Error performance of ultrawideband systems in a Poisson field of narrowband interferers," in *2006 IEEE Ninth International Symposium on Spread Spectrum Techniques and Applications*, 2006, pp. 410–416.

[2] M. Z. Win, "A mathematical model for network interference," IEEE Communication Theory Workshop, Sedona, AZ, May 2007.

[3] M. Z. Win, P. C. Pinto, and L. A. Shepp, "A mathematical theory of network interference and its applications," *Proc. IEEE*, vol. 97, no. 2, pp. 205–230, Feb. 2009.

[4] M. Haenggi, J. G. Andrews, F. Baccelli, O. Dousse, and M. Franceschetti, "Stochastic geometry and random graphs for the analysis and design of wireless networks," *IEEE J. Sel. Areas Commun.*, vol. 27, no. 7, pp. 1029–1046, Sep. 2009.

[5] H. ElSawy, E. Hossain, and M. Haenggi, "Stochastic geometry for modeling, analysis, and design of multi-tier and cognitive cellular wireless networks: A survey," *IEEE Commun. Surveys Tuts.*, vol. 15, no. 3, pp. 996–1019, 2013.

[6] L. Kleinrock and J. Silvester, "Optimum transmission radii for packet radio networks or why six is a magic number," in *Proceedings of the IEEE National Telecommunications Conference*, vol. 4, 1978, pp. 1–4.

[7] J. Silvester and L. Kleinrock, "On the capacity of multihop slotted ALOHA networks with regular structure," *IEEE Trans. Commun.*, vol. 31, no. 8, pp. 974–982, 1983.

[8] R. Nelson and L. Kleinrock, "The spatial capacity of a slotted ALOHA multihop packet radio network with capture," *IEEE Trans. Commun.*, vol. 32, no. 6, pp. 684–694, 1984.

[9] H. Takagi and L. Kleinrock, "Optimal transmission ranges for randomly distributed packet radio terminals," *IEEE Trans. Commun.*, vol. 32, no. 3, pp. 246–257, 1984.

[10] T.-C. Hou and V. O. Li, "Transmission range control in multihop packet radio networks," *IEEE Trans. Commun.*, vol. 34, no. 1, pp. 38–44, 1986.

[11] E. S. Sousa and J. Silvester, "Optimum transmission ranges in a direct-sequence spread-spectrum multihop packet radio network," *IEEE J. Sel. Areas Commun.*, vol. 8, no. 5, pp. 762–771, 1990.

[12] R. Mathar and J. Mattfeldt, "On the distribution of cumulated interference power in Rayleigh fading channels," *Wireless Networks*, vol. 1, no. 1, pp. 31–36, 1995.

[13] J. Ilow and D. Hatzinakos, "Analytic alpha-stable noise modeling in a Poisson field of interferers or scatterers," *IEEE Trans. Signal Process.*, vol. 46, no. 6, pp. 1601–1611, 1998.

[14] P. C. Pinto and M. Z. Win, "Communication in a Poisson field of interferers–Part I: Interference distribution and error probability," *IEEE Trans. Wireless Commun.*, vol. 9, no. 7, pp. 2176–2186, Jul. 2010.

[15] P. Pinto and M. Z. Win, "Communication in a Poisson field of interferers-Part II: Channel capacity and interference spectrum," *IEEE Trans. Wireless Commun.*, vol. 9, no. 7, pp. 2187–2195, Jul. 2010.

[16] E. S. Sousa, "Performance of a spread spectrum packet radio network link in a Poisson field of interferers," *IEEE Trans. Inf. Theory*, vol. 38, no. 6, pp. 1743–1754, 1992.

[17] C. L. Nikias and M. Shao, *Signal processing with alpha-stable distributions and applications*. Wiley-Interscience, 1995.

[18] M. Shao and C. L. Nikias, "Signal processing with fractional lower order moments: stable processes and their applications," *Proc. IEEE*, vol. 81, no. 7, pp. 986–1010, 1993.

[19] G. Samoradnitsky and M. S. Taqqu, *Stable non-Gaussian random processes: stochastic models with infinite variance*. CRC Press, 1994, vol. 1.

[20] M. Haenggi and R. K. Ganti, *Interference in Large Wireless Networks*. NOW Publishers (Foundations and Trends in Networking, Vol. 3), 2008.

[21] S. B. Lowen and M. C. Teich, "Power-law shot noise," *IEEE Trans. Inf. Theory*, vol. 36, no. 6, pp. 1302–1318, 1990.

[22] M. Franceschetti, "Stochastic rays pulse propagation," *IEEE Trans. Antennas Propag.*, vol. 52, no. 10, pp. 2742–2752, 2004.

[23] F. Baccelli, B. Blaszczyszyn, and P. Mühlethaler, "An ALOHA protocol for multihop mobile wireless networks," *IEEE Trans. Inf. Theory*, vol. 52, no. 2, pp. 421–436, 2006.

[24] A. Rabbachin, T. Q. S. Quek, H. Shin, and M. Z. Win, "Cognitive network interference," *IEEE J. Sel. Areas Commun.*, vol. 29, no. 2, pp. 480–493, Feb. 2011.

[25] A. Rabbachin, A. Conti, and M. Z. Win, "Wireless network intrinsic secrecy," *IEEE/ACM Trans. Netw.*, vol. 23, no. 1, pp. 56–69, Feb 2015.

[26] P. Pinto, J. Barros, and M. Z. Win, "Secure communication in stochastic wireless networks - Part I: Connectivity," *IEEE Trans. Inf. Forensics Security*, vol. 7, no. 1, pp. 125–138, Feb 2012.

[27] ——, "Secure communication in stochastic wireless networks - Part II: Maximum rate and collusion," *IEEE Trans. Inf. Forensics Security*, vol. 7, no. 1, pp. 139–147, Feb 2012.

[28] G. A. Tsihrintzis and C. L. Nikias, "Performance of optimum and suboptimum receivers in the presence of impulsive noise modeled as an alpha-stable process," *IEEE Trans. Commun.*, vol. 43, no. 2/3/4, pp. 904–914, 1995.

[29] J. Ilow, D. Hatzinakos, and A. N. Venetsanopoulos, "Performance of FHSS radio networks with interference modeled as a mixture of Gaussian and alpha-stable noise," *IEEE Trans. Commun.*, vol. 46, no. 4, pp. 509–520, 1998.

[30] S. Ambike, J. Ilow, and D. Hatzinakos, "Detection for binary transmission in a mixture of Gaussian noise and impulsive noise modeled as an alpha-stable process," *IEEE Signal Process. Lett.*, vol. 1, no. 3, pp. 55–57, 1994.

[31] E. Salbaroli and A. Zanella, "Interference analysis in a Poisson field of nodes of finite area," *IEEE Trans. Veh. Technol.*, vol. 58, no. 4, pp. 1776–1783, 2009.

[32] A. Rabbachin, T. Q. Quek, P. C. Pinto, I. Oppermann, and M. Z. Win, "Non-coherent UWB communication in the presence of multiple narrowband interferers," *IEEE Trans. Wireless Commun.*, vol. 9, no. 11, pp. 3365–3379, 2010.

[33] P. C. Pinto and M. Z. Win, "Spectral characterization of wireless networks," *IEEE Wireless Commun. Mag.*, vol. 14, no. 6, pp. 27–31, 2007.

[34] S. Srinivasa and M. Haenggi, "Modeling interference in finite uniformly random networks," in *International Workshop on Information Theory for Sensor Networks (WITS 2007)*, Santa Fe, NM, Jun. 2007.

[35] F. Baccelli, M. Klein, M. Lebourges, and S. Zuyev, "Stochastic geometry and architecture of communication networks," *Journal of Telecommunication Systems*, vol. 1, no. 7, pp. 209–227, Jun. 1997.

[36] T. Brown, "Cellular performance bounds via shotgun cellular systems," *IEEE J. Sel. Areas Commun.*, vol. 18, no. 11, pp. 2443–2455, Nov. 2000.

[37] J. G. Andrews, F. Baccelli, and R. K. Ganti, "A tractable approach to coverage and rate in cellular networks," *IEEE Trans. Commun.*, vol. 59, no. 11, pp. 3122–3134, Nov. 2011.

[38] A. Guo and M. Haenggi, "Spatial stochastic models and metrics for the structure of base stations in cellular networks," *IEEE Trans. Wireless Commun.*, vol. 12, no. 11, pp. 5800–5812, Nov. 2013.

This article has been accepted for publication in a future issue of this journal, but has not been fully edited. Content may change prior to final publication. Citation information: DOI 10.1109/COMST.2016.2624939, IEEE Communications Surveys & Tutorials

33

[39] B. Blaszczyszyn, M. Karray, and H. Keeler, "Using Poisson processes to model lattice cellular networks," in *Proc. the 32th Annual IEEE International Conference on Computer Communications (INFOCOM'13)*, Turin, Italy, Apr. 2013, pp. 773–781.

[40] M. Di Renzo and W. Lu, "The equivalent-in-distribution (EiD)-based approach: On the analysis of cellular networks using stochastic geometry," *IEEE Commun. Lett.*, vol. 18, no. 5, pp. 761–764, May 2014.

[41] L. H. Afify, H. ElSawy, T. Y. Al-Naffouri, and M.-S. Alouini, "The influence of Gaussian signaling approximation on error performance in cellular networks," *IEEE Commun. Lett.*, vol. 19, no. 12, pp. 2202–2205, Dec 2015.

[42] M. D. Renzo and P. Guan, "Stochastic geometry modeling of coverage and rate of cellular networks using the Gil-Pelaez inversion theorem." *IEEE Commun. Lett.*, vol. 19, no. 9, pp. 1575–1578, Sep. 2014.

[43] N. Deng, W. Zhou, and M. Haenggi, "The Ginibre point process as a model for wireless networks with repulsion," *IEEE Trans. Wireless Commun.*, vol. 14, no. 1, pp. 107–121, Jan. 2015.

[44] N. Miyoshi and T. Shirai, "A cellular network model with Ginibre configured base stations," *Advances in Applied Probability*, vol. 46, no. 3, pp. 832–845, Aug. 2014.

[45] ——, "Spatial modeling and analysis of cellular networks using the Ginibre point process: A tutorial," *arXiv preprint arXiv:1606.02828*, 2016.

[46] R. K. Ganti and M. Haenggi, "Asymptotics and approximation of the SIR distribution in general cellular networks," *IEEE Trans. Wireless Commun.*, vol. 15, no. 3, pp. 2130–2143, March 2016.

[47] A. Guo and M. Haenggi, "Asymptotic deployment gain: A simple approach to characterize the SINR distribution in general cellular networks," *IEEE Trans. Commun.*, vol. 63, no. 3, pp. 962–976, March 2015.

[48] M. Afshang and H. S. Dhillon, "Fundamentals of modeling finite wireless networks using binomial point process," *arXiv preprint arXiv:1606.04405*, 2016.

[49] H. S. Dhillon, R. K. Ganti, F. Baccelli, and J. G. Andrews, "Coverage and ergodic rate in K-tier downlink heterogeneous cellular networks," in *Proc. of the 49th Annual Allerton Conference on Communication, Control, and Computing (Allerton)*, Sep. 2011, pp. 1627–1632.

[50] H. Dhillon and J. G. Andrews, "Downlink rate distribution in heterogeneous cellular networks under generalized cell selection," *IEEE Wireless Commun. Lett.*, vol. 3, no. 1, pp. 42–45, Feb. 2014.

[51] M. D. Renzo, A. Guidotti, and G. E. Corazza, "Average rate of downlink heterogeneous cellular networks over generalized fading channels: A stochastic geometry approach," *IEEE Trans. Commun.*, vol. 61, no. 7, pp. 3050–3071, Jul. 2013.

[52] P. Madhusudhanan, J. G. Restrepo, Y. E. Liu, T. X. Brown, and K. R. Baker, "Downlink performance analysis for a generalized shotgun cellular system," *IEEE Trans. Wireless Commun.*, vol. 13, no. 12, pp. 6684–6696, Oct. 2014.

[53] W. C. Cheung, T. Quek, and M. Kountouris, "Throughput optimization, spectrum allocation, and access control in two-tier femtocell networks," *IEEE J. Sel. Areas Commun.*, vol. 30, no. 3, pp. 561–574, Apr. 2012.

[54] S. Singh, F. Baccelli, and J. Andrews, "On association cells in random heterogeneous networks," *IEEE Wireless Commun. Lett.*, vol. 3, no. 1, pp. 70–73, Feb. 2014.

[55] R. Heath, M. Kountouris, and T. Bai, "Modeling heterogeneous network interference using Poisson point processes," *IEEE Trans. Signal Process.*, vol. 61, no. 16, pp. 4114–4126, Aug. 2013.

[56] T. Bai, R. Vaze, and R. Heath, "Analysis of blockage effects on urban cellular networks," *IEEE Trans. Wireless Commun.*, vol. 13, no. 9, pp. 5070–5083, Sep. 2014.

[57] T. Bai and R. Heath, "Location-specific coverage in heterogeneous networks," *IEEE Signal Process. Lett.*, vol. 20, no. 9, pp. 873–876, Sep. 2013.

[58] B. Yu, L. Yang, H. Ishii, and S. Mukherjee, "Dynamic TDD support in macrocell-assisted small cell architecture," *IEEE J. Sel. Areas Commun.*, vol. 33, no. 6, pp. 1201–1213, Jun. 2015.

[59] S. Mukherjee, "Distribution of downlink SINR in heterogeneous cellular networks," *IEEE J. Sel. Areas Commun.*, vol. 30, no. 3, pp. 575–585, Apr. 2012.

[60] Y. Chun, M. Hasna, and A. Ghrayeb, "Modeling heterogeneous cellular networks interference using Poisson cluster processes," *IEEE J. Sel. Areas Commun.*, accepted 2015.

[61] H. Wei, N. Deng, W. Zhou, and M. Haenggi, "Approximate SIR analysis in general heterogeneous cellular networks," *IEEE Trans. Commun.*, vol. 64, no. 3, pp. 1259–1273, March 2016.

[62] A. M. Ibrahim, T. ElBatt, and A. El-Keyi, "Coverage probability analysis for wireless networks using repulsive point processes," in *2013 IEEE 24th Annual International Symposium on Personal, Indoor, and Mobile Radio Communications (PIMRC)*, Sept 2013, pp. 1002–1007.

[63] H. He, J. Xue, T. Ratnarajah, F. A. Khan, and C. B. Papadias, "Modeling and analysis of cloud radio access networks using Matérn hard-core point processes," *IEEE Trans. Wireless Commun.*, vol. 15, no. 6, pp. 4074–4087, June 2016.

[64] W. Bao and B. Liang, "Rate maximization through structured spectrum allocation and user association in heterogeneous cellular networks," *IEEE Trans. Commun.*, vol. 63, no. 11, pp. 4510–4524, Nov 2015.

[65] H. ElSawy and E. Hossain, "On stochastic geometry modeling of cellular uplink transmission with truncated channel inversion power control," *IEEE Trans. Wireless Commun.*, vol. 13, no. 8, pp. 4454–4469, Aug. 2014.

[66] L. H. Afify, H. ElSawy, T. Y. Al-Naffouri, , and M.-S. Alouini, "Error performance analysis in uplink cellular networks using a stochastic geometric approach," in *Proc. of the 4th International Workshop on Small Cell and 5G Networks (SmallNets)*, London, UK, Jun. 2015.

[67] M. D. Renzo and P. Guan, "Stochastic geometry modeling and system-level analysis of uplink heterogeneous cellular networks with multi-antenna base stations," *IEEE Trans. Commun.*, vol. 64, no. 6, pp. 2453–2476, June 2016.

[68] F. J. Martin-Vega, G. Gomez, M. C. Aguayo-Torres, and M. D. Renzo, "Analytical modeling of interference aware power control for the uplink of heterogeneous cellular networks," *IEEE Transactions on Wireless Communications*, accepted 2016.

[69] T. D. Novlan, H. S. Dhillon, and J. G. Andrews, "Analytical modeling of uplink cellular networks," *IEEE Trans. Wireless Commun.*, vol. 12, no. 6, pp. 2669–2679, Jun. 2013.

[70] S. Singh, X. Zhang, and J. G. Andrews, "Joint rate and SINR coverage analysis for decoupled uplink-downlink biased cell associations in HetNets," *IEEE Trans. Wireless Commun.*, accepted 2015.

[71] A. AlAmmouri, H. ElSawy, and M.-S. Alouini, "Load-aware modeling for uplink cellular networks in a multi-channel environment," in *Proc. of the 25th IEEE Personal Indoor and Mobile Radio Communications (PIMRC'14)*, Washington D.C., USA, Sep. 2014.

[72] M. Gharbieh, H. ElSawy, A. Bader, and M.-S. Alouini, "Tractable stochastic geometry model for IoT access in LTE networks," in *Proc. of the 2016 IEEE Global Communications Conference (GLOBECOM)*, Washington D.C., USA, Dec. 2016.

[73] P. Herath, C. Tellambura, and W. A. Krzymien, "Stochastic geometry modeling of cellular uplink power control under composite Rayleigh-Lognormal fading," in *2015 IEEE 82nd Vehicular Technology Conference (VTC Fall)*, Sept 2015, pp. 1–5.

[74] H. Y. Lee, Y. J. Sang, and K. S. Kim, "On the uplink SIR distributions in heterogeneous cellular networks," *IEEE Commun. Lett.*, vol. 18, no. 12, pp. 2145–2148, Dec. 2014.

[75] Z. Zeinalpour-Yazdi and S. Jalali, "Outage analysis of uplink two-tier networks," *IEEE Trans. Commun.*, vol. 62, no. 9, pp. 3351–3362, Sep. 2014.

[76] T. Kobayashi and N. Miyoshi, "Uplink cellular network models with Ginibre deployed base stations," in *International Teletraffic Congress (ITC)*, Sep. 2014, pp. 1–7.

[77] S. Singh, H. Dhillon, and J. Andrews, "Offloading in heterogeneous networks: Modeling, analysis, and design insights," *IEEE Trans. Wireless Commun.*, vol. 12, no. 5, pp. 2484–2497, May 2013.

[78] S. Singh and J. Andrews, "Joint resource partitioning and offloading in heterogeneous cellular networks," *IEEE Trans. Wireless Commun.*, vol. 13, no. 2, pp. 888–901, Feb. 2014.

[79] H. Dhillon, R. Ganti, and J. Andrews, "Load-aware modeling and analysis of heterogeneous cellular networks," *IEEE Trans. Wireless Commun.*, vol. 12, no. 4, pp. 1666–1677, Apr. 2013.

[80] M. Mirahsan, R. Schoenen, and H. Yanikomeroglu, "HetHetNets: Heterogeneous traffic distribution in heterogeneous wireless cellular networks," *IEEE J. Sel. Areas Commun.*, accepted 2015.

[81] Y. Lin, W. Bao, W. Yu, and B. Liang, "Optimizing user association and spectrum allocation in HetNets: A utility perspective," *IEEE J. Sel. Areas Commun.*, vol. 33, no. 6, pp. 1025–1039, Jun. 2015.

[82] R. K. Ganti and M. Haenggi, "Spatial analysis of opportunistic downlink relaying in a two-hop cellular system," *IEEE Trans. Commun.*, vol. 60, no. 5, pp. 1443–1450, May 2012.

[83] M. Di Renzo and W. Lu, "End-to-end error probability and diversity analysis of AF-based dual-hop cooperative relaying in a Poisson field of interferers at the destination," *IEEE Trans. Wireless Commun.*, vol. 14, no. 1, pp. 15–32, Jan 2015.

[84] ——, "On the diversity order of selection combining dual-branch dual-hop AF relaying in a Poisson field of interferers at the destination," *IEEE Trans. Veh. Technol.*, vol. 64, no. 4, pp. 1620–1628, April 2015.

[85] W. Lu and M. Di Renzo, "Stochastic geometry modeling and system-level analysis/optimization of relay-aided downlink cellular networks," *IEEE Trans. Commun.*, vol. 63, no. 11, pp. 4063–4085, Nov 2015.

[86] H. Elkotby and M. Vu, "Uplink user-assisted relaying in cellular networks," *IEEE Trans. Wireless Commun.*, vol. 14, no. 10, pp. 5468–5483, Oct 2015.

[87] H. ElSawy and E. Hossain, "Two-tier HetNets with cognitive femtocells: Downlink performance modeling and analysis in a multichannel environment," *IEEE Trans. Mobile Comput.*, vol. 13, no. 3, pp. 649–663, Mar. 2014.

[88] H. ElSawy, E. Hossain, and D. I. Kim, "HetNets with cognitive small cells: user offloading and distributed channel access techniques," *IEEE Commun. Mag.*, vol. 51, no. 6, pp. 28–36, Jun. 2013.

[89] H. ElSawy and E. Hossain, "On cognitive small cells in two-tier heterogeneous networks," in *Proc. of the 9th International Workshop on Spatial Stochastic Models for Wireless Networks (SpaSWiN'2013)*, Tsukuba Science City, Japan, May 2013.

[90] ——, "Channel assignment and opportunistic spectrum access in two-tier cellular networks with cognitive small cells," in *Proc. of the 2013 IEEE Global Communications Conference (GLOBECOM)*, Atlanta, USA, Dec. 2013.

[91] Y. S. Soh, T. Quek, M. Kountouris, and G. Caire, "Cognitive hybrid division duplex for two-tier femtocell networks," *IEEE Trans. Wireless Commun.*, vol. 12, no. 10, pp. 4852–4865, Oct. 2013.

[92] C. de Lima, M. Bennis, and M. Latva-aho, "Coordination mechanisms for self-organizing femtocells in two-tier coexistence scenarios," *IEEE Trans. Wireless Commun.*, vol. 11, no. 6, pp. 2212–2223, Jun. 2012.

[93] ——, "Statistical analysis of self-organizing networks with biased cell association and interference avoidance," *IEEE Trans. Veh. Technol.*, vol. 62, no. 5, pp. 1950–1961, Jun. 2013.

[94] P. Semasinghe and E. Hossain, "Downlink power control in self-organizing dense small cells underlaying macrocells: A mean field game," *IEEE Trans. Mobile Comput.*, accepted 2015.

[95] P. Semasinghe, E. Hossain, and K. Zhu, "An evolutionary game for distributed resource allocation in self-organizing small cells," *IEEE Trans. Mobile Comput.*, vol. 14, no. 2, pp. 274–287, Feb. 2015.

[96] R. Tanbourgi, H. S. Dhillon, and F. K. Jondral, "Analysis of joint transmit-receive diversity in downlink MIMO heterogeneous cellular networks," *IEEE Trans. Wireless Commun.*, accepted 2015.

[97] A. K. Gupta, H. S. Dhillon, S. Vishwanath, and J. G. Andrews, "Downlink multi-antenna heterogeneous cellular network with load balancing," *IEEE Trans. Commun.*, vol. 62, no. 11, pp. 4052–4067, Nov. 2014.

[98] H. S. Dhillon, M. Kountouris, and J. G. Andrews, "Downlink MIMO HetNets: Modeling, ordering results and performance analysis," *IEEE Trans. Wireless Commun.*, vol. 12, no. 10, pp. 5208–5222, Oct. 2013.

[99] R. Tanbourgi, H. S. Dhillon, J. G. Andrews, and F. K. Jondral, "Effect of spatial interference correlation on the performance of maximum ratio combining," *IEEE Trans. Wireless Commun.*, vol. 13, no. 6, pp. 3307–3316, Jun. 2014.

[100] ——, "Dual-branch MRC receivers under spatial interference correlation and Nakagami fading," *IEEE Trans. Commun.*, vol. 62, no. 6, pp. 1830–1844, Jun. 2014.

[101] M. Di Renzo and W. Lu, "Stochastic geometry modeling and performance evaluation of MIMO cellular networks using the equivalent-in-distribution (EiD)-based approach," *IEEE Trans. Commun.*, vol. 63, no. 3, pp. 977–996, Mar. 2015.

[102] M. D. Renzo and P. Guan, "A mathematical framework to the computation of the error probability of downlink MIMO cellular networks by using stochastic geometry," *IEEE Trans. Commun.*, vol. 62, no. 8, pp. 2860–2879, Aug. 2014.

[103] M. Di Renzo, C. Merola, A. Guidotti, F. Santucci, and G. E. Corazza, "Error performance of multi-antenna receivers in a Poisson field of interferers: A stochastic geometry approach," *IEEE Trans. Commun.*, vol. 61, no. 5, pp. 2025–2047, May 2013.

[104] S. Govindasamy, "Asymptotic data rates of receive-diversity systems with MMSE estimation and spatially correlated interferers," *IEEE Transactions on Communications*, vol. 62, no. 5, pp. 100–113, May 2014.

[105] J. Zhang and J. G. Andrews, "Distributed antenna systems with randomness," *IEEE Trans. Wireless Commun.*, vol. 7, no. 9, pp. 3636–3646, Sep. 2008.

[106] C. Li, J. Zhang, and K. Letaief, "Performance analysis of SDMA in multicell wireless networks," in *Proc. of the 2013 IEEE Global Communications Conference (GLOBECOM)*, Dec. 2013, pp. 3867–3872.

[107] N. Lee, D. Morales-Jimenez, A. Lozano, and R. Heath, "Spectral efficiency of dynamic coordinated beamforming: A stochastic geometry approach," *IEEE Trans. Wireless Commun.*, vol. 14, no. 1, pp. 230–241, Jan. 2015.

[108] Y. Lin and W. Yu, "Downlink spectral efficiency of distributed antenna systems under a stochastic model," *IEEE Trans. Wireless Commun.*, vol. 13, no. 12, pp. 6891–6902, Dec. 2014.

[109] A. Adhikary, H. S. Dhillon, and G. Caire, "Massive-MIMO meets HetNet: Interference coordination through spatial blanking," *IEEE J. Sel. Areas Commun.*, accepted 2015.

[110] L. H. Afify, H. ElSawy, T. Y. Al-Naffouri, and M.-S. Alouini, "Unified stochastic geometry model for MIMO cellular networks with retransmissions," *IEEE Trans. Wireless Commun.*, accepted 2016. [Online]. Available: http://http://arxiv.org/abs/1604.02960#

[111] Z. Chen, L. Qiu, and X. Liang, "Area spectral efficiency analysis and energy consumption minimization in multiantenna Poisson distributed networks," *IEEE Trans. Wireless Commun.*, vol. 15, no. 7, pp. 4862–4874, July 2016.

[112] H. Tabassum, A. H. Sakr, and E. Hossain, "Analysis of massive MIMO-enabled downlink wireless backhauling for full-duplex small cells," *IEEE Trans. Commun.*, vol. 64, no. 6, pp. 2354–2369, June 2016.

[113] N. Liang, W. Zhang, and C. Shen, "An uplink interference analysis for massive MIMO systems with MRC and ZF receivers," in *2015 IEEE Wireless Communications and Networking Conference (WCNC)*, March 2015, pp. 310–315.

[114] T. Bai and R. W. Heath, "Analyzing uplink SINR and rate in massive MIMO systems using stochastic geometry," *IEEE Trans. Commun.*, accepted 2016.

[115] L. H. Afify, H. ElSawy, T. Y. Al-Naffouri, , and M.-S. Alouini, "Error performance analysis in downlink cellular networks with interference management," in *Proc. of the 11th International Workshop on Spatial Stochastic Models for Wireless Networks (SpaSWiN'2015)*, Mumbai, India, May 2015.

[116] X. Zhang and M. Haenggi, "A stochastic geometry analysis of inter-cell interference coordination and intra-cell diversity," *IEEE Trans. Wireless Commun.*, vol. 13, no. 12, pp. 6655–6669, Dec. 2014.

[117] G. Nigam, P. Minero, and M. Haenggi, "Spatiotemporal cooperation in heterogeneous cellular networks," *IEEE J. Sel. Areas Commun.*, accepted 2015.

[118] ——, "Coordinated multipoint joint transmission in heterogeneous networks," *IEEE Trans. Commun.*, vol. 62, no. 11, pp. 4134–4146, Nov. 2014.

[119] A. Sakr and E. Hossain, "Location-aware cross-tier coordinated multi-point transmission in two-tier cellular networks," *IEEE Trans. Wireless Commun.*, vol. 13, no. 11, pp. 6311–6325, Nov. 2014.

[120] F. Baccelli and A. Giovanidis, "A stochastic geometry framework for analyzing pairwise-cooperative cellular networks," *IEEE Trans. Wireless Commun.*, vol. 14, no. 2, pp. 794–808, Jun. 2015.

[121] M. Wildemeersch, T. Quek, M. Kountouris, A. Rabbachin, and C. Slump, "Successive interference cancellation in heterogeneous networks," *IEEE Trans. Commun.*, vol. 62, no. 12, pp. 4440–4453, Dec. 2014.

[122] T. M. Nguyen, Y. Jeong, T. Quek, W. P. Tay, and H. Shin, "Interference alignment in a Poisson field of MIMO femtocells," *IEEE Trans. Wireless Commun.*, vol. 12, no. 6, pp. 2633–2645, Jun. 2013.

[123] C. Li, J. Zhang, M. Haenggi, and K. Letaief, "User-centric intercell interference nulling for downlink small cell networks," *IEEE Trans. Commun.*, vol. 63, no. 4, pp. 1419–1431, Apr. 2015.

[124] R. Tanbourgi, S. Singh, J. G. Andrews, and F. K. Jondral, "A tractable model for noncoherent joint-transmission base station cooperation," *IEEE Trans. Wireless Commun.*, vol. 13, no. 9, pp. 4959–4973, Sep. 2014.

[125] S. Akoum and R. Heath, "Interference coordination: Random clustering and adaptive limited feedback," *IEEE Trans. Signal Process.*, vol. 61, no. 7, pp. 1822–1834, Apr. 2013.

[126] H. S. Dhillon, Y. Li, P. Nuggehalli, Z. Pi, and J. G. Andrews, "Fundamentals of heterogeneous cellular networks with energy harvesting," *IEEE Trans. Wireless Commun.*, vol. 13, no. 5, pp. 2782–2797, May 2014.

[127] A. H. Sakr and E. Hossain, "Analysis of K-tier uplink cellular networks

with ambient RF energy harvesting," *IEEE J. Sel. Areas Commun.*, accepted 2015.

[128] ——, "Cognitive and energy harvesting-based D2D communication in cellular networks: Stochastic geometry modeling and analysis," *IEEE Trans. Commun.*, vol. 63, no. 5, pp. 1867–1880, May 2015.

[129] Y. S. Soh, T. Quek, M. Kountouris, and H. Shin, "Energy efficient heterogeneous cellular networks," *IEEE J. Sel. Areas Commun.*, vol. 31, no. 5, pp. 840–850, May 2013.

[130] M. Wildemeersch, T. Quek, C. Slump, and A. Rabbachin, "Cognitive small cell networks: Energy efficiency and trade-offs," *IEEE Trans. Commun.*, vol. 61, no. 9, pp. 4016–4029, Sep. 2013.

[131] C. Li, J. Zhang, and K. Letaief, "Throughput and energy efficiency analysis of small cell networks with multi-antenna base stations," *IEEE Trans. Wireless Commun.*, vol. 13, no. 5, pp. 2505–2517, May 2014.

[132] D. Cao, S. Zhou, and Z. Niu, "Optimal combination of base station densities for energy-efficient two-tier heterogeneous cellular networks," *IEEE Trans. Wireless Commun.*, vol. 12, no. 9, pp. 4350–4362, Sep. 2013.

[133] ——, "Improving the energy efficiency of two-tier heterogeneous cellular networks through partial spectrum reuse," *IEEE Trans. Wireless Commun.*, vol. 12, no. 8, pp. 4129–4141, Aug. 2013.

[134] M. Di Renzo and W. Lu, "System-level analysis/optimization of cellular networks with simultaneous wireless information and power transfer: Stochastic geometry modeling," *IEEE Trans. Veh. Technol.*, accepted 2016.

[135] Y. Deng, L. WANG, M. Elkashlan, M. Di Renzo, and J. Yuan, "Modeling and analysis of wireless power transfer in heterogeneous cellular networks," *IEEE Trans. Commun.*, accepted 2016.

[136] T. Lam, M. Di Renzo, and J. Coon, "System-level analysis of SWIPT MIMO cellular networks," *IEEE Commun. Lett.*, accepted 2016.

[137] M. D. Renzo, "Stochastic geometry modeling and analysis of multi-tier millimeter wave cellular networks," *IEEE Trans. Wireless Commun.*, accepted 2015.

[138] S. Singh, M. Kulkarni, A. Ghosh, and J. Andrews, "Tractable model for rate in self-backhauled millimeter wave cellular networks," *IEEE J. Sel. Areas Commun.*, accepted 2015.

[139] T. Bai and R. Heath, "Coverage and rate analysis for millimeter-wave cellular networks," *IEEE Trans. Wireless Commun.*, vol. 14, no. 2, pp. 1100–1114, Feb. 2015.

[140] E. Turgut and M. C. Gursoy, "Average error probability analysis in mmwave cellular networks," in *Proc. of the IEEE 82th Vehicular Technology Conference (VTC-Fall)*, Sep. 2015, pp. 1–5.

[141] J. Lee and T. Q. S. Quek, "Hybrid full-/half-duplex system analysis in heterogeneous wireless networks," *IEEE Trans. Wireless Commun.*, vol. 14, no. 5, pp. 2883–2895, May 2014.

[142] H. Alves, C. de Lima, P. Nardelli, R. Demo Souza, and M. Latvaaho, "On the average spectral efficiency of interference-limited full-duplex networks," in *Proc. of the 9th International Conference on Cognitive Radio Oriented Wireless Networks and Communications (CROWNCOM)*, Jun. 2014, pp. 550–554.

[143] A. Alammouri, H. ElSawy, O. Amin, and M. S. Alouini, "In-band α-duplex scheme for cellular networks: A stochastic geometry approach," *IEEE Trans. Wireless Commun.*, accepted 2016.

[144] A. AlAmmouri, H. ElSawy, and M. S. Alouini, "Flexible design for α-duplex communications in multi-tier cellular networks," *IEEE Trans. Commun.*, vol. 64, no. 8, pp. 3548–3562, Aug 2016.

[145] I. Randrianantenaina, H. Elsawy, and M.-S. Alouini, "Limits on the capacity of in-band full duplex communication in uplink cellular networks," in *Workshop. of IEEE Global Communications Conference (Globecom'15)*, San Diego, CA, Dec. 2015.

[146] N. Deng, W. Zhou, , and M. Haenggi, "Heterogeneous cellular network models with dependence," *IEEE J. Sel. Areas Commun.*, accepted 2015.

[147] M. Di Renzo, "A stochastic geometry approach to the rate of downlink cellular networks over correlated Log-Normal shadowing," in *Proc. of the IEEE 78th Vehicular Technology Conference (VTC-Fall)*, Sep. 2013, pp. 1–5.

[148] H. ElSawy, E. Hossain, and M.-S. Alouini, "Analytical modeling of mode selection and power control for underlay D2D communication in cellular networks," *IEEE Trans. Commun.*, vol. 62, no. 11, pp. 4147–4161, Nov. 2014.

[149] X. Lin, J. G. Andrews, and A. Ghosh, "Spectrum sharing for device-to-device communication in cellular networks," *IEEE Trans. Wireless Commun.*, vol. 13, no. 12, pp. 6727–6740, Dec. 2014.

[150] M. Peng, Y. Li, T. Quek, and C. Wang, "Device-to-device underlaid cellular networks under Rician fading channels," *IEEE Trans. Wireless Commun.*, vol. 13, no. 8, pp. 4247–4259, Aug. 2014.

[151] H. Sun, M. Wildemeersch, M. Sheng, and T. Quek, "D2D enhanced heterogeneous cellular networks with dynamic TDD," *IEEE Trans. Wireless Commun.*, accepted 2015.

[152] M. Khoshkholgh, Y. Zhang, K.-C. Chen, K. Shin, and S. Gjessing, "Connectivity of cognitive device-to-device communications underlying cellular networks," *IEEE J. Sel. Areas Commun.*, vol. 33, no. 1, pp. 81–99, Jan. 2015.

[153] K. Aly, H. ElSawy, and M. S. Alouini, "Modeling cellular networks with full duplex D2D communication: A stochastic geometry approach," *IEEE Trans. Commun.*, accepted 2015.

[154] M. Afshang, H. S. Dhillon, and P. H. J. Chong, "Fundamentals of cluster-centric content placement in cache-enabled device-to-device networks," *IEEE Trans. Commun.*, vol. 64, no. 6, pp. 2511–2526, June 2016.

[155] X. Lin, R. Ganti, P. Fleming, and J. G. Andrews, "Towards understanding the fundamentals of mobility in cellular networks," *IEEE Trans. Wireless Commun.*, vol. 12, no. 4, pp. 1686–1698, Apr. 2013.

[156] W. Bao and B. Liang, "Stochastic geometric analysis of user mobility in heterogeneous wireless networks," *IEEE J. Sel. Areas Commun.*, accepted 2015.

[157] S. Sadr and R. Adve, "Handoff rate and coverage analysis in multi-tier heterogeneous networks," *IEEE Trans. Wireless Commun.*, vol. 14, no. 5, pp. 2626–2638, May 2015.

[158] R. Arshad, H. Elsawy, S. Sorour, T. Y. Al-Naffouri, and M.-S. Alouini, "Handover management in dense cellular networks: A stochastic geometry approach," in *IEEE International Conference on Communications (ICC).*, Malaysia, Kuala Lumpur, May 2016.

[159] ——, "Cooperative handover management in dense cellular networks," in *IEEE Global Conference on Communications (Globecom).*, Washington, DC, Dec 2016.

[160] H. Ibrahim, H. ElSawy, U. T. Nguyen, and M.-S. Alouini, "Mobility-aware modeling and analysis of dense cellular networks with c-plane/u-plane split architecture," *IEEE Trans. Commun.*, accepted 2016. [Online]. Available: http://http://arxiv.org/abs/1604.02960#

[161] D. Chen, T. Quek, and M. Kountouris, "Backhauling in heterogeneous cellular networks: Modeling and tradeoffs," *IEEE Trans. Wireless Commun.*, accepted 2015.

[162] V. Suryaprakash, P. Rost, and G. Fettweis, "Are heterogeneous cloud-based radio access networks cost effective?" *IEEE J. Sel. Areas Commun.*, accepted 2015.

[163] N. Lee, R. Heath, D. Morales-Jimenez, and A. Lozano, "Base station cooperation with dynamic clustering in super-dense cloud-RAN," in *IEEE Globecom Workshops*, Dec. 2013, pp. 784–788.

[164] G. Geraci, H. S. Dhillon, J. G. Andrews, J. Yuan, and I. B. Collings, "Physical layer security in downlink multi-antenna cellular networks," *IEEE Trans. Commun.*, vol. 62, no. 6, pp. 2006–2021, Jun. 2014.

[165] H. Wang, X. Zhou, and M. Reed, "Physical layer security in cellular networks: A stochastic geometry approach," *IEEE Trans. Wireless Commun.*, vol. 12, no. 6, pp. 2776–2787, Jun. 2013.

[166] F. Baccelli and B. Baszczyszyn, *Stochastic Geometry and Wireless Networks, Volume I – Theory*.   NoW Publishers, 2009.

[167] ——, *Stochastic Geometry and Wireless Networks, Volume II – Applications*.   NoW Publishers, 2009.

[168] M. Haenggi, *Stochastic Geometry for Wireless Networks*.   Cambridge University Press, 2012.

[169] S. Weber and J. G. Andrews, *Transmission Capacity of Wireless Networks*.   NOW Publishers (Foundations and Trends in Networking, Vol. 5), 2012.

[170] S. Mukherjee, *Analytical Modeling of Heterogeneous Cellular Networks*.   Cambridge University Press, 2014.

[171] R. Vaze, *Random Wireless Networks*.   Cambridge University Press, 2015.

[172] M. Abramowitz and I. A. Stegun, Eds., *Handbook of Mathematical Functions, Tenth Printing*.   Dover Publications, Dec. 1972.

[173] I. S. Gradshteyn and I. M. Ryzhik, *Table of Integrals, Series, and Products, Seventh Edition*.   Academic Press, 2007.

[174] A. Baddeley, *Spatial Point Processes and their Applications in Lecture Notes in Mathematics: Stochastic Geometry*.   Springer Verlag, 2007.

[175] D. Stoyan, W. S. Kendall, and J. Mecke, *Stochastic Geometry and Its Applications*.   second edition, Wiley, 1996.

[176] D. Daley and D. Vere-Jones, *An Introduction to the Theory of Point Processes, Volume II: General Theory and Structure*.   Springer, 2008.

[177] ——, *An Introduction to the Theory of Point Processes, Volume I: Elementary Theory and Methods*.   Springer, 2003.

[178] L. Li and A. J. Goldsmith, "Capacity and optimal resource allocation for fading broadcast channels. Part I: ergodic capacity," *IEEE Trans. Inf. Theory*, vol. 47, no. 3, pp. 1083–1102, March 2001.

[179] A. Okabe, B. Boots, K. Sugihara, and S. Chiu, *Spatial Tessellations: Concepts and Applications of Voronoi Diagrams*. second edition, Wiley, 2000.

[180] G. L. Stüber, *Principles of mobile communication*. Springer Science & Business Media, 2011.

[181] H. H. Andersen, *Linear and graphical models: for the multivariate complex normal distribution*. Springer Science & Business Media, 1995, vol. 101.

[182] G. Alfano, M. Garetto, and E. Leonardi, "New directions into the stochastic geometry analysis of dense CSMA networks," *IEEE Trans. Mobile Comput.*, vol. 13, no. 2, pp. 324–336, Feb. 2014.

[183] M. Kaynia, N. Jindal, and G. Oien, "Improving the performance of wireless ad hoc networks through MAC layer design," *IEEE Trans. Wireless Commun.*, vol. 10, no. 1, pp. 240–252, Jan. 2011.

[184] H. ElSawy, E. Hossain, and S. Camorlinga, "Spectrum-efficient multi-channel design for coexisting IEEE 802.15.4 networks: A stochastic geometry approach," *IEEE Trans. Mobile Comput.*, vol. 13, no. 7, pp. 1611–1624, Jul. 2014.

[185] H. ElSawy and E. Hossain, "A modified hard core point process for analysis of random CSMA wireless networks in general fading environments," *IEEE Trans. Commun.*, vol. 61, no. 4, pp. 1520–1534, Apr. 2013.

[186] M. Haenggi, "Mean interference in hard-core wireless networks," *IEEE Commun. Lett.*, vol. 15, no. 8, pp. 792–794, Aug. 2011.

[187] Y. Kim, F. Baccelli, and G. de Veciana, "Spatial reuse and fairness of mobile ad-hoc networks with channel-aware CSMA protocols," in *Proc. of the 2011 International Symposium on Modeling and Optimization in Mobile, Ad Hoc and Wireless Networks (WiOpt),*, May 2011, pp. 360–365.

[188] H. Nguyen, F. Baccelli, and D. Kofman, "A stochastic geometry analysis of dense IEEE 802.11 networks," in *Proc. of the 26th IEEE International Conference on Computer Communications (INFOCOM)*, May 2007, pp. 1199–1207.

[189] W. Lu and M. Di Renzo, "Stochastic geometry modeling of cellular networks: Analysis, simulation and experimental validation," in *ACM Int. Conf. Modeling, Analysis and Simulation of Wireless and Mobile Systems*, Oct 2015, pp. 1–4. [Online]. Available: http://arxiv.org/pdf/1506.03857.pdf

[190] ——, "Stochastic geometry modeling of mmwave cellular networks: Analysis and experimental validation," in *2015 IEEE International Workshop on Measurements and Networking (M&N)*, Oct 2015, pp. 1–4.

[191] B. Matérn, *Spatial Variation*. Springer-Verlag, 1986, vol. 2nd Edition. Vol. 36 of Lecture Notes in Statistics.

[192] M. Haenggi, "Mean interference in hard-core wireless networks," *IEEE J. Sel. Areas Commun.*, vol. 15, no. 8, pp. 792–794, Aug. 2011, available at http://www.nd.edu/~mhaenggi/pubs/cl11.pdf.

[193] ——, "The mean interference-to-signal ratio and its key role in cellular and amorphous networks," *IEEE Wireless Commun. Lett.*, vol. 3, no. 6, pp. 597–600, Dec 2014.

[194] E. Lukacs, "Applications of Faà di Bruno's formula in mathematical statistics," *The American Mathematical Monthly*, vol. 62, no. 5, pp. 340–348, 1955.

[195] ——, *Characteristic Functions*, 2nd ed. New York: Hafner Pub. Co., 1970.

[196] A. Conti, M. Z. Win, and M. Chiani, "Slow adaptive M-QAM with diversity in fast fading and shadowing," *IEEE Trans. Commun.*, vol. 55, no. 5, pp. 895–905, May 2007.

[197] L. Toni and A. Conti, "Does fast adaptive modulation always outperform slow adaptive modulation?" *IEEE Trans. Wireless Commun.*, vol. 10, no. 5, pp. 1504–1513, May 2011.

[198] M. K. Simon and M.-S. Alouini, *Digital Communication over Fading Channels*. Wiley-Interscience, 2005, vol. 95.

[199] K. A. Hamdi, "A useful technique for interference analysis in Nakagami fading," *IEEE Trans. Wireless Commun.*, vol. 55, no. 6, pp. 1120–1124, Jun. 2007.

[200] A. Giorgetti and M. Chiani, "Influence of fading on the Gaussian approximation for BPSK and QPSK with asynchronous cochannel interference," *IEEE Trans. Wireless Commun.*, vol. 4, no. 4, pp. 384–389, Aug. 2005.

[201] M. Chiani, A. Conti, and O. Andrisano, "Outage evaluation for slow frequency hopping mobile radio systems," *IEEE Trans. Commun.*, vol. 47, no. 12, pp. 1865–1874, Dec. 1999.

[202] A. Conti, M. Z. Win, M. Chiani, and J. H. Winters, "Bit error outage for diversity reception in shadowing environment," *IEEE Commun. Lett.*, vol. 7, no. 1, pp. 15–17, Jan. 2003.

[203] M. D. Renzo, W. Lu, and P. Guan, "The intensity matching approach: A tractable stochastic geometry approximation to system-level analysis of cellular networks," *IEEE Trans. Wireless Commun.*, vol. 15, no. 9, pp. 5963–5983, Sept 2016.

[204] S. Guruacharya, H. Tabassum, and E. Hossain, "Integral approximations for coverage probability," *IEEE Commun. Lett.*, vol. 5, no. 1, pp. 24–27, Feb 2016.

[205] K. A. Hamdi, "A useful lemma for capacity analysis of fading interference channels," *IEEE Trans. Commun.*, vol. 58, no. 2, pp. 411–416, 2010.

[206] A. Gupta, H. Dhillon, S. Vishwanath, and J. G. Andrews, "Downlink coverage probability in MIMO HetNets with flexible cell selection," in *Proc. of the 2014 IEEE Global Communications Conference (GLOBECOM)*, Dec. 2014, pp. 1534–1539.

[207] A. Conti, W. M. Gifford, M. Z. Win, and M. Chiani, "Optimized simple bounds for diversity systems," *IEEE Trans. Commun.*, vol. 57, no. 9, pp. 2674–2685, Sep. 2009.

[208] H. Elsawy, H. Dahrouj, T. Al-naffouri, and M.-S. Alouini, "Virtualized cognitive network architecture for 5G cellular networks," *IEEE Commun. Mag.*, vol. 53, no. 7, pp. 78–85, July 2015.

[209] M. Afshang, H. S. Dhillon, and P. H. J. Chong, "Modeling and performance analysis of clustered device-to-device networks," *IEEE Trans. Wireless Commun.*, accepted. 2016.

[210] A. Guo, Y. Zhong, W. Zhang, and M. Haenggi, "The Gauss-Poisson process for wireless networks and the benefits of cooperation," *IEEE Trans. Commun.*, vol. 64, no. 5, pp. 1916–1929, May 2016.

[211] Y. Li, F. Baccelli, H. S. Dhillon, and J. G. Andrews, "Fitting determinantal point processes to macro base station deployments," in *Proc. of the 2014 IEEE Global Communications Conference (GLOBECOM)*, Dec. 2014, pp. 1534–1539.

[212] I. Flint, X. Lu, N. Privault, D. Niyato, and P. Wang, "Performance analysis of ambient RF energy harvesting with repulsive point process modeling," *IEEE Trans. Wireless Commun.*, vol. 14, no. 10, pp. 5402–5416, Oct 2015.

[213] R. K. Ganti, J. G. Andrews, and M. Haenggi, "High-SIR transmission capacity of wireless networks with general fading and node distribution," *IEEE Trans. Inf. Theory*, vol. 57, no. 5, pp. 3100–3116, May 2011.

[214] R. Giacomelli, R. K. Ganti, and M. Haenggi, "Outage probability of general ad hoc networks in the high-reliability regime," *IEEE/ACM Trans. Netw.*, vol. 19, no. 4, pp. 1151–1163, Aug 2011.

[215] J. Lee and C. Tepedelenlioglu, "Stochastic ordering of interference in large-scale wireless networks," *IEEE Trans. Signal Process.*, vol. 62, no. 3, pp. 729–740, Feb. 2014.

[216] A. Sabharwal, P. Schniter, D. Guo, D. Bliss, S. Rangarajan, and R. Wichman, "In-band full-duplex wireless: Challenges and opportunities," *IEEE J. Sel. Areas Commun.*, vol. 32, no. 9, pp. 1637–1652, Sep. 2014.

[217] S. Hong, J. Brand, J. Choi, M. Jain, J. Mehlman, S. Katti, and P. Levis, "Applications of self-interference cancellation in 5G and beyond," *IEEE Commun. Mag.*, vol. 52, no. 2, pp. 114–121, Feb. 2014.

[218] E. Bastug, M. Bennis, and M. Debbah, "Living on the edge: The role of proactive caching in 5G wireless networks," *IEEE Commun. Mag.*, vol. 52, no. 8, pp. 82–89, Aug 2014.

[219] B. Blaszczyszyn and A. Giovanidis, "Optimal geographic caching in cellular networks," *CoRR*, vol. abs/1409.7626, 2014. [Online]. Available: http://arxiv.org/abs/1409.7626

[220] M. J. Farooq, H. ElSawy, and M. S. Alouini, "A stochastic geometry model for multi-hop highway vehicular communication," *IEEE Trans. Wireless Commun.*, vol. 15, no. 3, pp. 2276–2291, March 2016.

[221] A. Ali, H. Elsawy, T. Y. Al-Naffouri, and M. S. Alouini, "Narrowband interference parameterization for sparse bayesian recovery," in *2015 IEEE International Conference on Communications (ICC)*, June 2015, pp. 4530–4535.

[222] D. Dardari, A. Conti, C. Buratti, and R. Verdone, "Mathematical evaluation of environmental monitoring estimation error through energy-efficient wireless sensor networks," *IEEE Trans. Mobile Comput.*, vol. 6, no. 7, pp. 790–802, Jul. 2007.

[223] R. Cai, J.-K. Zhang, T. Davidson, W. Zhang, K. Wong, and P. Ching, "A power allocation strategy for multiple Poisson spectrum-sharing networks," *IEEE Trans. Wireless Commun.*, vol. 14, no. 4, pp. 1785–1799, April 2015.

This article has been accepted for publication in a future issue of this journal, but has not been fully edited. Content may change prior to final publication. Citation information: DOI 10.1109/COMST.2016.2624939, IEEE Communications Surveys & Tutorials

37

[224] T. Samarasinghe, H. Inaltekin, and J. Evans, "On optimal downlink coverage in Poisson cellular networks with power density constraints," *IEEE Trans. Commun.*, vol. 62, no. 4, pp. 1382–1392, April 2014.

[225] J.-S. Ferenc and Z. Néda, "On the size distribution of Poisson Voronoi cells," *Physica A: Statistical Mechanics and its Applications*, vol. 385, no. 2, pp. 518–526, 2007.

[226] H. S. Jo, Y. J. Sang, P. Xia, and J. G. Andrews, "Heterogeneous cellular networks with flexible cell association: A comprehensive downlink SINR analysis," *IEEE Trans. Wireless Commun.*, vol. 11, no. 10, pp. 3484–3495, October 2012.

Hesham ElSawy (S'10, M'14) received the B.Sc. degree in Electrical Engineering from Assiut University, Assiut, Egypt, in 2006, the M.Sc. degree in Electrical Engineering from Arab Academy for Science and Technology, Cairo, Egypt, in 2009, and the Ph.D. degree in Electrical Engineering from the University of Manitoba, Winnipeg, MB Canada, in 2014. Currently, he is a postdoctoral fellow with the Computer, Electrical, and Mathematical Sciences and Engineering Division, King Abdullah University of Science and Technology (KAUST), Saudi Arabia, and an adjunct member at the school of Computer Science & Engineering, York University, Canada. During the period of 2006-2010, he worked at the National Telecommunication Institute, Egypt, where he conducted professional training both at the national and international levels, as well as research on network planning. From 2010 to 2014, he worked with TRTech, Winnipeg, MB, Canada, as a Student Researcher. For his academic excellence, he has received several academic awards, including the NSERC Industrial Postgraduate Scholarship during the period of 2010-2013, and the TRTech Graduate Students Fellowship in the period of 2010-2014. He also received the best paper award in the ICC 2015 workshop on small cells and 5G networks. He is recognized as an exemplary reviewer by the *IEEE Transactions of communication* in 2015 & 2016. His research interests include statistical modeling of wireless networks, stochastic geometry, and queueing analysis for wireless communication networks.

Ahmed Sultan-Salem (M'07) received the B.S. and M.S. degrees in electrical engineering from Alexandria University, Egypt. He finished his Ph.D. from the Electrical Engineering Department at Stanford University in 2007. His thesis work was focused on the development of new models and signal analysis techniques to infer planetary surface parameters from data acquired by earth-based and spaceborne remote sensing experiments.
He is currently a visiting faculty to King Abdullah University of Science and Technology (KAUST), Saudi Arabia. His current research interests are energy harvesting, cognitive radio technology, dynamic spectrum access, cooperative communications, distributed and sequential detection, physical layer-based secrecy and OFDM for optical communications.

Mohamed-Slim Alouini (S'94, M'98, SM'03, F?09) was born in Tunis, Tunisia. He received the Ph.D. degree in Electrical Engineering from the California Institute of Technology (Caltech), Pasadena, CA, USA, in 1998. He served as a faculty member in the University of Minnesota, Minneapolis, MN, USA, then in the Texas A&M University at Qatar, Education City, Doha, Qatar before joining King Abdullah University of Science and Technology (KAUST), Thuwal, Makkah Province, Saudi Arabia as a Professor of Electrical Engineering in 2009. His current research interests include the modeling, design, and performance analysis of wireless communication systems.

Moe Z. Win (S'85-M'87-SM'97-F'04) received both the Ph.D. in Electrical Engineering and the M.S. in Applied Mathematics as a Presidential Fellow at the University of Southern California (USC) in 1998. He received the M.S. in Electrical Engineering from USC in 1989 and the B.S. (*magna cum laude*) in Electrical Engineering from Texas A&M University in 1987.
He is a Professor at the Massachusetts Institute of Technology (MIT) and the founding director of the Wireless Information and Network Sciences Laboratory. Prior to joining MIT, he was with AT&T Research Laboratories for five years and with the Jet Propulsion Laboratory for seven years. His research encompasses fundamental theories, algorithm design, and experimentation for a broad range of real-world problems. His current research topics include network localization and navigation, network interference exploitation, intrinsic wireless secrecy, adaptive diversity techniques, and ultra-wideband systems.
Professor Win is an elected Fellow of the AAAS, the IEEE, and the IET, and was an IEEE Distinguished Lecturer. He was honored with two IEEE Technical Field Awards: the IEEE Kiyo Tomiyasu Award (2011) and the IEEE Eric E. Sumner Award (2006, jointly with R. A. Scholtz). Together with students and colleagues, his papers have received numerous awards, including the IEEE Communications Society's Stephen O. Rice Prize (2012), the IEEE Aerospace and Electronic Systems Society's M. Barry Carlton Award (2011), the IEEE Communications Society's Guglielmo Marconi Prize Paper Award (2008), and the IEEE Antennas and Propagation Society's Sergei A. Schelkunoff Transactions Prize Paper Award (2003). Highlights of his international scholarly initiatives are the Copernicus Fellowship (2011), the Royal Academy of Engineering Distinguished Visiting Fellowship (2009), and the Fulbright Fellowship (2004). Other recognitions include the International Prize for Communications Cristoforo Colombo (2013), the *Laurea Honoris Causa* from the University of Ferrara (2008), the Technical Recognition Award of the IEEE ComSoc Radio Communications Committee (2008), and the U.S. Presidential Early Career Award for Scientists and Engineers (2004).
Dr. Win was an elected Member-at-Large on the IEEE Communications Society Board of Governors (2011–2013). He was the Chair (2005–2006) and Secretary (2003–2004) for the Radio Communications Committee of the IEEE Communications Society. Over the last decade, he has organized and chaired numerous international conferences. He is currently serving on the advisory board of the IEEE COMMUNICATION LETTERS. He served as Editor-at-Large (2012–2015) for the IEEE WIRELESS COMMUNICATIONS LETTERS, as Editor (2006–2012) for the IEEE TRANSACTIONS ON WIRELESS COMMUNICATIONS, and as Area Editor (2003–2006) and Editor (1998–2006) for the IEEE TRANSACTIONS ON COMMUNICATIONS. He was Guest-Editor for the PROCEEDINGS OF THE IEEE (2009) and for the IEEE JOURNAL ON SELECTED AREAS IN COMMUNICATIONS (2002).